2015 年度

博士学位論文

高温超伝導テープ線材の通電電流及び永久電流モードの特性に関する研究

Study of the current feeding effect on transport and remnant current characteristics of HTS tapes

中部大学大学院

工学研究科　電気電子工学専攻

TALLOULI MOHAMED

ABSTRACT

The development of the superconducting power transmission lines based on long-length High-Temperature Superconducting (HTS) tapes requires high production quality of these tapes. Due to fault conditions or technical errors during the operation of the power transmission line an over-current pulse, which its value reaches more than several times the rated current, could occur.

To avoid the cable damage in any urgent case, a quick interruption of the transport current is necessary. Comprehensive understanding of the current cut off time of HTS tape is required to restart the operation of power transmission line.

In this thesis, the redistribution of the transport and remnant current densities in HTS tapes after over-current pulse application and current switch off intervention was studied. One and three-dimensional transport and residual magnetic field scanning for different HTS tapes by a Hall probe system were made. After the software was developed, one and two-dimensional current density distributions data in HTS tapes from the magnetic field profiles around these tapes were obtained. The results show that after a short over-current pulse, that doesn't harm the HTS tape, a long time relaxation of the magnetic field above HTS tape's edges was observed. This relaxation process is related to the redistribution of the current density inside HTS tapes. It depends on the HTS tape structure and existence of stabilizer. For the redistribution of the remnant current density in HTS tapes, we found that the speed of intervention to cut current has a direct effect on the residual magnetic fields and then to the current distribution. This redistribution depends also on the type of the HTS tape where it is more important for laminated tapes than filamentary ones. These results should be considered in the design of HTS cables.

要約

長尺の高温超伝導（HTS）テープ線材を使った超伝導送電ケーブルの開発は、HTS テープ線材の高い均一性-を必要とする。そして、システム故障や誤操作等によって、短い時間ではあるが定格電流の数倍の電流にケーブルが耐える必要がある。また、ケーブル損傷を避けるためは、短い時間で電流遮断をする遮断器の利用は必要不可欠で有り、同時に遮断後システムが回復したときには、早い再通電が求められる。つまり、 HTS テープの電流が遮断された後の送電システムの再起動の検討も必要となる。

本論文では、過電流パルスおよび電流遮断後の HTS テープ線材に残る電流の分布を実験的に計測し、テープ線材中の磁場の拡散及び均一性について検討した。このため、異なるタイプの HTS テープをモデル化し、一次元電流密度分布及び二次元電流密度分布（テープのため、厚さは無視した）を求めた。これは、1 次元及び 2 次元の磁場分布測定を行うためのホールプローブを利用した実験装置を開発し、磁場分布をデータとして計算機に取り込んだ。次ぎに、Biot Savart 法則の逆問題を解くための数値ソフトウェアを開発し HTS テープ内に一次元、二次元の電流密度分布が得た。また、磁場測定の時定数を評価して、磁場のテープ線材中の拡散について議論を行った。

その結果、十分に安定化材で保護された HTS テープ線材は短い過電流パルスによって破壊されることは観測されなかったが、Bi2223 系線材では、磁場拡散時間が通常の見積もりとは大きく異なった。一方、Y123 系線材は、磁場拡散時間は通常の見積もりにしたがった。このような違いは現在検討中である。

また、HTS テープ線材の残留電流密度分布によって、線材の均一性について議論ができることが分かった。特に、電流密度分布が Vortex を作ることが観測され、これが再スタートにどの様な影響を与えるかについての検討が必要になることが分かった。

今後は、単一のテープ線材だけではなく、ケーブル状に加工したときにどの様な振る舞いをするかに重点を置いて調べる必要があることが重要で有り、今回の結果はこのための基礎データを与えると考えている。

ACKNOWLEDGEMENTS

This work was carried out between March 2013 and December 2015 at the Centre of Applied Superconductivity and Sustainable Energy Research (CASER) laboratory, and the Department of Electric engineering, at Chubu University. I spent very exciting and fruitful time in this laboratory.

I would first like to thank my supervisor, **Prof. Satarou Yamaguchi**. Thanks for his support, encouragement, and guidance; I learned a lot of things, which are not limited to research topics.

I would like to thank also:

Prof. Atsuo Iiyoshi, Chancellor of Chubu University; For his continuous encouragement through this thesis.

Prof. Ishihara Osamu, **Prof. Noriko Chikumoto**, **Prof. Edmund Soji Otabe**, and **Prof. Toshio Kawahara** (Thesis committee); For their comments and suggestions to improve the quality of this thesis. Also for participating in the thesis panel. My deepest appreciation..

Dr. Jian Sun, (CASER member); For multiple assistance with measurements required for this thesis and many precious advice and discussions on research, experimental setups and exchange of viewpoints.

Mr. Koji Yoshimura, (CASER member); For preparing and designing of the measurement equipment, devices and his continued assistance during this thesis.

Dr. Tosin Famakinwa for the kindness and all the advice He gave to me during his visit CASER laboratory and on this thesis.

Prof. Oleg Shyshkin (Kharkiv University, Ukraine); For having the time to discuss many research topics as well as this work and developing simulation programs and calculations, which makes this thesis possible.

M. Kyomi Muto, Mariko Yamakoshi, and Hikaru Akiyama, (CASER members); For their encouragement and moral assistance that allowed me to have joyful living in Japan. Without them, my working condition would be probably less pleasant.

Mr. Hisato Ohara and **Toki Yoshinubu**; For to first introducing me to Japanese life style and culture .

Prof. Samia Charfi Kaddour (El Manar University, Tunisia); For first inviting me to do this thesis in Japan and for his continuous support.

My family, mother, father, brother and sisters; For all encouragements, supports and, their continuous love.

My fiancée Ines and all my friends especially **Jakula, Uejima, and Vyatkin**; For invaluable help, great encouragement, and everything.

Japanese government; For funding me with doctoral scholarship and for giving me the chance to discover this beautiful country.

To my parents and siblings

LIST OF FIGURES AND TABLES

Figures

Tables

Table of Contents

PREFACE

The world is still living in the era of fuels energy, however, no one can say for sure when this era is going to end, because almost more than half of the world reserves of oil and gas has been consumed. This situation calls for the consideration of renewable energies with the fact that fuel energy have very strong impact on our environment. This consideration results in many worldwide projects. Sahara Solar Breeder project (SSB project) is among these projects. The goal of SSB is to generate electricity through photovoltaic panels and and transport it from the North African Sahara desert to European continent via a High Temperature Superconducting Cables (HTSC). These superconducting power cables is planned to transport high DC current from the south of the Mediterranean Sea to the north. Recent remarkable progress in superconducting DC power cables (cooled by liquid nitrogen LN2) constructed at Chubu University makes it possible to transmit large electric power with much less loss than normal copper cables.

This thesis was completed in the Centre of Applied Superconductivity and Sustainable Energy Research (CASER) laboratory of Chubu University where a DC Superconducting Power Transmission line (DCSC-PT) was constructed. The redistribution of the current density in HTS tapes after a fault condition or quick cut-off operation is needed to operate and restart power lines. Normal and over-current operation of HTS tape was experimentally simulated, as a result software was developed, Transport and remnant currents and magnetic multi-dimensional distributions were measured and calculated. In this thesis long time relaxation and redistribution of magnetic field and current density, dependence on the cut-off speed and HTS tape characteristics are discussed. The above are common phenomena and they should be considered in the design of DC HTS power cables.

Previous researchers made magnetic field scanning method to calculate current density but they use basically micro-scale scanning aimed to detect the defect in tapes and difficult model to calculate current density. Our method is sample and direct. It is based on resolving linear equations and millimeter-scale scanning to get current density configuration.

The thesis is outlined is as follows:

In chapter 1 is an introduction to superconductivity. Brief history and background information of superconducting parameters and applications are described.

In chapter 2, the electromagnetic and thermodynamic properties of HTS tapes are discussed, specifically, the characteristics of BSCCO and YBCO tapes, which have more potential for application in power engineering. Current density in HTS tapes and contactless method of current calculation is also described here.

In chapter 3, the power cable parameters of normal and superconductor power cables are discussed. The advances of DC power cable compared to AC superconducting power cables are also mentioned. The DC superconducting power transmission line constructed at Chubu University is also discussed.

Chapter 4, a brief discussion of the importance of cryogenic engineering for superconducting power cables technology.

The experimental layout, method and setup are discussed in chapter 5. The experimental results using the Hall probe technique after applying a normal current feeding operation and an over-current pulse to BSCCO and YBCO tapes are presented. Measurement of the self-magnetic field above tapes' edges, self and remnant magnetic field scanning by one and three-dimensional Hall probe sensors are shown. The homogeneity of the remnant magnetic field of the HTS tapes used in this thesis was also investigated.

In chapter 6 we present current density distribution calculation. A solution method is proposed based on the resolution of simple linear equations from the inverse problem of Biot-Savart law.

The results of the over-current pulse operation on the current density distribution of the BSCCO and YBCO tapes are presented in **chapter 7**. The effect of the self-magnetic field penetration on the current density near HTS tapes both near the edges and at the center of the used HTS tapes is included in this chapter.. In this chapter also, presented is the current density calculation results of one and two-dimensional remnant current density distributions. Homogeneity of the HTS tapes and the current cut-off operation effect on the remnant current density profiles are discussed.

In **Chapter 8** the main conclusion of this thesis's experimental work and numerical calculations is presented. This chapter also gives some considerations for the possible continuation of the experimental works and current density calculations.

Sahara Solar Breeder project (SSB), construct a dream and hope not only for North African civilizations but also to the global world. The exploration and transport of huge energy hidden in the Sahara Desert from one continent to another give a solution for our future generations. SSB project plans to connect the world via a net of renewable and clean energy. This thesis tries to contribute to the advantages of the superconducting power transmission technology and hence to the SSB project.

CHAPTER 1: AN INTRODUCTION TO SUPERCONDUCTIVTY

1.1 History of superconductivity

The superconductivity, discovered by the Dutch physicist Kammerlingh Onnes in 1911, is considered as one of the greatest scientific discoveries. Its applications, especially in energy transport, become more and more numerous. Originally trying to melt the pure mercury, Onnes remarked that the resistance of mercury decreases rapidly to zero below 4.2 K [1]. To proof that the resistivity of mercury is correctly zero, Onnes used the technique of estimating the upper limit of the resistivity by studying the decay rate of the persistent current in a superconducting ring. Once established, the time dependence of the current I(t) through the ring is given by $I(t)=I0\ e^{-(R/L)t}$ where I0 is the current at t=0, R is the resistance, and L is the inductance of the ring. The current showed no decay even for infinitely long times, which means that the superconductor had zero resistance.

This phenomenon discovered also in other materials is called superconductivity. Resistivity of certain element or compound decreases to zero below certain temperature and it is called the critical temperature (Tc). In addition to the critical temperature Tc, Superconductivity has other critical parameters, which are: critical magnetic field Hc and critical current density Jc. Another major characteristic of superconductivity is the Meissner effect that is when superconductors expelled magnetic field lines.

Many physicists such as London, Ginzburg-Landau [2] and Bardeen-Cooper-Shriffer (or BCS) t [3] have put forward different theories to explain the superconducting phenomenon. These theories explain various phenomena observed in the superconducting state such as the drop of resistivity, critical temperature, critical current density, Meissner effect etc.

BCS theory (Nobel prize winners in 1971) is the complete theory among the previous one. It suggests that at very low temperatures the electrons are put at couples to form Cooper pairs. This ordered state is due to the existence of an attraction between electrons through the atomic lattice vibrations, which can be explained as follow: an electron moves in the metal and causes a local and momentary lattice strain by the attraction between the electron and the positive ions. These ions movement creates a surplus of positive charge. A second electron will be subjected to the excess of positive charge that shields the negative charge of the first electron. As electrons flow much faster than the ions (ions are much heavier), the second electron experiences the persistent effect of the positive charge when the first electron is away from it. The interaction between two electrons is therefore of great significance. Electron pairs thus formed move then without dissipation of energy in the crystal lattice. Electrons become as fermions, which means that they can be at the same location in the same physical condition. [4,5]. BCS theory gives then an almost complete explanation of the superconductivity, However, superconductivity mechanism in this theory does not allow to obtain a critical temperature higher than tens of Kelvins for the maximum Tc [6]. The superconductor in which this theory is valuable is called conventional superconductors or **low-temperature superconductors**.

In 1986 new superconducting materials were discovered (see Fig. 1). These are the CuO2 planes based on cuprate materials with critical temperatures up to Tc = 135 K (at ambient pressure). These new superconductors, however, have undermined by the BCS theory. They are called **high-temperature superconductors**. Since the discovery of the cuprates, then the oxypnictides, researchers are quickly trying to understand the properties of these materials, particularly the transport current characteristics. The transport properties of these materials are considered "abnormal" in the non-superconducting phase.

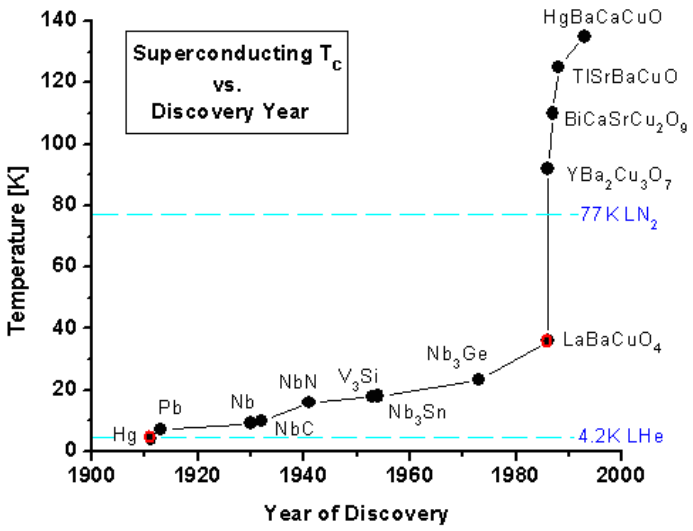

Fig. 1 Evolution of the critical current in the 20Th century. [7]

1.2 Superconductivity parameters

The superconductivity state is defined by three main parameters: the critical temperature Tc, the critical magnetic field Hc, and the critical current density J_c. And every superconductor material is characterized by these three parameters, which constitute what we call critical surface or phase diagram as in Fig. 2.

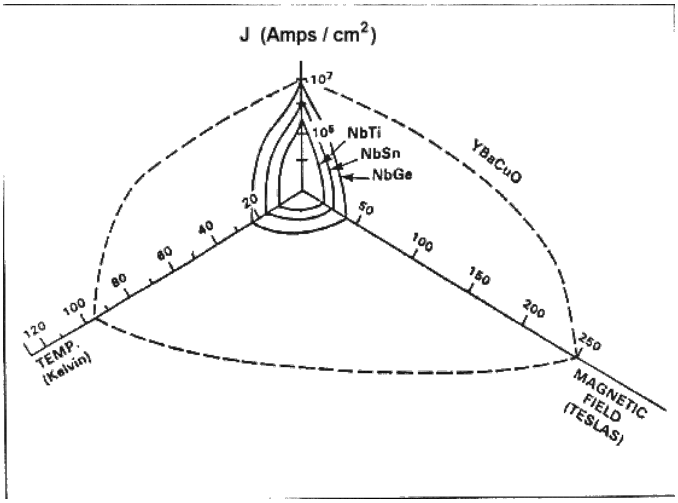

Fig. 2 Phase diagrams of superconductor materials. [7]

1.2.1 *Critical temperature*

Superconductivity is a state of matter that appears below a temperature called critical temperature or T_c. In fact, the superconductivity state is observed in many materials when their temperature is close to 0 K. However, T_c is higher in the case of bad conductor materials with a high resistivity such as mercury.

Fig.3 shows the variation of the resistivity for normal and superconductor materials versus the temperature. For the normal conductors the variation of the resistivity or R (T) in low temperatures is related, except the temperature, to the Debye temperature and precisely to the maximum mode frequency $\theta_d = \sim \omega_d/k$ [8]. For $T << \theta d$ the resistivity R (T) goes as T^3 and for $T >> \theta_d$ the resistivity R (T) corresponds to a linear variation and we can right R (T) as: $R(T) = R_0 [1 + \alpha (T-T_0)]$ where α is the temperature coefficient of the material and R_0 is determined by impurities and lattice defects [8]. We can observe in Fig. 3 that for T = 0 K the resistivity of normal conductor is not zero. However, for superconductor materials R (T) drops quickly to zero close to T_c, which characterizes the superconducting state.

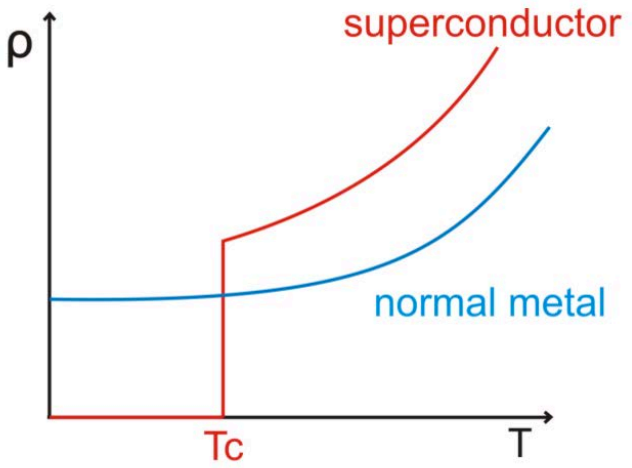

Fig. 3 Critical temperature of superconductor compared to normal metal [9]

1.2.2 Critical magnetic field

The superconducting state can be destroyed by the application of a magnetic field if this one is above a value named critical magnetic field or H_c. This magnetic field depends on the temperature by $H_c(T) = H[1-(\frac{T}{T_c})^2]$ as in Fig.4. The critical magnetic field is then maximal for a temperature equal to zero.

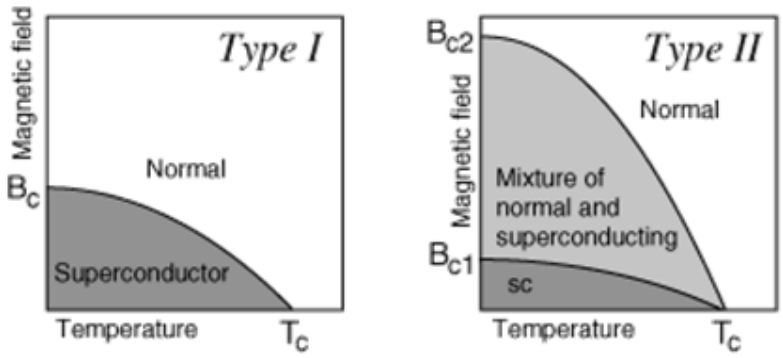

Fig. 4 Critical magnetic field as a function of temperature for Type-I and Type-II superconductor [10]

Superconducting materials are characterized also by an effect called Meissner effect. This is when superconductors expel the magnetic field lines when it is cooled below T_c with or without an applied magnetic field. In a superconducting material the magnetic field B is then equal to $\vec{B} = \mu_0(\vec{M} + \vec{B}_{int}) = 0 \Rightarrow \vec{M} = -\vec{B}_{int} = \chi\vec{B}_{int} \Rightarrow \chi = -1$ where μ_0 is the vacuum permeability, χ is the volume magnetic susceptibility, M is the magnetization and B_{int} is the interior magnetic field. Meissner effect indicates that the superconducting materials are perfect diamagnetic materials.

The transport currents in superconducting materials flow through the inner surface of a thickness equal to λ_L called the London penetration length and given by $\lambda_L^2 = \frac{m}{n_s\mu_0 e^2}$ (n_s is the number of Cooper electrons, e is the electron charge and m is the mass of the electron) with the range of

(100 to 1000) Å at lower temperature T << T_c. These currents make a screen shielding to the applied magnetic fields. The screening is incomplete for thin superconducting tapes and it is inferior to λ_L.

The magnetic field penetration length is given by London Maxwell equations [11] as follow:

$\Delta\vec{B} - \frac{1}{\lambda^2_L}\vec{B} = \vec{0}$ And $\Delta\vec{J} - \frac{1}{\lambda^2_L}\vec{J} = \vec{0}$.

For a superconductor thin tape and if a perpendicular magnetic field or a perpendicular current density vector are applied to the tape's surface, *B* and *J* are written as follow:

$\vec{B}(z) = \vec{B}(0) \times e^{-\frac{z}{\lambda_L}}$ And $\vec{J}(z) = \vec{J}(0) \times e^{-\frac{z}{\lambda_L}}$. Means that *B* and *J* decrease exponentially from the superconductor surface.

Superconductors are divided into two types: type I and type II.

- Type I superconductors are characterized by the fact that if the external magnetic field reaches the critical value Hc the Meissner effect stops immediately. Diamagnetism is then perfect for an applied magnetic field lower than Hc. Many pure conductors are in fact superconductors type I, however they are not used in superconductor magnets because of their low critical magnetic fields inferior to 10^7 Tesla.

- Type II superconductors are characterized by an incomplete diamagnetism which disappears gradually from a characteristic magnetic field value named H_{c1} and disappears totally for a second characteristic magnetic field named H_{c2} as in Fig. 5.

The diamagnetism profile of the type II superconductors have three zones (see Figs. 5)

- First one is for H< H_{c1}. The Meisner effect is then complete and the behaviour of the type II superconductors is identical to type I superconductors. In this zone the type II superconductor is in a **superconducting state**.

- Second one is a zone where $H_{c1} < H < H_{c2}$ and it is named **mixed state**. It is characterized by the partial penetration of magnetic fluxes in form of tubes as in Fig. 6. These tubes of penetrated magnetic fields are named vortices and they are arranged in the superconductor type II materials as a configuration proposed by the physicist Abrikozov. The core of the vortex tube with ξ size ($\xi < \lambda_L$) is in normal state and around it the superconductor state. In Abrikozov model ξ is named superconducting coherence length and it is given by the Ginzburg-Landau theory. The superconducting currents circulating around vortex induces a quantified fluxes Φ_0 given by

$\Phi_0 = \frac{h}{2e} = 2.067 \times 10^{-15}$ J. s. e^{-1}, where *h* is the Planck constant and e is the electron charge. For

n_v vortices we have then $n_v * \Phi_0$.

- The third region corresponds to the **normal state**.

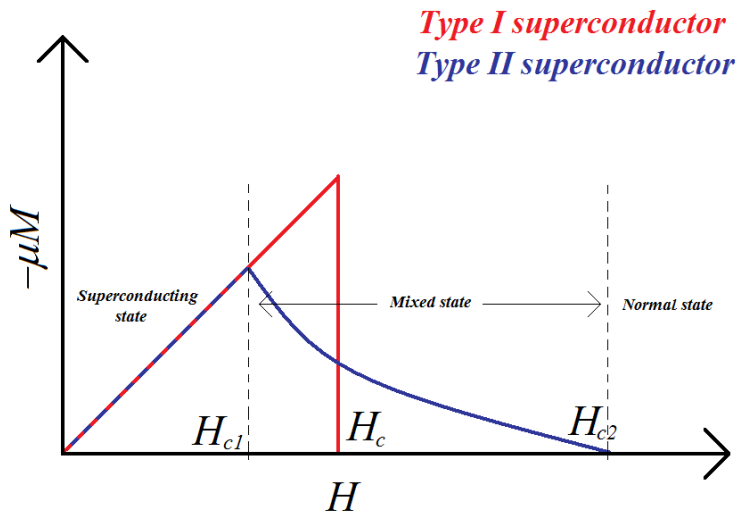

Fig. 5 Magnetization of the superconductors. [12]

It exists in fact in another zone, not shown in Fig. 5, situated between the mixture and the normal zones and in which only a thin surface of the superconducting material conducts currents. The superconductivity disappears totally if the magnetic field decreases this third critical magnetic field named H_{c3}.

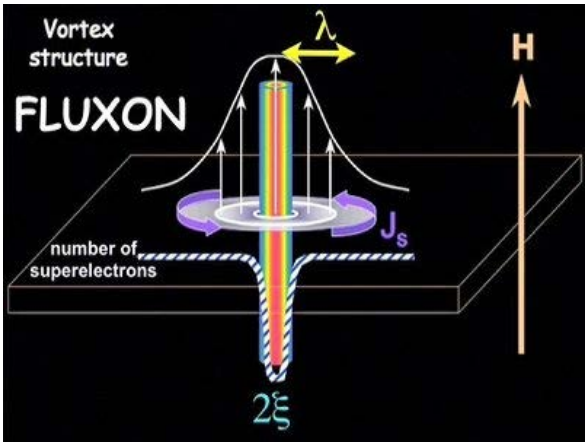

Fig. 6 Vortex structure in type II superconductors. [13]

The higher critical magnetic field H_{c2} can be very high for some superconductors and it can reach even up to 250 T for some material (see table). For this reason, Type II materials are the most used in the superconductor magnets. Other compounds except pure metals are almost all type II superconductors.

Materials	T_c (K)	H_{c1} (T=0)	H_{c2} (T=0)
Nb	9.3	5.0	0.1
NbTi	9.5	-	13
Nb_3Sn	18.5	0.0035	23
YBCO	91.2	0.0032	250
BSCCO (2223)	131	0.0045	110

Table 1. Critical parameters of some superconductor materials. [14]

1.2.3 Critical current density, flux-creep and flux-flow

The critical current density is the maximum value beyond which a resistivity reappears in the superconducting materials, which means that the superconductor state is destroyed. In superconducting state, the electrons are insensitive to all excitations and behave as a non-viscous fluid in the material. This fact is related to the existence of a superconducting gap and explains the absence of any loss of energy in superconductors.

For the type I superconductors, the current distribution is not homogeneous. The transport current flows only on the surface within the London penetration thickness as we saw in the previous section. However, for the type II superconductors, the transport current density depends strongly on the induced magnetic field B and on the presence of vortices in the material penetrated as an Abrikosov configuration. The applied current density reacts with the vortices in the type II superconductors under the Lorentz force [15]. If the Lorentz force is higher than a characteristic force named pinning force F_0 the vortices move and a dissipation lost is then produced in the material. This movement of the vortices by a distance d is called hopping and has a characteristic frequency Ω. But when the current density exceeds Jc the vortices are torn. This regime is called flow regime. The vortices move then freely and an electric field is then created in the superconductor material. For large critical current density superconductors, vortices must be anchored in the material with a high pinning force [16].

The dependence of the electric field in function of the applied current density in superconductors is divided then into three zones as in Fig. 7.

The first zone is named thermally activated flux-flow zone. This zone is for small current densities, where the vortex on averages moves in the same direction. This zone is also not yet

well defined and depends on the temperature, that's why we could not see it in the figure. Losses are totally negligible in this zone [17].

- The second zone is located around the critical current, and it is called flux-creep. The vortices density is strong enough and also the interactions between them and the Lorentz forces [18].

- The third zone is for currents above the critical current, called flux-flow zone. In this zone the Lorentz force is much greater than the vortices pinning forces, leaving the vortices moving collectively and freely [19].

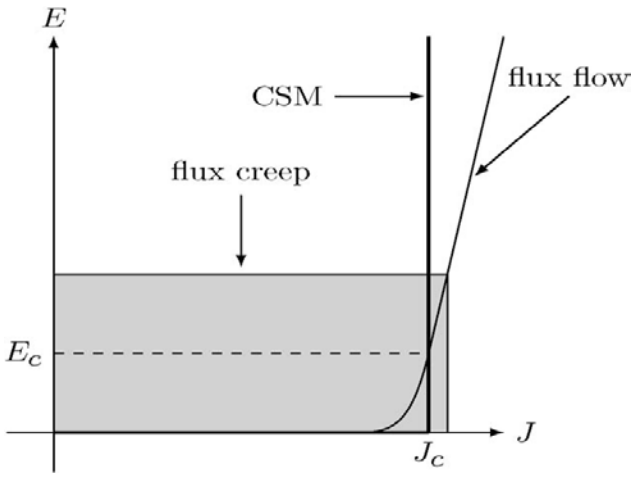

Fig. 7 Electric field dependence on the applied current density [20].

1.3 Superconductor's current density calculation

To calculate the current density in superconductor, various methods are used. However, some of these techniques have the disadvantage of not maintaining stable measurement conditions and require special preparation of the sample and a precise calibration of the measuring instruments. Therefore, to improve the current transport capability and its longitudinal uniformity of the superconductor other techniques named contactless or non-destructive techniques are utilized to

characterize the current density distribution. These techniques help to detect any defect of HTS tapes after a fatigue or strained processes.

We can cite from these techniques:

- First the scanning Hall-probe Microscopy (SHM), which is known as one of the most useful non-destructive technique for magnetic evaluation of several materials such as stainless steel and low carbon steel largely used in industry. It has been also applied to characterize current density distributions in filamentary HTS tapes such as the BSCCO tapes or coated conductors such as YBCO tapes. [21]

- The second non-destructive technique is the Superconducting Quantum Interference Devices (SQUID), which is a high-resolution magnetometer using Josephson junctions, that can detect a magnetic flux density. We can detect with such technique, for example, local current densities flowing around artificial defects in YBCO tapes. [22],

- Magneto-optical imaging, which is based on an effect discovered in 1845 by the scientist Michal Faraday [23, 24]. Faraday law is a physical law that relates the polarization vector of a linearly polarized light beam propagating in a material parallel to a magnetic field H rotated through an angle ϕ to the Verdet constant ν which is material-specific and temperature- and frequency-dependent constant. In fact, ν depends on the dispersion of the refractive index after interacting with the material, where n is the index of refraction, λ is the wavelength, e/m is the charge to mass ratio of the electron and c is the speed of light by $\nu = \frac{\phi}{dB} - \frac{1}{2}\frac{e}{m}\frac{\lambda}{c}\frac{dn}{d\lambda}$ [23].

We propose in this thesis to reconstruct the distribution of current in HTS tapes using the measurement of its self-magnetic field measured above the tapes' surface using one-dimensional and three-dimensional Hall probe sensors. This method did not require special preparation. The

calculation of the current density will be calculated by an inverse method technique. We present the experiment results and current density calculation in chapter 5, 6, and 7.

Many models described the current density distribution in superconductors, and it is difficult to have an analytical macroscopic model that can characterize completely the current density for complicated configurations. However, these models can carry out complete analytical calculations of the current densities for simple geometries such as a single HTS tape conducted by a DC current. The first proposed model is the Bean model named also the critical state model, which is a simplified one. For the dependence of Jc as a function of the self-magnetic field, power low model and Kim model may be used also. In this case, the superconducting material works around its critical current density. The use of each model depends then on the physical parameters and the configuration of the HTS tape. We summarize each model as follow:

- Bean suggested the first model in 1962, named also critical state model. It mainly gives a macroscopic explanation of the irreversible magnetization of hard Type-II superconductors and assumes that the current in HTS tapes flows at a constant current equal to Jc. The current density in this model is independent of the induced magnetic field and it's related to the current density by: $\nabla B_{\text{int}} = \mu J_c$ [25]. This model has the advantage of being relatively simple for sample geometries of superconductors. It gives analytical expressions of J and B, which makes easy to get some important variables such as AC losses. This model makes also some difficulties in the use of digital developments and does not give satisfactory results for the calculation of the current density distribution in HTS tapes.

- The power law model describes well the behaviour of HTS tapes around the critical state. The model's parameters are the critical current density Jc and the exponent *n*. It relates the current density *J* to the electric field *E* in the superconductor material by: $\frac{E(J)}{E_c} = (\frac{J}{J_c})^n$. Its possible also

with this model to vary the curves *E (J)* so that we can model a normal conductor for $n = 1$ (linear behaviour of the law) or to have a curve as in the critical state model for $n > 100$. In this model E_C is the electric field strength at $I = I_c$. The temperature and magnetic field are dependent on n and can provide an insight into the property of the dissipation process. For engineers the critical current corresponds to the criterion $E_c = 1$ μV/cm. An example of the *E, J* profile of the BSCCO tape used in this thesis is shown in Fig. 16 and for a high temperature superconductor tape for example the critical current Ic is given by $I_c = J_c * S$ with S is the cross section of the tape. We show Fig. 8 the E, J profile measured in our lab for the BSCCO tape and we can see in this figure that the I_c is equal to 200 A.

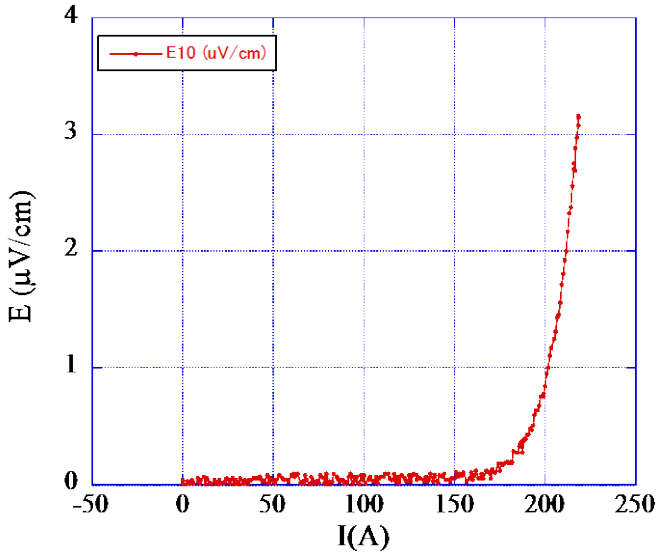

Fig. 8 Variation of the electric field of the BSCCO tape as function of an applied DC current.

- The Bean model and the power law model consider the superconducting material as isotropic and insulated. They do not take into account any heating of the conductor as a result of losses that might be originated from the interaction of the current density with the vortices. The critical current density is assumed then to be constant regardless of the transported current. In fact the current density is highly dependent on the interaction with the vortices. B. Kim et al [26] gave

the expression of the current density *J* and relates it not only to the applied current density and magnetic field but also to the pinning strength F_0 of vortices and the critical electric field by the equation: $J_c(T) = J_c(0)[(1 - k_B T / F)\ln(Bd\Omega / E_c)]$ where J_c *(0)* is the critical current density for T = 0 and *d, Ω* are parameters depending on superconductor vortices.

1.4 Superconducting applications

Superconductors with low and high temperature are already used in many fields: electricity, medical, electronics or even trains. They are also central parts of many devices such as: power cables, magnetic sensors, SQUID, or to produce very strong magnetic fields. (See Figs. 9-11).
We can name some of the main superconductor's applications as follow:

- Superconductor magnets [27].

A **superconducting magnet** is an electromagnet made from coils (See Fig. 9) of superconducting wire. They must be cooled and maintain cryogenic temperatures during operation. In its superconducting state the wire can conduct much larger electric current than ordinary wire, creating intense magnetic fields. Superconducting magnets can produce greater magnetic field and can be cheaper to operate because no energy is dissipated as heat in the windings. They are used in MRI machines in hospitals, and in scientific equipment such as NMR spectrometers and particles accelerator. [28]

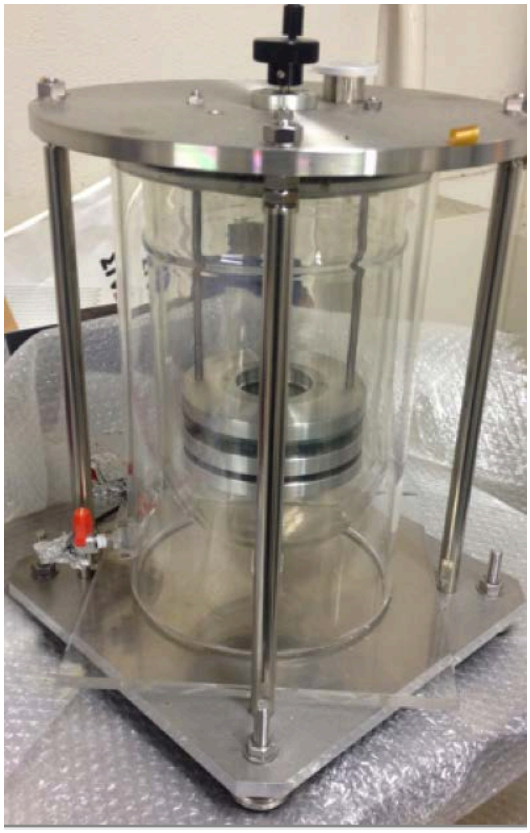

Fig. 9 Photo of an HTS superconducting coil in CASER laboratory.

- Transmission lines [29]. It will be discussed in more detail in chapter 3.
- Superconductor motors [30].

Superconducting motors (as shown in Fig. 10) are new types of AC synchronous motors that employ HTS (high-temperature superconductor) windings in place of conventional copper coils. Because HTS wire can carry significantly larger currents than can copper wire, these windings are capable of generating much more powerful magnetic fields in a given volume of space. The smaller size and compact nature of superconducting motors allow them to be manufactured at lower cost than equivalent conventional motors. In addition, the motor's increased efficiency results in lower operating costs than conventional motors. [31]

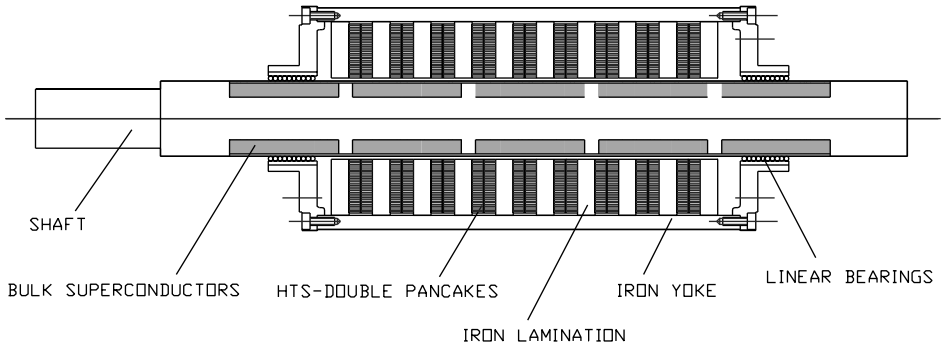

Fig. 10 Structure of superconducting motor [30]

- SQUID [32]

Superconducting Quantum Interference Device is used to measure very weak magnetic fields. It usually consists of two Josephson junctions connected in parallel in a superconducting loop as in Fig, 11.

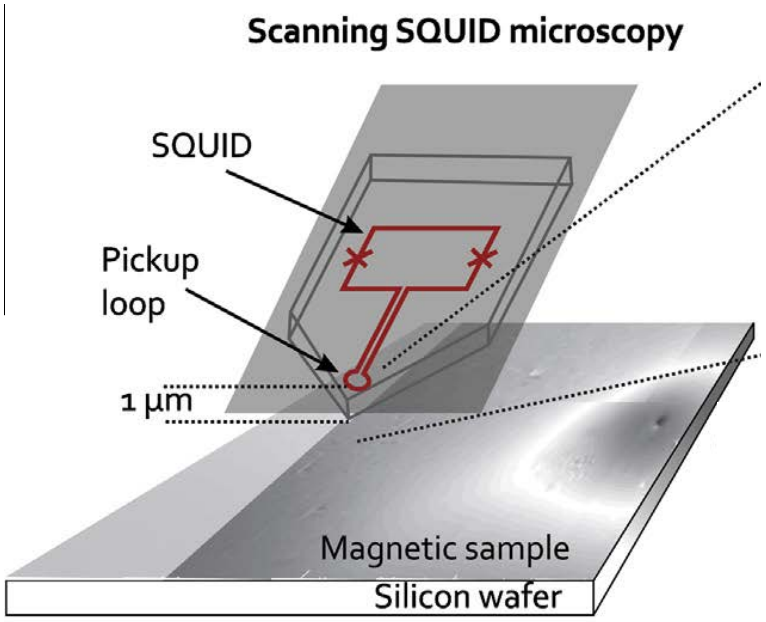

Fig. 11 Magnetic filed measurement set-up by SQUID [32]

- Microwave detectors. [33]

Superconductor is used also to fabricate microwave detectors and antenna (see Fig. 12). With its high sensitivity it is largely used in many fields and especially in astronomy.

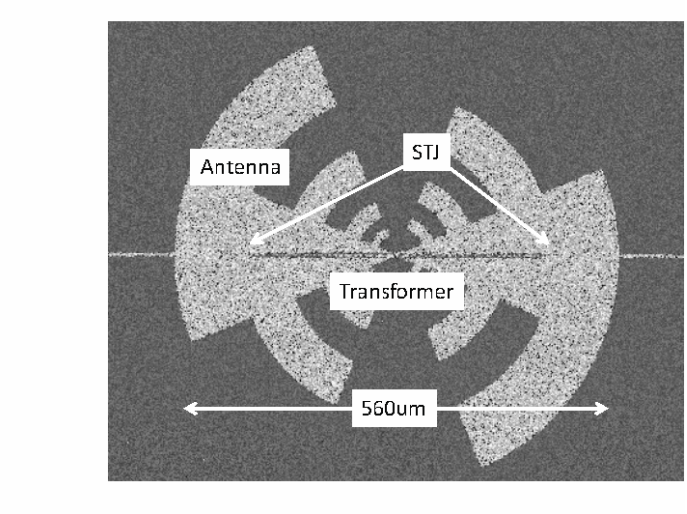

Fig. 12 Microwave detector using superconducting tunnel junction [33]

Even if superconductors work only in very low temperatures many applications are already operational in the laboratory and could spread throughout our cities, because cooling methods are becoming more and more less expensive and better and we will discuss cryogenics engineering in chapter 3. Superconductors, can lead to progress not only in energy and the environment but also transport or IT.

1.5 Summary

Even if superconductors work only at very low temperatures many applications are already operational in the laboratory and could spread throughout our cities because cooling methods are becoming more and less expensive and better and we will discuss cryogenics engineering in

chapter 3. Superconductors, can lead to progress not only in energy and the environment but also transport or IT.

In this chapter, we showed that low temperature and high-temperature superconductors have the property of transporting current with much lower losses than conventional conductors and also that they have special physical characteristics. These properties and characteristics have interested industries for a large variety of applications that continues to emerge.

CHAPTER 2: HIGH-TEMPERATURE SUPERCONDUCTOR TAPES AND MODULES OF CURRENT DENSITY CALCULATION

2.1 Introduction

High temperature superconducting tapes (HTS), mainly YBCO and BSCCO tapes, are more and more considered as the future solution for the high current power transmission technology. They are also used in transformers, fault current limiters, and magnets, because of their high critical current density and critical temperature, which gives them advantage compare to low temperature superconductors or normal conductors.

HTS tapes are fabricated commercially in large scale including two forms: filamentary form (example: BSCCO tapes) where superconductor filaments are packed in a matrix, and lattice form where the superconductor lattice (ex: YBCO tapes) of a thin layer is coated with other layers. The current density distribution investigation in these tapes is then important for more development of their applications.

2.2 Properties and manufacturing of High-Temperature Superconductor Tapes

2.2.1 Properties and manufacturing of BSCCO tapes

Bismuth strontium calcium copper oxide (BSCCO) is a high-temperature superconductor, (formula: $Bi_2Sr_2Ca_{n-1}Cu_nO_{2n+4+y}$), and one of the most used cuprate material with the YBCO materials in the superconductivity applications. BSCCO material was discovered in Japan in 1988 and its structure is Perovskite [34]. The superconductor part in a BSCCO crystal is the very anisotropic two-dimensional layer of the copper oxide plane (See Fig. 13).

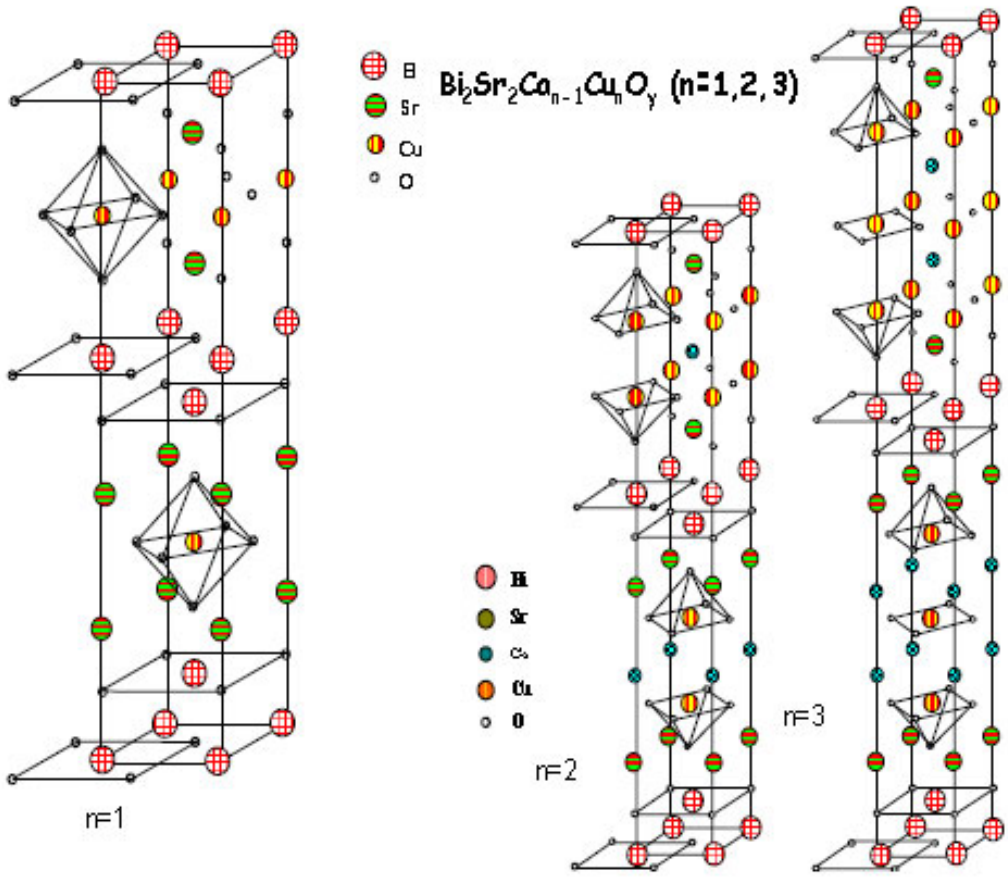

Fig. 13 BSCCO Crystal structure. [35]

BSCCO materials have a big critical magnetic field H_{c2} that can reach 110 T in 77K and a high critical temperature, which can reach more than 100 K. In industry, the most used BSCCO materials are the Bi-2223 filaments and Bi-2212 polycrystalline.

However, Bi-2223 has several phases and it is difficult to obtain pure Bi-2223 (unlike in 2212) because it depends on the oxygen partial pressure. The PIT powder in tube method is the general way to fabricate Bi-2223 tapes. A powder mixture is prepared from Bi_2O_3, PbO, $SrCO_3$, $CaCO_3$ and CuO compounds and then inserted into a silver cylinder. Silver material made the cylinder because it does not chemically react with the bismuth compound and allows the diffusion of oxygen at high temperature. The processing of the tape is done then in a controlled oxygen atmosphere. That's why the silver is used as silver based matrix in Bi2223 tapes (see Figs. 13 and

14). This silver-based matrix as silver-copper or silver-gold improves also the tape mechanical properties and limits the AC losses because of its resistivity. The assembly of the BSCCO tape is fabricated after some industrial processes such as drawing, rolling and heat treatments [36].

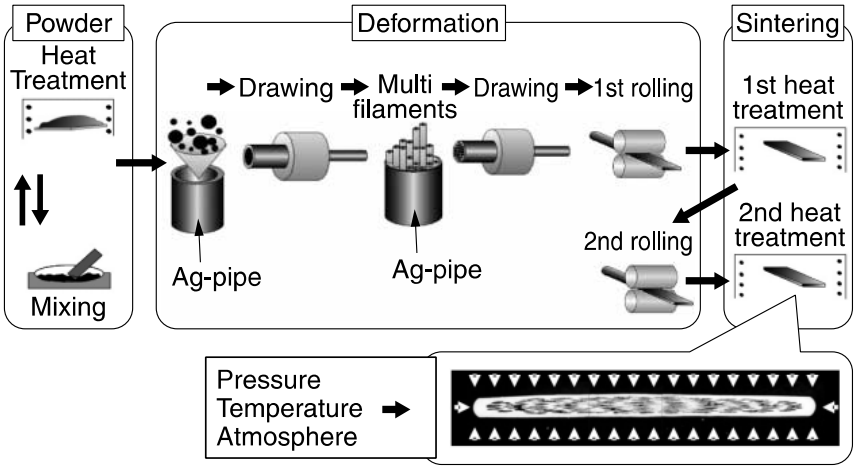

Fig. 14 Manufacturing process of DI-BSCCO (PIT method). [37]

Figure 14 shows the Bi-2223 filaments embedded in the silver-copper matrix. A series of specific thermal treatments (about a hundred hours) under reduced oxygen atmosphere at 840 ° C allows obtaining the final product by reacting the powder of bismuth to form the HTS silver matrix with the two types H and HT used in this thesis. In fact, Sumitomo Electric Industries, Ltd manufacturing specific BSCCO tapes named DI-BSCCO with various features, Type H (High critical current), Type S (Slim), Type HT (High critical current and Tough), Type ST (Slim and Tough) and Type AC (AC use). Type H has the same structure as the conventional high Ic wire with a cross-sectional area of around 1 mm^2 but features dramatically higher Ic. Type S is manufactured at half the raw material cost because its cross-sectional area is a half that of Type H. Type HT and Type ST are the high strength wires made by reinforcing Type H and Type S with metallic tapes such as stainless tapes. They have the same I_c values as Type H and Type S

and show remarkably high mechanical strengths. Type AC has the lowest AC loss among all types of DI-BSCCO and is the most suitable for an AC use. The feature of each type of DI-BSCCO is summarized in Table 2. [37] The symbols used in Table 2 is the double circle for very good, one circle for good, and triangle for medium.

Type of DI-BSCCO	I_c	Permissible tensile stress	Permissible bending diameter	AC loss	Price
Type H	◎	○	△	△	○
Type S	○	△	○	○	◎
Type HT	◎	◎	◎	△	○
Type ST	○	◎	◎	○	◎
Type AC	△	△	○	◎	○

Table 2. Various features of different types of DI-BSCCO. [37]

These processes lead to the production of a rectangular wire having a filamentary structure. Bi-2223 is a ceramic material, which means that the fabrication of a Bi-2223 cable with one filament, as copper ,for example, is difficult. Ceramic materials are also weak and any twist of the Bi-2223 filaments broke it easily. However, by modifying the sheath material from pure silver to silver-alloy and improving the Young's modulus of Bi2223 filaments by raising the density of filaments using the CT-OP sintering process, the maximum permissible tensile stress could be increased to more than 150 MPa.

Bi-2223 tapes have also a large critical current (200 A at 77 K for the BSCCO tapes made by Sumitomo and used in this thesis), and can reach 500A at 20 K. The Bi-2223 tapes are popular for their good pinning properties [38]. However, the high cost of the silver material remain one of the most serious problems to produce BSCCO tapes in large amount, the research of another

material that can substitute the silver is one of the active area in research. A cross section photo of one BSCCO tape used in this thesis is shown in Fig. 15.

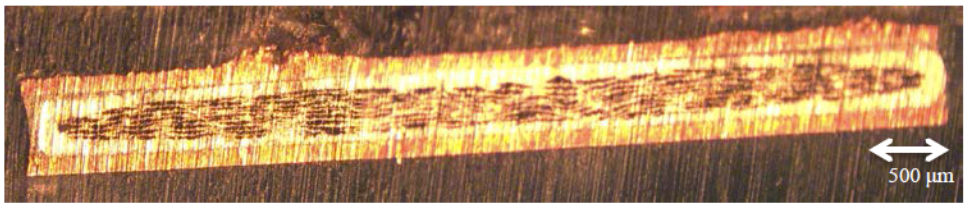

Fig. 15 Cross-section photo of the BSCCO tape (DI-BSCCO, Sumitomo tape).

2.2.2 Properties and manufacturing of YBCO tapes

Georg Bednorz and Karl Müller at IBM in Zurich discovered YBCO materials in 1986. The YBCO crystal is constituted by Yttrium, Barium and Copper Oxide (formula: $YBa_2Cu_3O_{7-y}$) with Perovskite structure as in Fig. 16. YBCO was at that time the first material to be superconducting above 77 K, the boiling point of liquid nitrogen [39].

YBCO materials have many strong advantages among them: a high critical temperature, high current density and strong irreversibility field. However, the silver matrix and the pressure techniques used in BSCCO tapes fabrication couldn't be used in the case of YBCO materials. Because, the silver is permeable to oxygen, but its melting point is lower than YBCO one. Furthermore, the grain orientation of the YBCO crystals in the lattice is not sufficient to enable this HTS tape to carry high currents because the critical current density J_c depended on different grain boundary disorientation. Higher Jc, for the sample texture, is attributed to the improvement of the grain orientations [40].

That's why, a new HTS tapes using YBCO materials, called second-generation HTS tapes (as AMSC tape with I_c =500 A, used in this thesis and shown in Fig. 17, 18), have been developed. This YBCO tapes called coated conductors are laminated with different layers as: Buffer layers,

Shunt, Copper stabilizer etc. which every layer has a different role and the current is mainly transported by the YBCO layer.

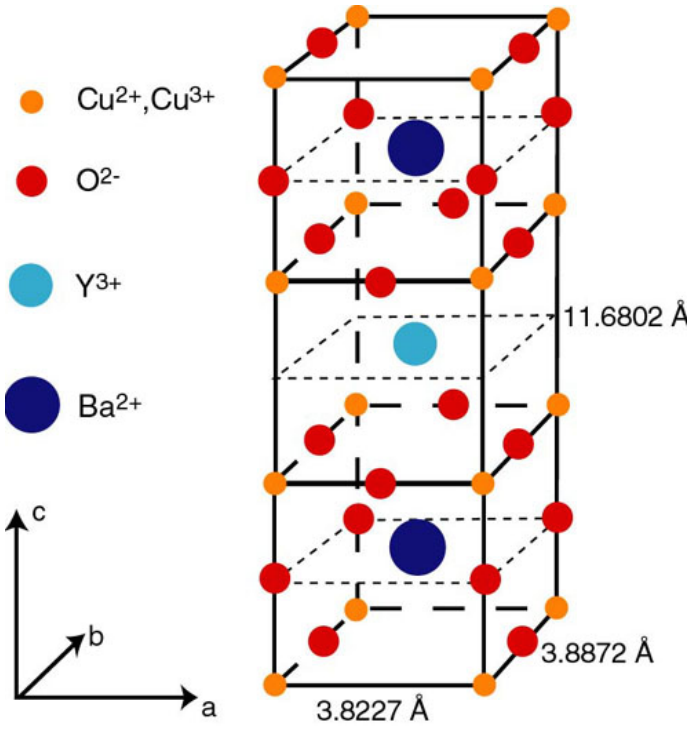

Fig. 16 YBCO Cristal structure. [41]

The fabrication process of these coated conductors differs from one company to another. But they typically have common shapes with a width of several millimetres and a thickness of hundreds of micrometres. Largely used fabrication process employs ion-beam assisted deposition (IBAD) for orienting MgO as buffer layers [42]. Fujikura Ltd. developed first this process in Japan. Another fabrication process of superconducting layers developed by Fujikura Ltd. is a process named pulsed-laser-deposition (PLD) as a method for depositing YBCO superconducting layer [43-44].

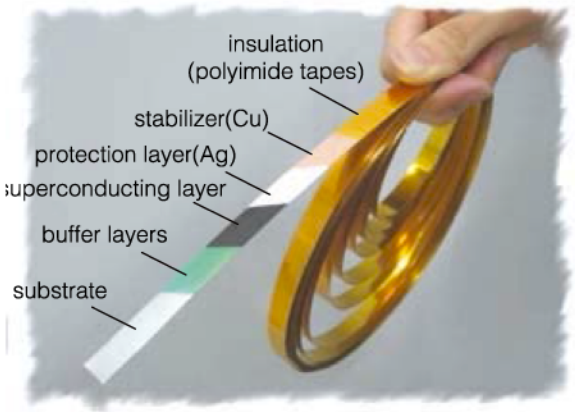

Fig. 17 Photo of the Fujikura HTS tape's general structure. [45]

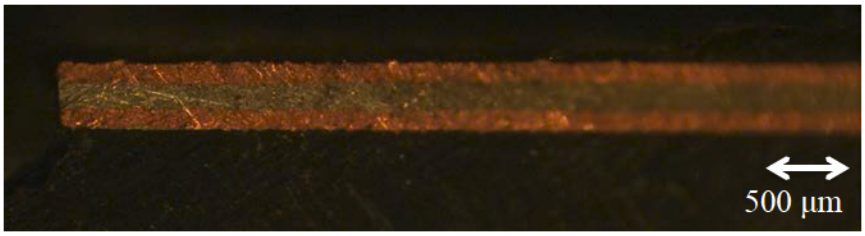

Fig. 18 Cross-section photo of the YBCO AMSC tape.

Another issue on YBCO tapes is the difficulty of obtaining a homogeneous critical current for tapes longer than hundred of meters. The distribution profiles of the critical current of the YBCO tapes show that, even if the current can be relatively homogeneous if the tape's length is several centimetres, it is difficult to obtain a homogeneous current for hundreds of meters of YBCO tapes. Fig, 19 show the longitudinal Ic distribution of Fujikura YBCO tapes used in this thesis. The Fujikura tape's length is longer than 600 m and we can see that the current distribution is not constant for this distance especially for the wire A. The standard deviation (StD) of the wire A, for example, is for 14.7(A/cm) and the Average I_c ($\overline{I_c}$) is 649 A/cm. The uniformity of this YBCO tape equal to $\frac{StD}{\overline{I_c}} \times 100$ is 2.2%. This inhomogeneity can be problematic for reliable superconducting magnets and other YBCO tape's applications. [45]

Fig. 19 Longitudinal Ic distribution of YBCO (Fujikura) tape. [45]

2.3 Current density distribution in BSCCO and YBCO tapes

The knowledge of the current distribution in BSCCO and YBCO tapes is important also to understand their conductive properties, such as the dynamic distribution of the current in the HTS tape, the over-current effect, the remnant current homogeneity, etc.

The calculation of the one-dimensional (1D) and two-dimensional (2D) current density distribution in HTS tapes can be used then to study the HTS tape's homogeneity and control process quality because it will allow the localization of faults in the HTS samples.

For the current density calculation, we relate the self-magnetic field to the current density J by the Biot-Savart law in which for a surface current is given by $B(r) = \frac{\mu_0}{4\pi} \int \frac{[J \times R]}{R^3} dS$, where dS points normal to the surface and R separate an elementary electric charge to the magnetic field position.

The YBCO tapes used in this thesis are commercial tapes. Their thicknesses are between 10 and 12 mm. The thickness of the superconductor layer of these HTS tapes is around 0.1 μm. The

model of thin films works then well with YBCO tapes. We can apply the Biot-Savart law for one or two-dimensional current density distribution in thin films cited above.

For the BSCCO tapes, used also in this thesis, some other facts should be considered before applying the Biot-Savart law to study their current densities. In fact, BSCCO tapes are a filamentary HTS tapes. Superconductor filaments are twisted and packed in a normal metal matrix having a low resistivity at a low temperature (usually copper-silver matrix).

The filamentary structure is used to eliminate instabilities in the superconductor. The twist of the filaments is introduced to reduce magnetic field coupling effect between filaments, and the matrix is used to shunt filaments current when the BSCCO tape is at the normal state. The matrix plays then a role in stabilizing. The used commercial BSCCO has as width 4.5 mm; the thickness is 0.35 mm including the stabilizer's thickness, which is 0.1 mm. If we consider these different phenomena producing in the filamentary HTS tapes for the current density analyse, the model of two-dimensional current distribution will be also acceptable for BSCCO tapes.

2.4 Summary

HTS tapes are nowadays the main part of different technology especially electric power devices, motors and magnets using commonly copper and aluminium wires. HTS tapes represent a progress to produce and transport energy. However, more development of their structure for more efficiency and strength is necessary.

BSCCO and YBCO are the main two kinds of HTS tapes commercially produced for the majority of big companies such as Sumitomo, Fujikura, AMSC, and SWCC etc. In this chapter, we described briefly the properties of this two kind of HTS tapes. The use of these HTS tapes in superconductor cables requires the study of the current density distribution in these tapes on different conditions of current feeding that a DC power grid can front.

The investigation of the current density distribution in HTS tapes is necessary also to understand its characteristics including homogeneity, self-magnetic field properties, and the effect of normal and over currents on the distribution of the current in direct and permanent phases. We discussed in this chapter some of the methods to measure the self-magnetic field profiles of the HTS tapes, especially contactless methods.

CHAPTER 3: SUPERCONDUCTOR TAPES IN POWER CABLES

3.1 Introduction

Electric cables (Copper or aluminium cables, superconducting power cables etc.) are nowadays an essential part in the energy transportation for short or long distance. Almost all technologies and industries need electric cables to transport energy from one point to another. Therefore, electric cables become an essential part of human life. The DC superconducting power transmission lines were developed last decades in many countries worldwide including Europe, America and Japan. In the same period, several international projects also developed AC superconducting power transmission lines. Both AC and DC superconducting power transmission lines were thought then to construct a smart worldwide grid. We think that DC power transmission lines are good for such smart grids because of its advantages compare to AC superconducting power cables and its ability to be extended to thousands of kilometres, and because of many other benefits.

3.2 Normal electric cables

Electric cables have an essential function to conduct electricity from one point to another. They represent the active elements of the electrical connections. However, they should be characterized by a very low resistivity to limit losses and should be properly insulated.

Electric conductors and cables are then varied and depend on materials, with which we fabricate cables, and some other parameters such as electric resistance, size, voltage, weight, mechanical strength, capacitance, and inductance. We give in table 3 some of the characteristics of normal electric cables made by SWCC [46].

Cross section of the conductor	Outer Diameter of the conductor	Thickness of the insulator	Thickness of the shielding copper	Thickness of the sheath
60	9.3	5.0	0.1	2.1
100	12.0	=	=	2.2
150	14.7	=	=	2.3
200	17.0	=	=	2.4
250	19.0	=	=	2.5
325	21.7	=	=	2.6
400	24.1	=	=	2.7
500	26.9	=	=	2.8
600	29.5	=	=	2.9
800	34.0	=	=	3.2
1000	38.0	=	=	3.3
1200	41.7	=	=	3.5
1400	45.0	=	=	3.6

Table 3. SWCC copper cable geometry. [46]

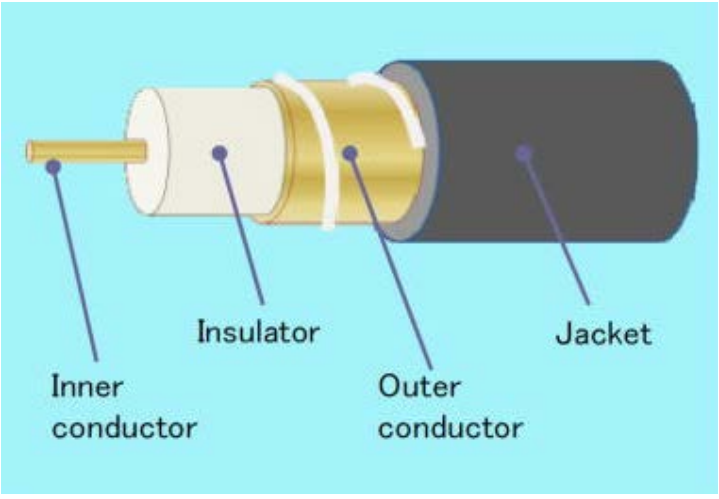

Fig. 20 copper cable's structure. [47]

We find in one electric cable different parts such as conductor material, sheath and insulation as shown in table 3 and Fig. 19. Depending on the applications we distinguish a diversity of cables, which can be unipolar or multipolar cables used for low or high-frequency transmission and for AC or DC current. In table 3 we show general information about the size and the geometry of the copper cable. In table 4, we give some physical characteristic of the electric cable such as resistance, voltage and capacitance. These characteristics are very important to choose which cable is more adaptable for the electric applications.

Outer Diameter of the cable	Weight per length [Kg/km]	Max electric DC resistance @ 20° C	Tested Voltage insulation	Mini insulation resistance	Max Capacitance of cable per length [µF/km]
25	1.050	0.305	26	2,500	0.29
28	1.500	0.183	=	2,000	0.35
31	2.050	0.133	=	=	0.40
33	2.600	0.0915	=	1,500	0.45
36	3.100	0.0739	=	=	0.49
38	3.900	0.0568	=	=	0.54
41	4.650	0.0462	=	=	0.59
44	5.700	0.0369	=	1,000	0.65
47	6.870	0.0308	=	900	0.74
54	9.200	0.0231	=	800	0.85
58	11.000	0.0187	=	700	0.94
62	13.100	0.0156	=	=	1.01
66	15.000	0.0133	=	=	1.08

Table 4. SWCC copper cable characteristics. [46]

In the other hand, direct current or DC and the alternative current or AC are the main two kinds of currents used in energy transportation. DC and AC current advantages depend on where we use each kind of current.

The direct current is an electric current in which electrons circulate continuously in the same direction, means from the negative to the positive pole. Its propagation is at the speed of light. All circuit powered by a battery or generator works with direct current.

However, in alternative current the electrons flow alternatively in both directions of the circuit. The rotation of an alternator generates a movement of the electrons that produces the alternative current. In this case, the movement of electrons is limited to a few thousandths of a millimetre. The alternating current is measured by its frequency (in hertz).

In Japan, for example, the frequency is 50 Hz in Tokyo, because it has been using alternating current devices imported from Germany in the 19^{th} century and they worked on 50 Hz. which means that electron makes 50 trips per second. However, In Osaka, for example, frequency is 60 Hz, because generators are imported from the United States and worked with 60 Hz.

If the intensity of the current is limited which is the major case in electric cable applications, AC cables are the most used. In this case, the heat loss is lower in the AC electric cables than those in DC electric cables. That's why; alternating current is used mainly in the distribution of electricity.

However, DC electric cables are preferred, if the electric power is transported for long distances by buried cables or underwater cables. We call this the retroactive power.

Another advantage of the DC electric cables is the fact that we need in this case two cables while three cables are required for AC cables, which has an impact on the cost. We will see in this thesis that these advantages are also available for DC superconducting power cables.

3.3 Superconducting power cables

3.3.1 Conventional Superconducting power cables

Low-temperature superconducting materials as (NbTi) are now used to construct cables called conventional superconducting cables. These cables are used in advanced physics and in the development of high magnetic field coils. These coils are used in many applications and projects such as the Large Hadron Collider accelerator made by the European Organization for Nuclear Research (CERN) in Europe and the magnetic resonance imaging (MRI), which is the main industrial application for the superconducting magnets. All these applications require a low temperature that can be provided only by liquid helium a provided from industry. In CERN Large Hadron Collider the magnets are connected to the current feeding by the superconducting cables. The cables house 36 strands of superconducting wire and each strand being exactly 0.825 mm in diameter. Each strand houses 6300 superconducting filaments of Niobium-titanium (NbTi). Each filament is about 0.006 mm thick, i.e. 10 times thinner than a normal human hair and round each filament there is a 0.0005 mm layer of high-purity copper. Based on physical measurements it is a Rutherford cable. Copper is an insulation material between the filaments in the superconductive state when the temperature is below -263 C. When leaving the superconductive state, copper acts as a conductor transferring the electric current and the heat. [48]

NbTi and Nb3Sn are two main low-temperature superconductor materials commonly used in the industrial production of conventional superconducting power cables because of their superconducting properties and ability to be shaped. NbTi has good superconducting properties (T_c = 9 K, H_{c2} = 12 T) and also very good mechanical properties. It has the best characteristics of superconducting metal alloys (T_c = 18.3 K, H_{c2} = 23 T), but not good mechanical properties and

used only over 8 T. We show in Fig. 21 an example of NbTi conventional power cable. [49]

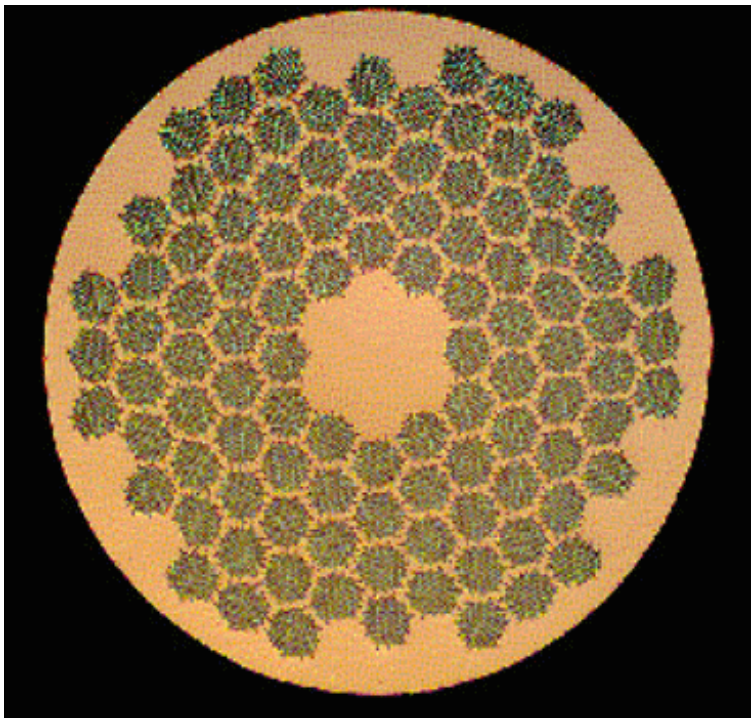

Fig. 21 Superconductor cable made by NbTi material [48].

Because of their capability to carry high currents, superconducting magnets are good devices for magnetic resonance imaging than normal magnets.

Another major contribution of superconducting coils is MAGLEV trains. In fact in these trains, called also magnetic levitation trains, NbTi superconducting magnets shown in Fig. 22 are used.

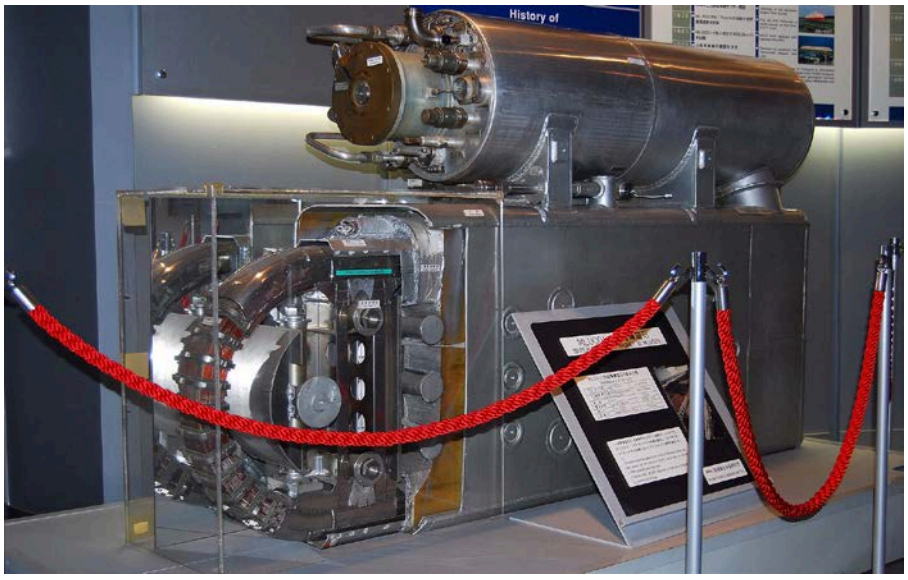

Fig. 22 Superconducting magnets used for Maglev trains. [50]

3.3.2 High temperature superconducting power cables

Importance of the DC superconductor power cables

HTS tapes have been developed in industry to transport large currents. Its development leads to the construction of new electric cables using these high-temperature-superconducting tapes called superconducting power cables. Cryogenic technology is also now well developed which provides a remarkable help to make future power cable grid possible and will be discussed in the next chapter. However, the HTS tapes used in the superconductor power cables cannot do many conventional operations. They are a special material and their properties are different than copper or aluminium commonly used in normal electric cables. The development of the electrical and mechanical properties of the HTS tapes and then the superconductor power cables becomes a major challenge. The demand for electrical energy is the day after day increasing, that's the reason why some power lines and electrical network projects must increase more and more the amplitude of the transported energy. For these reasons, superconducting power cables represent a

serious solution to these effects. Power cables can carry currents up to five times more than normal cables (aluminium or copper). In cities where the power consumption is steadily increasing, it will be possible in near future to transport much more current than those transported by normal cables. Sahara Solar Breeder project is a good example of this future challenge then. The second big advantage for the superconductor power cables is the fact that they have almost zero resistance and especially DC superconductor power cables. Heat losses produced by normal cables can be then avoided.

Advantages of DC superconductor power cables comparing to AC power cables

DC superconducting power transmission (DCSC-PT) line is proposed for the next generation power transmission system. Because the resistance is almost zero for DC system completely, DCSC-PT will be able to use a low voltage system in order to reduce the cost of the inverter, and it will be planed from 10 to 30 kV. Instead of the low voltage, the magnitude of the current is high as 10 kA to 30kA. The high current system can store high magnetic energy in the transmission line like the superconducting magnetic energy storage system. In the other hand, one of the key issues of the AC applications is to reduce the AC losses of the HTS tape conductor, and if the AC losses will be reduced enough to the practical level, the AC applications will have large markets. In this sense, the DC superconducting system has lots of benefits for power applications because no AC loss in DCSC-PT.

In point of view of the geometry of cables, AC cables are composed of two layers. One inner layer is used to carry the electric current and the other layer is used to shield the magnetic field produced by the inner layer current in order to reduce the eddy current loss of the cryogenic pipe. Two layers are insulated each other because the magnetic shielding layer is connected into. Therefore, an AC cable is used for the DC transmission cable because there are the insulated two

layers. Three-phase AC system needs then three cables and DC system need only one cable to transmit the power. In this sense, the cost of the DC cable is cheaper than that of AC cables.

Moreover, since the DC cable is free from AC losses the short-circuit current of AC cables is quite higher than that of DC system, and the rated current in DC cables is almost twice of those of AC cables.

Another important advantage of the DC superconducting cables is related to cryogenic engineering. In fact, the diameter of the inner pipe of the cryogenic pipe for the DC cable is smaller than those of AC cables, because the same-size three cables must be installed into the inner pipe for AC's. The cost of the inner pipe of DC cable is cheaper and the heat leakage to the inner pipe is lower. The pressure of the liquid nitrogen flow is lower for DC cable system because in AC cable the three-cables are twisted and the performance is higher in the case of DC cables independently from the performance of the HTS tapes.

DC power cable constructed in Chubu University

In 2010 in Chubu University, Japan, a 200 m superconducting power cable has been constructed successfully for DC transmission (named CASER-2 and shown in Fig. 23) [51]. The length of the cable could contract about 60 cm by the change from 300 K to 70 K. To manage the thermal contraction and expansion, the cable ends are not fixed at the terminals and can move with respect to the terminals. This thermal expansion, was proved to be partly composed by the movement of the cable, was confirmed by feeding the rated current of the cable.

CASER-2 DC power cable is a coaxial power cable composed of two superconducting conductors of DI-BSCCO tapes spirally surrounding a copper former as in Fig. 24. The tapes are arranged closely to make the magnetic field lines surrounding the cable uniformly. The number of tapes in each conductor is different because of their different radii. [52, 53]

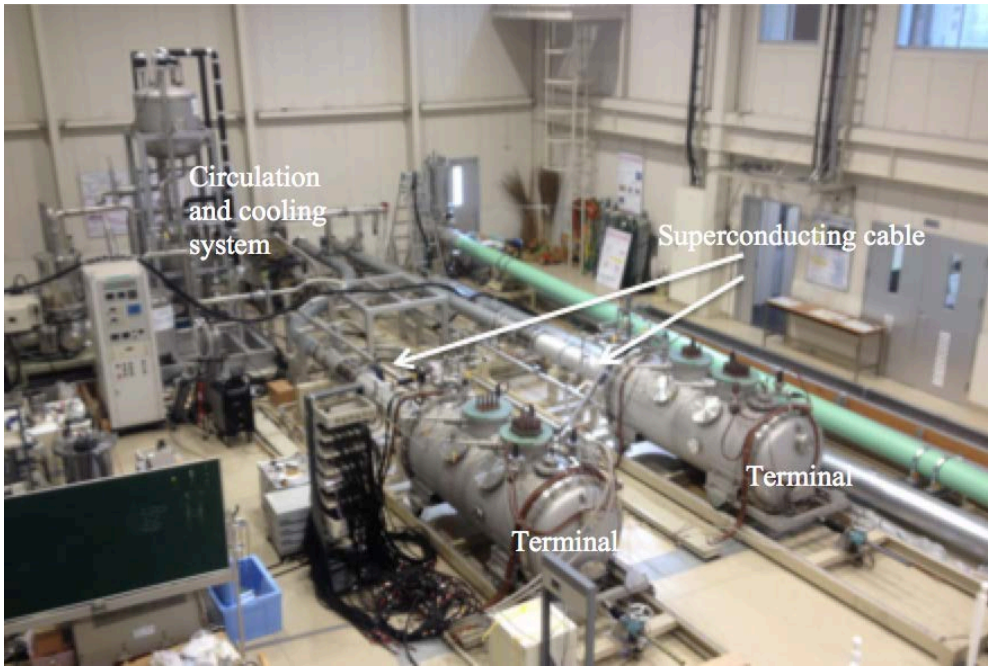

Fig. 23 Power cable facilities, (Chubu University, Japan).

The HTS cable is installed into a vacuum insulated cryogenic pipe and operated at about 77 K by the circulation of the liquid nitrogen. A measurement system composed of 600 channels was developed to monitor the system and to collect sufficient information for the evaluation of the test facility performance. In fact, the data recorded including the temperature, pressure, level and flow rate of liquid nitrogen cooling, loading current, voltage and temperature of the conductors and pressure of the vacuum. In the cable, there are 23 tapes for the inner conductor and 16 tapes for the outer conductor, as shown in Fig. 24. Since the current of one HTS tape is limited, numerous tapes were utilized and arranged in the multi-layer structure, improved the performance of the power cable. [53]

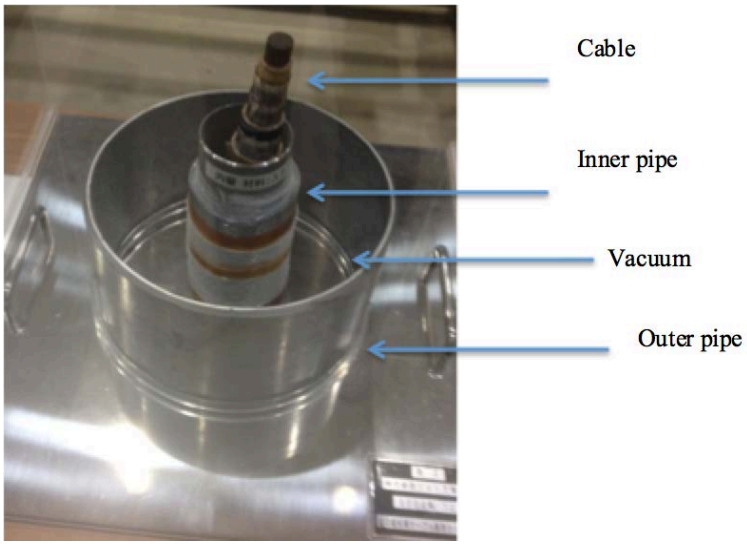

Fig. 24 DC power cable structure (Chubu University power cable).

3.4 Summary

Superconducting power cables nowadays are considered among one of the most important application of HTS tapes. We presented in this chapter some specifications of normal and superconductor power cables. We discussed also the importance of the DC power cables and its advantages comparing to AC ones. We showed finally the DC superconducting power cable and some of its facilities constructed at Chubu University.

CHAPTER 4. CRYOGENIC ENGINEERING

4.1 Introduction

The study of the current distribution in HTS tapes and the effect of the DC current feeding operations on this distribution are important best running and maintenance of the DC power transmission lines. However, the cryogenic engineering for superconducting power cable and HTS tapes is also important. We should then focus on the cryogenic engineering and pay an effort to achieve high-performance cryogenic systems. In this chapter, we will present some important features of the cryogenic engineering applied to superconducting power cables and its rule for high current stability, reliable security and protection. Different parts of the cryogenic engineering study in this chapter are based on the cryogenic techniques used in superconductor DC power transmission line (CASER-2) constructed in Chubu University, which was described in the previous chapter of this thesis.

4.2 Liquid nitrogen cooling system for the HTS power cable

As we discussed previously, HTS tapes are a high-temperature superconductor materials that their critical temperature exceeds 77 K, which is the temperature of the liquid nitrogen (LN_2). For that reason, LN2 is used commonly in superconductor power cables to cool down the HTS tapes leading to transport current almost 5 to 10 times the rated current for normal copper cables with similar geometry. LN2 must circulate inside the cropping of power cables. And for that reason, pumps are used. For the LN2 circulation inside the cable, many system configurations have been analysed including the thermal siphon with a counter-flow circulation loop composed of a cryogen flow channel and an inner cable channel proposed by Prof. S. Yamaguchi and shown in Fig. 25. [54]

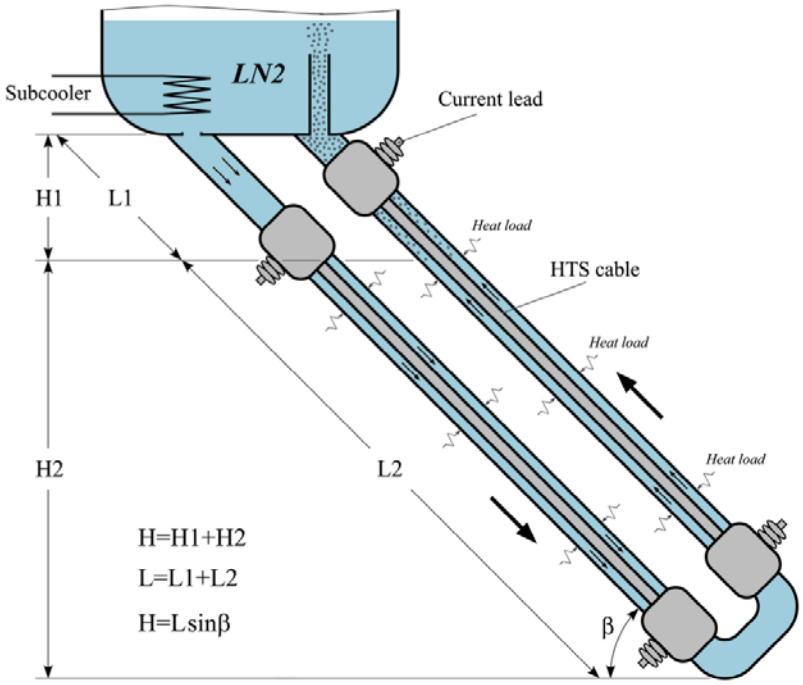

Fig. 25 HTS cable cooling system [54].

The system is comprised of a liquid coolant reservoir placed at the top of the circuit, and two channels, connected at its bottom. It is required that the vaporization happens only in the second channel, significantly reducing the average density of the two-phase fluid.

The reservoir at the top of the thermal siphon has to contain the coolant at the atmospheric pressure p_0 = 1 atm = 0.1013 MPa. Assuming LN2 for the coolant the boiling temperature at the inlet is T_0 = 77.35 K. The temperature in the first line must be below the boiling temperature to prevent the formation of the two-phase flow. The pressure and the boiling temperature grow as we move down along the first channel, and all that we need is a sufficiently low heat load to prevent temperature rise from exceeding the boiling temperature as a function of local pressure. The hydraulic head above it and the flow friction in the first line define the pressure at the bottom point of the thermal siphon. There is no boiling here, and the flow goes up the hill absorbing the heat load due to the thermal capacity of the coolant at a rate defined by its mass

flow. At some point, the temperature and the pressure of LN2 reach the boiling. That is where the two-phase flow begins. Above this point, the heat load is absorbed by the heat capacity of the liquid coolant, and its heat of vaporization. The temperature of the gas-liquid mixture is the boiling temperature of the coolant at the local pressure. The flow returns the coolant into the atmospheric pressure reservoir at the top of the line. Nitrogen vapour is vented to the atmosphere, while the liquid is returned to the inlet of the cooling circuit [54].

4.3 Cryogenic pipe for DC power transmission

The high performance of the superconducting power cable needs good and sophisticated pipes. In fact, many losses of energy in DC-SCPT can be related to many reasons such as heat radiations and heat leak, which can affect the liquid nitrogen and the HTS tapes inside the cryogenic pipes. Pipe systems with various lengths should be constructed then in order to avoid such losses. In the AC superconducting power transmission lines, it exists also the AC losses but they are avoided in DC-SPT, and that's why we will focus in this section on the characteristics of the pipes used in this power transmission method.

Generally, the pipes in the DC-SCPT are constructed with outer and inner pipes as shown in Fig. 26. The space between the outer pipe and the inner pipe is in vacuum for the thermal isolation. The superconducting power cable of 40 mm in diameter is installed inside the inner pipe. As the cryogen, liquid nitrogen (LN_2) flows through both the outside and the inside of the superconducting power cable in the same direction. The heat influx from the outer pipe to the inner pipe is aimed to be 1 W/m. To reduce the heat influx by radiation from the room temperatures side a multilayer insulator is generally used in these pipes, which is a multilayer of thin polyethylene foils with aluminium-coated surfaces [55].

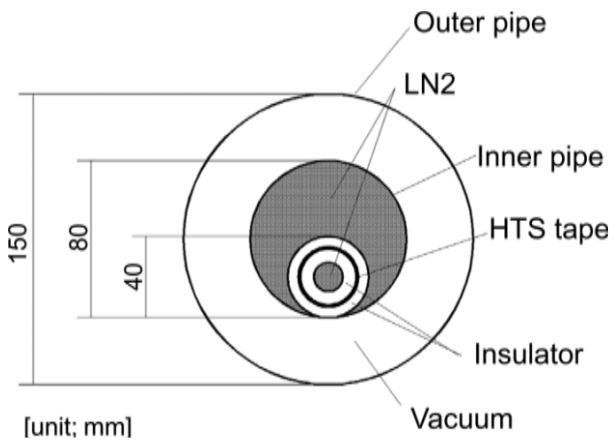

Fig. 26 Cross-section of the DC superconducting power transmission line. [55]

4.4 Refrigeration features

For the stable LN2 circulation in the pipes, a system of pumping is commonly used in the DC-SCPT lines. We will give in this section some details about the refrigeration system used in the CASER-2. Two LN2 tanks are used and their vertical drop is 2 m. The capacity of the tank is 200 L for each. The pressure difference between two tanks can circulate the LN2 along the design values the flow rate. The flow rate reaches 5 L/min to 15 L/min by the control of the valve experimentally. After cooling down is started, the cable will contract with the temperature decreases. The thermal contraction ratio ~0.3 per cent and the contraction length is 60 cm for the 200 m cable [55].

4.5 Summary

Even the main subject of this thesis is to study the current distribution of the current density in the HTS tapes after different DC current feeding operations. We think that the cryogenic engineering and techniques applied on the HTS tapes and the DC superconducting power transmission lines are very important to be discussed briefly.

CHAPTER 5. MEASUREMENT EXPERIMENT AND RESULTS

5.1 Introduction

The development of the power transmission lines based on long-length HTS tapes requires the high production quality of these tapes. High-Temperature superconductor tapes with high homogeneity along their lengths are required on superconducting devices, and power cables. On the other hand, a serious damage can happen to the power cable manufactured from the high temperature superconducting (HTS) tapes due to overcurrent conditions or because of technical errors during the cable assembling. To avoid the cable damage in any urgent case, a quick interruption of the transport current is necessary. Comprehensive understanding of the permanent current and the effect of the over-current pulses on current density in HTS tapes are required to restart the operation of power transmission lines and to estimate the uniformity of the HTS tape along the longitudinal direction, which is also very important for many other applications of HTS cables. In this chapter, we present the experiment set-up to simulate the normal and the over-current pulse operations to study the current feeding effect on the self-magnetic field and the current-density distribution in BSCCO and YBCO tapes.

5.2 HTS tapes used in this thesis

In this thesis two kinds of HTS tapes are used, which are one BSCCO tape that is a filamentary HTS tape and four YBCO tapes that are a coated tapes, made by four different companies. Sumitomo, SWCC, Fujikura and AMSC consecutively make these tapes [45], [56 - 58]. The table 5 below summarizes their different characteristics. The HTS tapes were chosen with different structure and critical currents to make a comparison of the behaviour of each tape with different current feeding operation including normal and over-current conditions. The HTS

tapes were chosen also with different layer structure; including the existence of stabilizer layer or not and different dimensions (width and thickness).

Table 5. HTS tapes characteristics.

HTS tapes	BSCCO [56] (SUMITOMO)	YBCO [57] (SWCC)	YBCO [58] (AMSC)	YBCO [45] (Fujikura, tape1)	YBCO [45] (Fujikura, tape 2)
Critical current @77K	200 A	160 A	300 A	572 A	572 A
Width	4.5 mm	5 mm	12 mm	10 mm	10 mm
Tape thickness	0.35 mm	~ 0.12 mm	~ 0.2 mm	~ 0.2 mm	~ 0.1 mm
Architecture	Two Cu reinforced alloys (50 μm)	Ag stabilizer layer (~15 μm)	Two Cu stabilizer strips (~50 μm)	Cu stabilizer layer (100 μm)	-
	BSCCO filaments (10 μm x 250 μm)	YBCO HTS layer (~ 1.5 μm)	Ag layer (~3 μm)	Ag layer (8.2 μm)	Ag layer (8.2 μm)
	Ag matrix (0.25 mm)		YBCO HTS layer (~ 0.8 μm)	GdBaCuO HTS layer (1.8 μm)	GdBaCuO HTS layer (1.8 μm)
				Tin (2 μm ~ 4 μm)	Tin (2 μm ~ 4 μm)
		Buffer layer: [GZO, etc.] (~ 1.4 μm)	Buffer layer: [Y_2O_3, etc.] (~ 1.4 μm)	Buffer layer: [MgO, etc.] (~ 0.6 μm)	Buffer layer: [MgO, etc.] (~ 0.6 μm)
		Hastelloy texture (100 μm)	NiW (5 at.%) texture (75 μm ~ 100 μm)	Hastelloy texture (75 μm)	Hastelloy texture (75 μm)
Processing of HTS	Powder in tube	TFA-MOD	MOD	*PLD*	*PLD*

5.3 Experimental device

Our experimental device is constituted by an open cryostat on which different devices are mounted: the scanning system, Hall probe, HTS tape and an FRP (fibre reinforced plastic) plate. See Fig. 27.

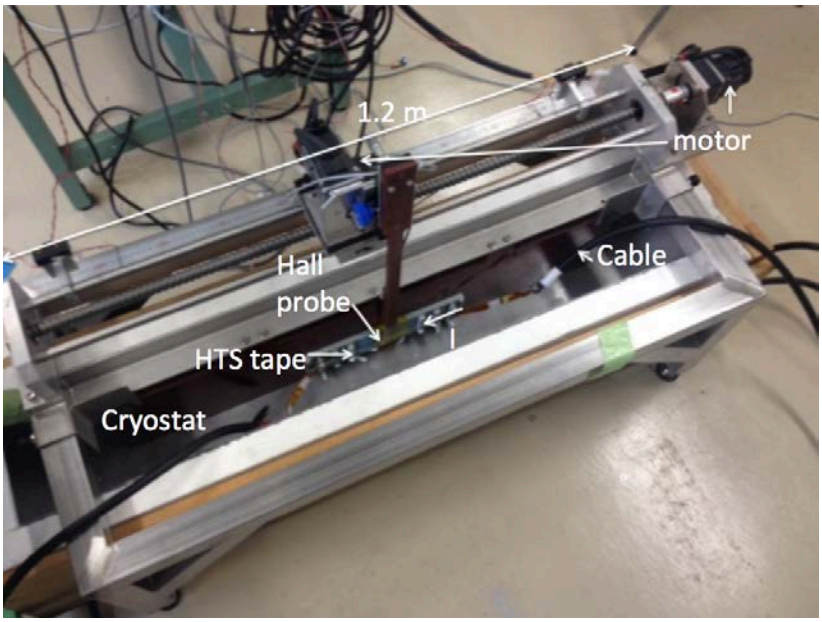

Fig. 27 Experiment setup.

We fixed the HTS tape that we will measure its self-magnetic field on the plate by Kapton tapes and small FRP plastics as in Fig. 28.

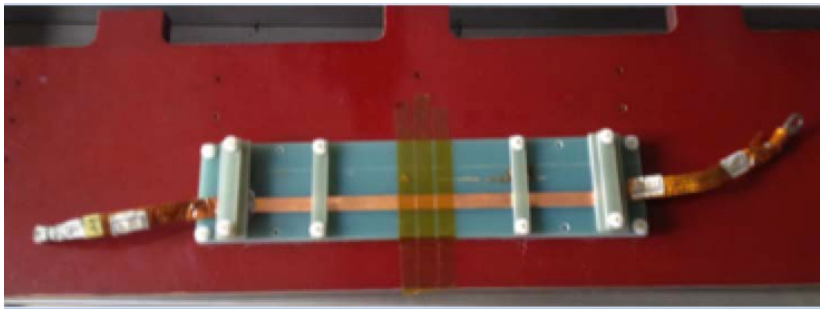

Fig. 28 HTS tape fixed on the FRP plate.

The FRP plate is then put in the cryostat. The configuration of the experiment axis is chosen as follow: The X- axis is within the HTS tape's length, and it is also the direction of the applied current. The Y-axis is within the HTS tape's width and the Z-axis is perpendicular to the HTS tape's surface as in Fig. 29. Two rulers are fixed near the Y-axis motor to check the Y position of the Hall probe sensor (Hall probe characteristics will be discussed in section 5.5) and another ruler fixed on the cryostat to read the X position of the Hall probe sensor.

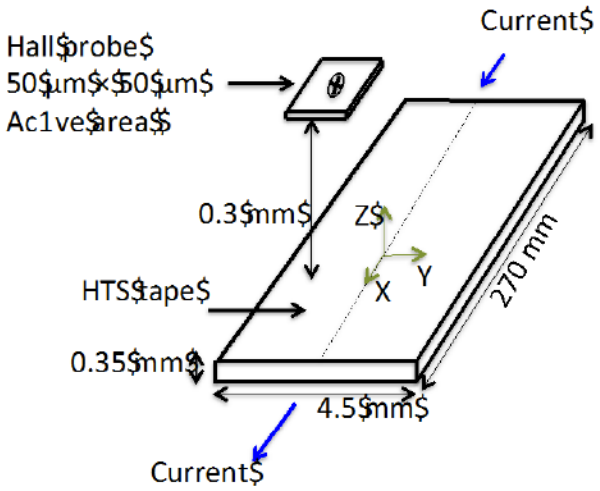

Fig. 29 Configuration to measure the magnetic field.

We fix the Hall probe supporter with the Y-axis motor. This motor is a brushless DC motor made by ORIENTAL MOTOR LTD and its steps are controlled via a Labview (Fig. 30). In this thesis, we used a 0.05 mm and 0.1 mm as steps length.

The Y positions are directly read from the Y-axis ruler and the position Y = 0 corresponds to the Hall probe at the bottom of the cryostat. The FRP plate is situated between Y=70 and Y= 100.

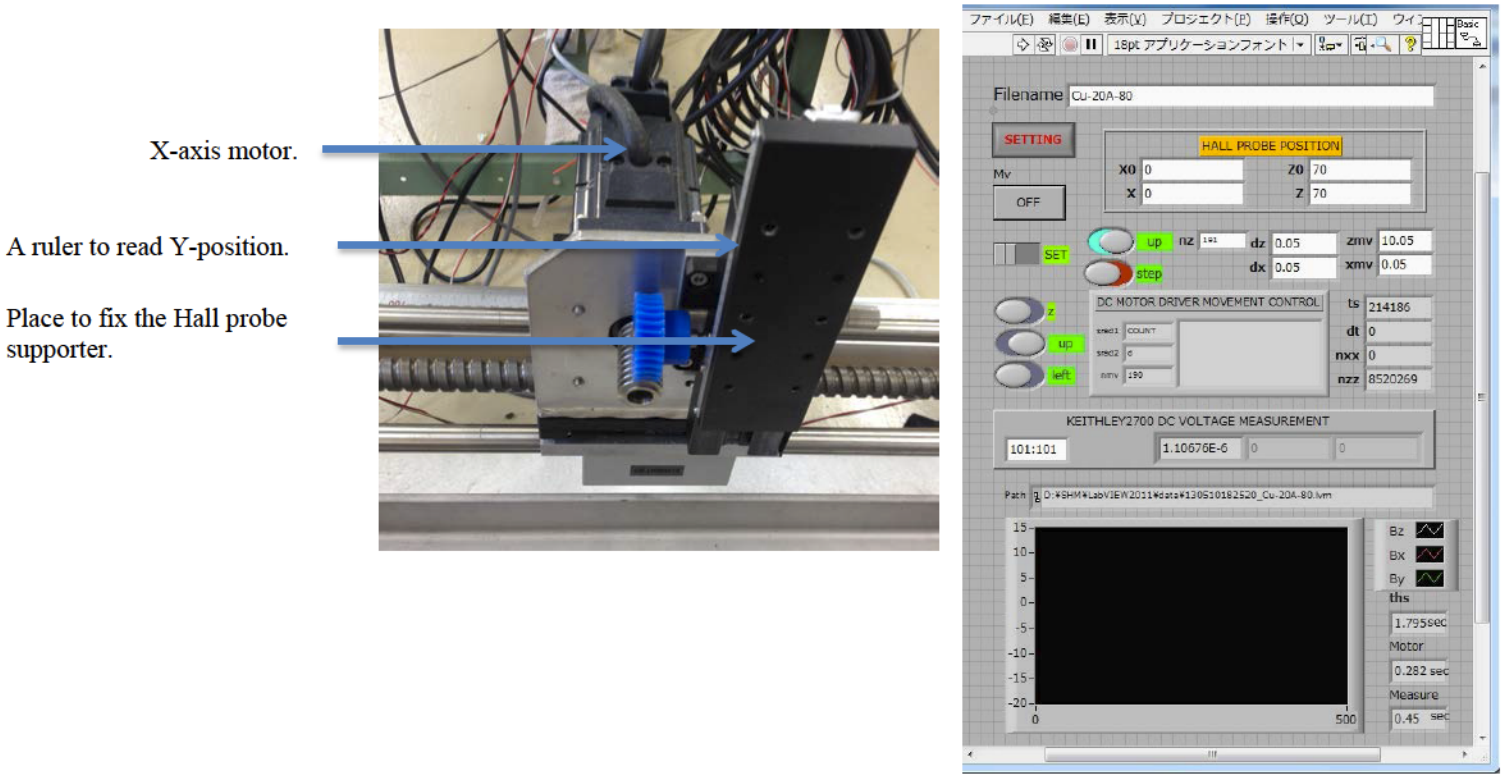

Fig. 30 Y-axis motors and Labview program.

The Hall probe attached to the end of the Hall probe plate will be above the tape surface. The distance between the Hall probe sensor and the HTS tape's surface is adjusted manually and we fix this altitude at 0.3 mm for all experiments, because at smaller altitudes (inferior to 0.3mm) the accuracy becomes larger and the altitude of the Hall probe would be difficult to keep it fix.

The Hall probe supporter (Fig. 32, 33) fixed with the Y-axis motor can move within the X-axis via a step X-axis motor (Fig. 31) with same characteristics of the Y-axis motor. We can change with this system then the X position of the Hall probe supporter means the Hall probe X position. The same Labview program also controls the Y-axis step motor.

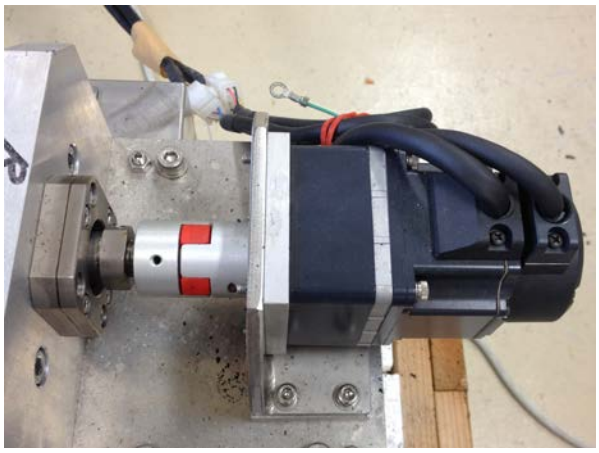

Fig. 31 X-axis step motor.

The Hall probe moves above the tape's surface by the stepping motors system and its current is set to be 10 mA. It is connected also to a Keithly data acquisition system with one data/second as data sampling to measure the voltage gave by the Hall probe sensor (see Fig. 34). In this thesis we use two Hall probes; the first one is 1D hall probe that measures only the perpendicular component of the magnetic field. We used this Hall probe for the calculation of the one-dimensional current density distribution. The second one is a 3D Hall probe, shown in Fig. 29, that measures the three perpendicular components of the magnetic field profiles.

Fig. 32 Plate of the 1D Hall probe sensor.

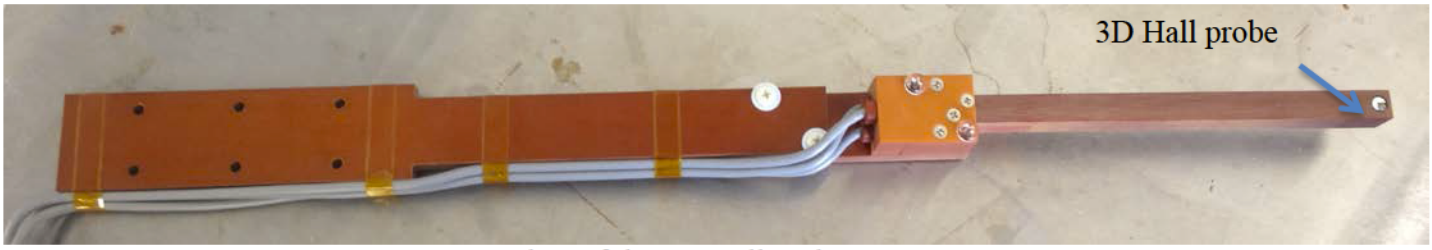

Fig. 33 Plate of the 3D Hall probe sensor.

Fig. 34 Hall probe current source (up) and Keithly instrument (down).

After fixing the HTS tape and the Hall probe supporter in the cryostat we fill it with liquid nitrogen (LN2) to cover the HTS tape. The level of the LN2 is kept fix along the experiment and its level is adjusted manually by filling the cryostat, with LN2 liquid during the experiment. The HTS tape is connected to DC current via copper connectors (Fig. 28). To simulate different DC current feed scenarios we used in this thesis a DC current power supply (DCPS) which has its own switch and current controller, shown in Fig. 37. The maximum current of DCPS is 100 A. DCSP is connected to a shunt resistor and current transducer (CT) to measure the current and

show it in a voltmeter (Fig. 36). A mechanical switch is connected to the circuit, and it is a no-fuse-breaker (NFB). The electric circuit of the experiment is shown in Fig. 35.

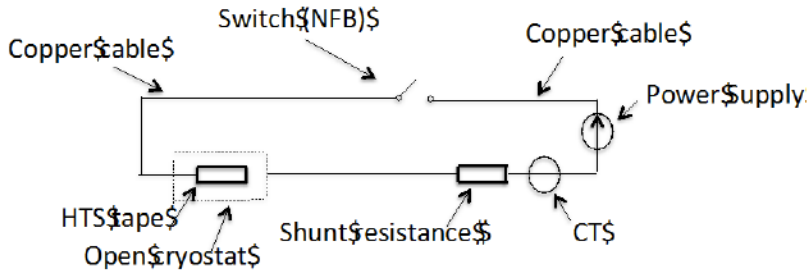

Fig. 35 The electric circuit used in the experiment.

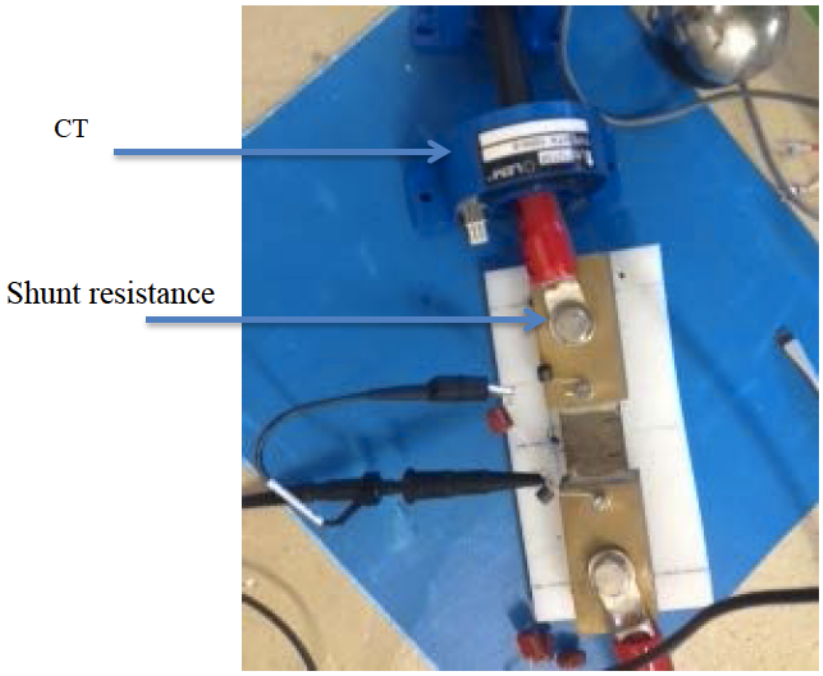

Fig. 36 Image of CT and shunt resistance.

Fig. 37 DC current power supply.

5.4 Set-up for DC current feed operations

For the direct DC current operation, we simulate to scenarios. In fact, our electric circuit provides two current feed operations, which are called normal and over-current pulse operations.

- The over-current pulse operation simulates the fault current condition. At first, the NFB is open. The DCSP is set to 100 A where its voltage is maximum at 10 V by the power supply controller. When the NFB is switched on, and because the low resistivity of the HTS tape, an overcurrent pulse reaches 900 A is provided during 5 ms by the DCSP, then the current is constant at the DC maximum current after some oscillations at 100 A within 0.1 s. The accuracy of the current controller is less than 0.1%.

Figure 38 shows the current waveform of over-current pulse operation at the first 10 ms after the switch ON for the BSCCO tape. The peak current is ~ 900 A, and its duration is ~5 ms. The critical current of the BSCCO tape is 200 A listed in Table 5, and it is lower than 900 A. Therefore, mainly the HTS tape matrix carries the current during the pulse. The material of the matrix is copper and silver, and their resistivity's are ~ 10^{-9} Ωm at liquid nitrogen temperature, where the thicknesses of the HTS tapes is less than 0.3 mm. The self-magnetic field diffusion time is shorter than 1 ms, and the current density profile might be flat over the tape thickness during the pulse, because the critical current of the BSCCO tape is lower than 900 A. We will

discuss the self-magnetic field diffusion process [59] and these different predictions in detail in the next chapters. Figure 38 shows the waveform of the over-current pulse operation in a long time axis, and the current continues ~60 min as the experiment, shown in Fig. 39. The over-current pulse cannot be shown in Fig. 38 because it is too short. The accuracy of the current is within 0.1%. We will measure the self-magnetic fields near the HTS tapes' edge after 20 min of data gathering.

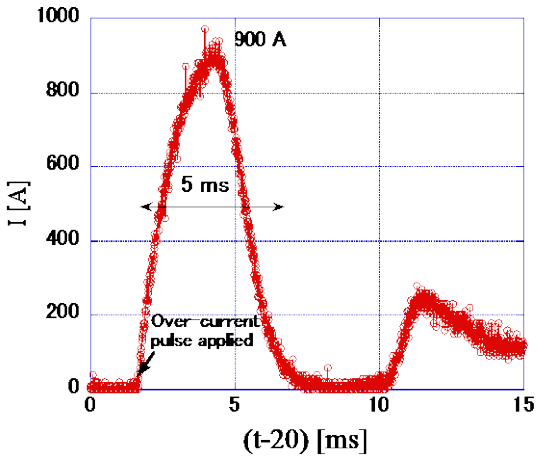

Fig. 38 Current waveform of the over-current pulse.

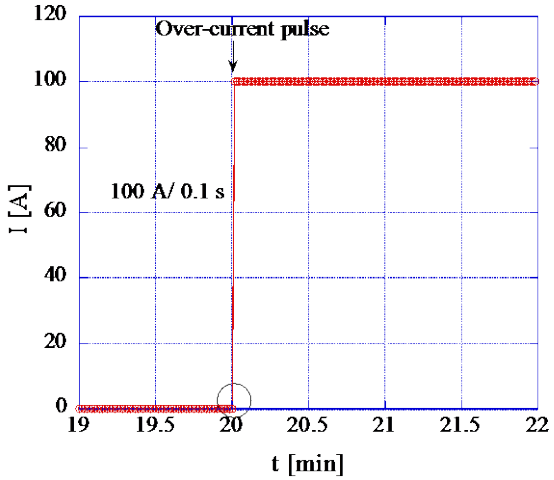

Fig. 39 Current waveform of the over-current pulse operation.

Once we applied this overcurrent pulse to HTS tape it doesn't harm BSCC and YBCO tapes. But in the case of the YBCO (Fujikura) tape that its structure doesn't contain the copper layer, it burns. We can see in Fig. 40 a burnt Fujikura tape after the over-current pulse application.

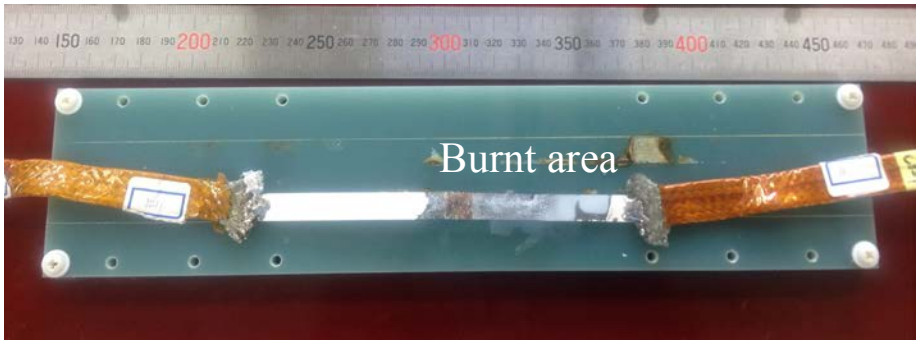

Fig. 40 Burnt Fujikura tape after over-current pulse application.

- The second operation for the direct DC current simulates the normal operation. The electric circuit is closed and the current is raised by 1 A/s to 100A of DC current, controlled by the DCSP, which is a normal scenario for the DC superconducting power cable current feeding. The waveform of the current is shown in Fig. 41.

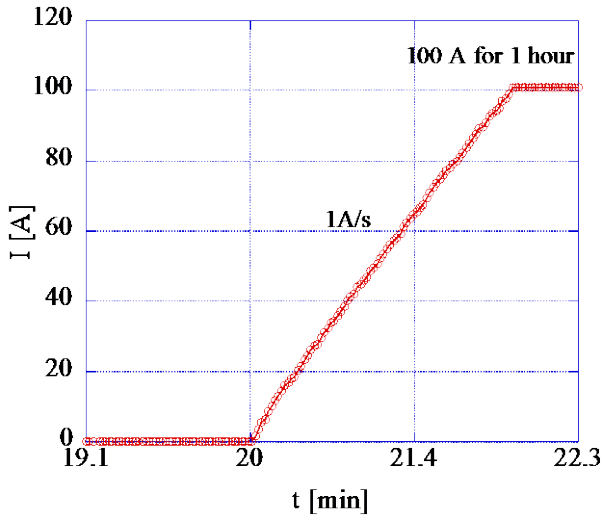

Fig. 41 The current waveform of the current rising in normal operation.

For the remnant current we simulate also two scenarios. The first one is the quick interruption of the DC current and the second one is a slow decrease of the DC current. The transport DC current of 100 A applied to each HTS tape was switched off then by two operations; first operation is a quick switch off by just switching off the electric switcher manually we called this

operation Fast op. Second operation is decreasing the current manually by 1A/s and we call this operation Slow op. Both switch off operations profiles are shown in Figs. 41 and 42.

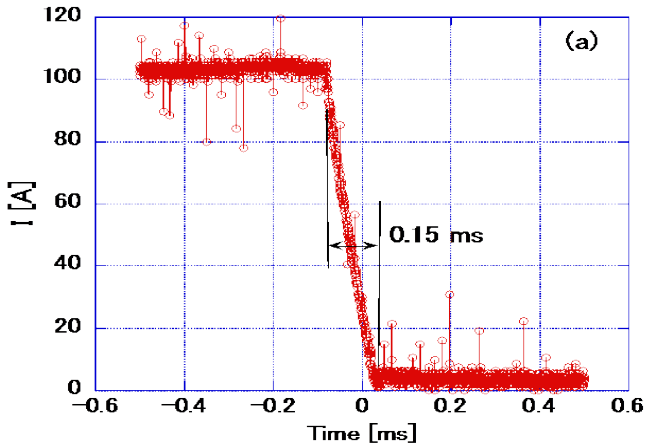

Fig. 42 The current waveform of the fast switch off.

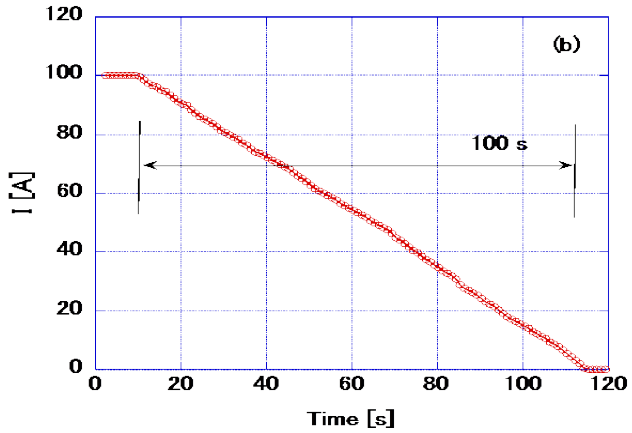

Fig. 43 The current waveform of the slow switch off.

We start scanning the perpendicular component of the residual magnetic field of each HTS tape along the Y direction for these different current feed operations. We change the X position of the Hall probe sensors along the longitudinal direction and we repeat the measurements. During the experiment as is mentioned above, we keep the constant level of LN2 in the open cryostat.

5.5 Hall probe measurement

5.5.1 Scanning technique

The field mapping is a measurement technique that has been known for many years. One of the main measurement techniques which have been developed and chosen in this thesis is the Scanning Hall probe measurement technique, which consists in fixing a Hall probe sensor on a moving Hall probe supporter moving above a sample. The sample can be magnetized by an external magnetic field source (permanent magnet or electromagnet) or simply conducted by an applied current (DC or AC current). This method provides a good spatial resolution and a high accuracy of the values of the magnetic field. [60-61]

In the other hand, the characterization of the HTS tapes by Hall probe measurement and scanning method used to be very suitable to investigate the current feeding operation effect on the current density distribution in the tapes. We chose this method not only because it's contactless and non-destructive but also because it's fast and useful in reel-to-reel condition. Hall probe scanning method consists then of measuring a data collection of the self-magnetic fields amplitudes produced by BSCCO and YBCO tapes. The data obtained by this measurement can be used to view one-dimensional magnetic field profile using a 1D Hall probe sensor or the profiles of the three components of the magnetic fields using a 3D Hall probe sensor. We approximate the results of the magnetic field profiles by a model in order to obtain the distribution of the current density of the tape, which is difficult to do with an electrical measurement. [62,63]

5.5.2 One and three-dimensional magnetic field scanning set-up

❖ **One-dimensional magnetic field scanning set-up**

The Hall probe used for the 1D Hall probe measurement in this thesis is a Cryogenic Hall probe

made by AREPOC s.r.o [64]. In this Hall probe, four leads are connected to the midpoints of opposite sides. When the control current $\mathbf{I_{cont}}$ is flowing trough the semiconductor layer and a magnetic field **B** is applied, a resultant Hall voltage $\mathbf{U_H}$ can be measured on the sides of the semiconductor layer. If the constant control current supplies the Hall probe a Hall voltage is directly proportional to the magnetic flux density. Voltage output varies with the angle between the vector of the magnetic flux lines and the plane of the sensing area. Maximum value is reaching when the magnetic flux lines are perpendicular to the sensing area.

Parameter	Unit	300 K	77 K	4.2 K
Normal control Current, In	**mA**	**10**	**10**	10
Maximum control current	mA	12	15	15
Sensitivity at In	**mV/T**	**49.7**	-	-
Offset voltage at In	μV	< 50	< 30	-
Input resistance	Ω	64	68	-
Output resistance	Ω	58	61	-
Linearity error up to 1T	%	< 0.2	-	-
Change of sensitivity due to reversing of the magnetic field	%	< 1	-	-

Table 6. 1 D Hall probe characteristic.

This linear Hall probe is also ratio metric, which means that its output voltage is proportional to the control current. The Hall probe sensor is for (50 x 50) μm^2 active area and for (5 x 7 x 1) mm^3 overall dimension. The table 6 resumes the different characteristics of our 1D Hall probe. [64]

We scan the perpendicular component of the magnetic field of the HTS tape along the Y-axis from down to up by a step of 0.05 mm in 0 A of the applied current (background) as in Fig. 29. We calculate then the average of the measured magnetic field that corresponds to the background. We subtract after, this average from the measured magnetic field. Fig. 44 shows an example of the background measurement. As it is shown the average of the magnetic field measured across the tape is 0.655 mT. This magnetic field amplitude corresponds to the magnetic field background. We apply after this a DC current and we measure the self-magnetic field above the tape and we subtract finally background amplitude from the measured self-magnetic field data. Fig. 45 shows the self-magnetic field profile of the BSCCO tape after subtraction of the magnetic field background. We get then a symmetric profile.

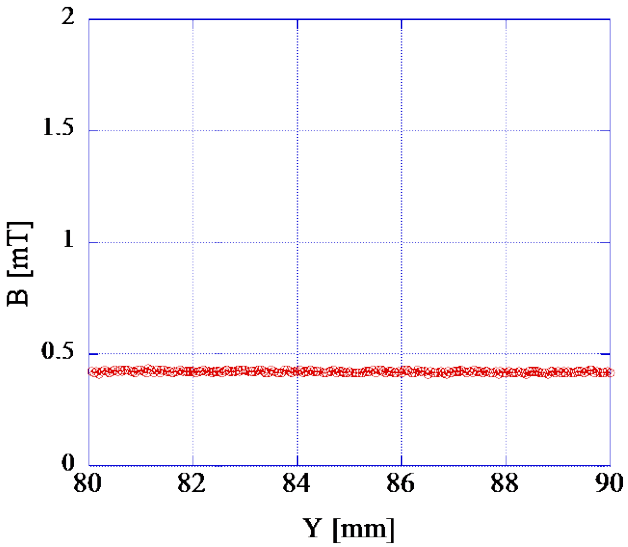

Fig. 44 Profile of the magnetic field background.

Because the tape is in the LN2 bath and might be a shrink, we need to exactly know its position. For that, we had to fix its center position. The symmetric self-magnetic field profile gives, in this case, the possibility to know precisely where is the position of the tape's centre. In fact, the

center of the tape is the position corresponds to zero self-magnetic fields. In Fig. 45 the center of the BSCCO tape is at Y= 77.25 mm.

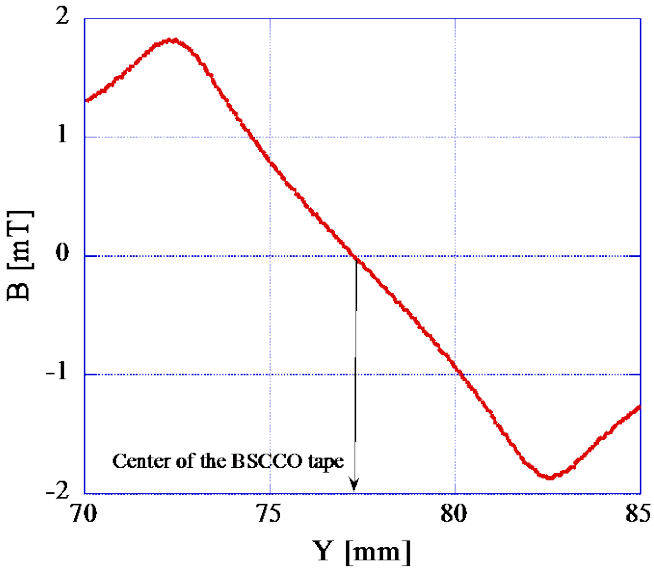

Fig. 45 YBCO tape magnetic field profile.

❖ **Three-dimensional magnetic field scanning set-up**

The Hall probe used in the 3D magnetic field measurement is developed for operations at a temperature range of 1.5 - 350 K and in magnetic fields up to 5 T. This Hall probe is also made also by AREPOC s.r.o. [64]. The Hall probe is desi three perpendicular components of the magnetic field using (250 x 250) μm^2 Hall probe sensors as in Fig. 46. This type of Hall probes is appropriate for the measurement of fringing fields from magnets, coils, and for other homogeneity characterizations. The active area of each elementary sensor is (50 x 50) μm^2. The probe sensitivity of each sensor is 70 mV/T at the nominal control current of 10 mA and the overall dimensions are ∅(8 x 20) mm. [64]

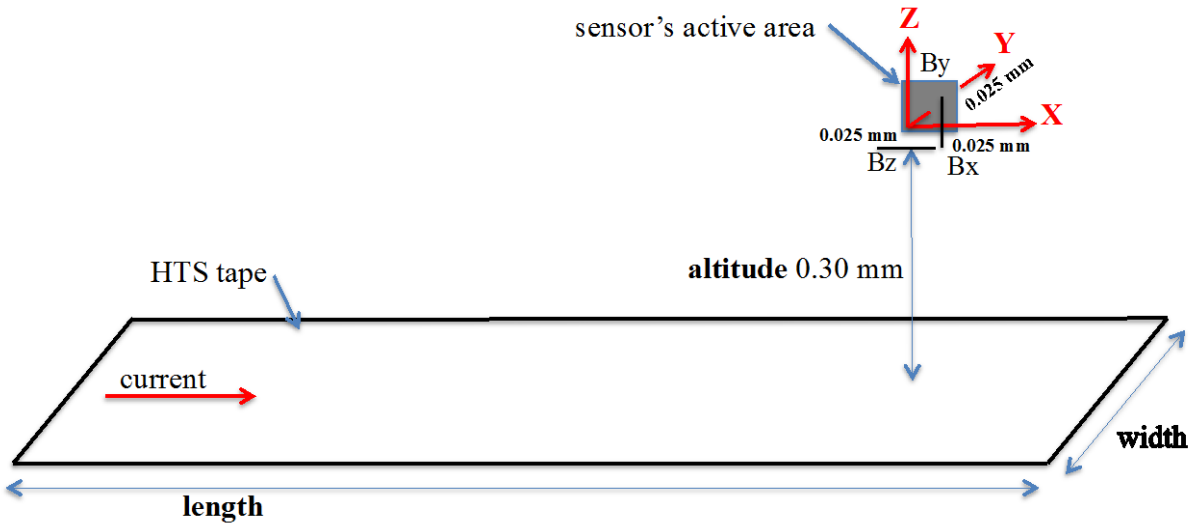

Fig. 46 3D Hall probe configuration.

In the case of the 3D hall probe measurement, we apply the same method to measure the background magnetic field used in the 1D magnetic field measurement. We scan the three perpendicular components of the magnetic field of the HTS tapes along the Y-axis from down to up by a step of 0.1 mm in 0 A. We calculate the average of each component of the measured magnetic field that corresponds to the background and we subtract after that the average of theses three averages from the measured magnetic field. Fig. 47 shows the three components of the magnetic field profiles measured by our 3D Hall probes sensors.

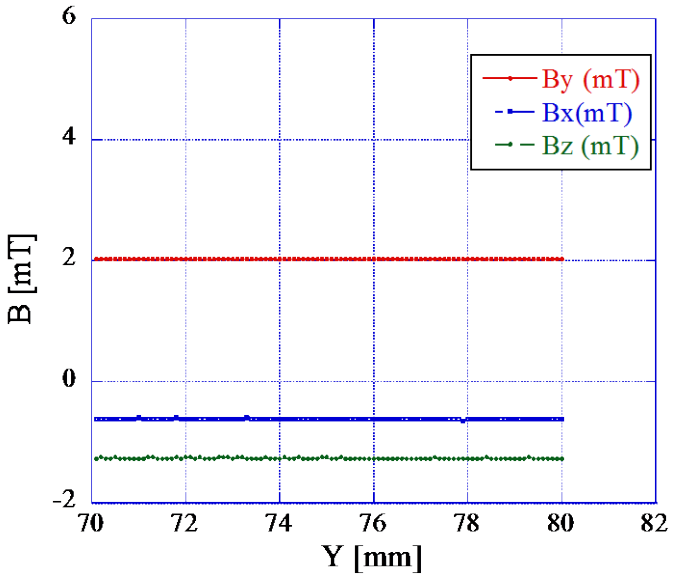

Fig. 47 Profiles of the 3D magnetic field background.

After that, we apply a 100A of DC current to the HTS tape, we scan a Hall probe above the tape by the step of 0.1 mm and we get Bz, By and Bx graphs. The center of the tape is the position corresponds to zero Bz magnetic field and the maximum of the By magnetic field. Fig. 48 shows the center position of the BSCCO tape situated at Y= 78.4 mm.

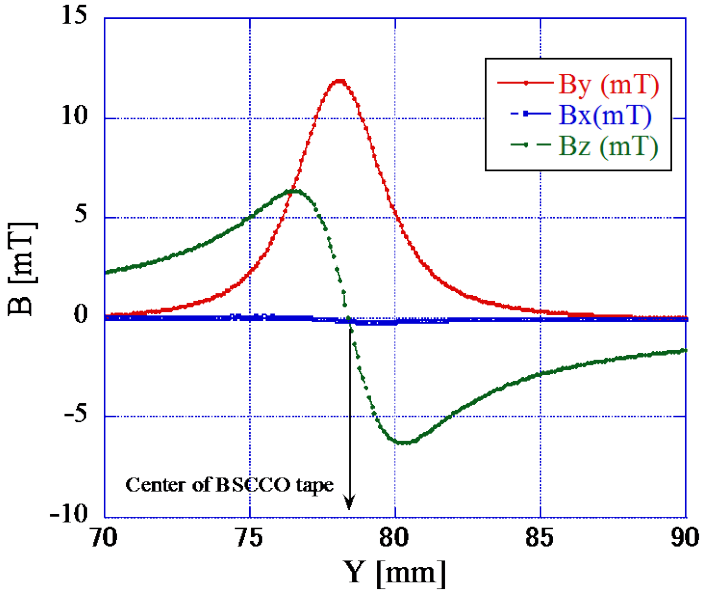

Fig. 48 YBCO tape's 3D magnetic field profiles.

5.6 Over-current pulse operation experiment

5.6.1 Magnetic field measurement above the HTS tapes' edge

We measured the self-magnetic fields near the HTS tapes' edge after 20 min of data gathering as in Fig. 49 for the over-current pulse operation and the normal operation. The tapes chosen for this experiment are BSCCO, AMSC and Fujikura (tape 1).

In the over-current pulse operation, the self-magnetic field of the BSCCO tape increases quickly, and then decreases gradually for the next 60 minutes. See Fig. 49. However, the self-magnetic

field remains constant for the YBCO (AMSC) tape in Fig. 45. YBCO (Fujikura) tape, used in this thesis, has no stabilizing copper layer to protect it from the over-current, as in the YBCO (AMSC) tape. The tape characteristic changes after the over-current pulse and it burn easily. Fortunately, one YBCO (Fujikura) tape did not burn and we can measure the self-magnetic field profile across the tape's width but not the self-magnetic field near the tape's edge.

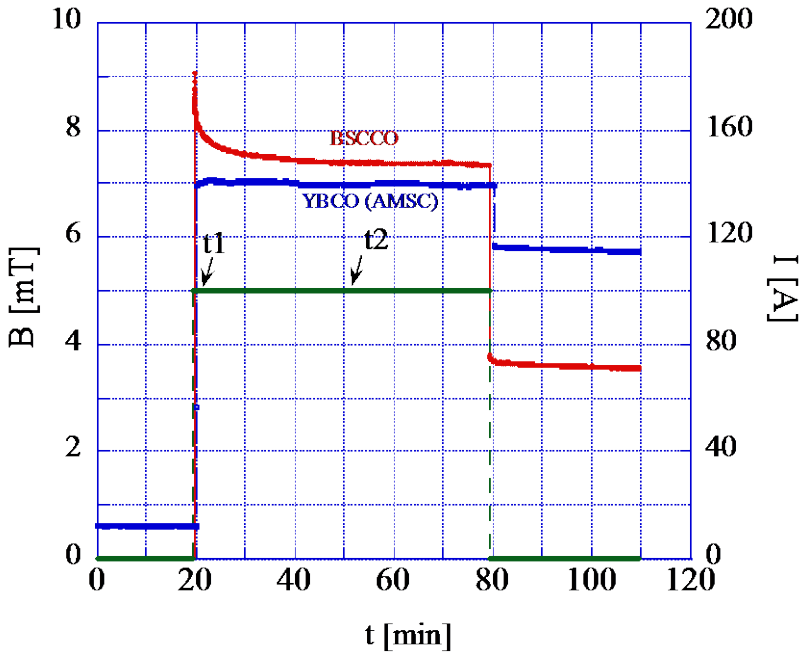

Fig. 49 Magnetic field profiles above HTS tapes edge on the over-current pulse operation.

However in the case of the normal operation, a small increase of the self-magnetic field is found for the BSCCO tape but not for the YBCO tapes after the current reaches 100 A. Fig. 50 shows it with the waveforms of the current near the edge of the HTS tapes. It increases gradually for the last one hour for the BSCCO tape but remain constant for the YBCO tapes. Although the width of the Fujikura's YBCO tape is not wider than that of AMSC's, the self-magnetic field at the edge for Fujikura's is lower than AMSC's. It suggests that the current density profile of Fujikura's is different from AMSC's and that the current density profile of Fujikura's is not peaked near the edge like the AMSC's. Both BSCCO tape and YBCO (AMSC) tape have copper layer protection

convenient to absorb the pulse and protect the tape after for long time current feeding in opposition to the YBCO (Fujikura) tape. This characteristic will have an impact on the current density distribution in both cases.

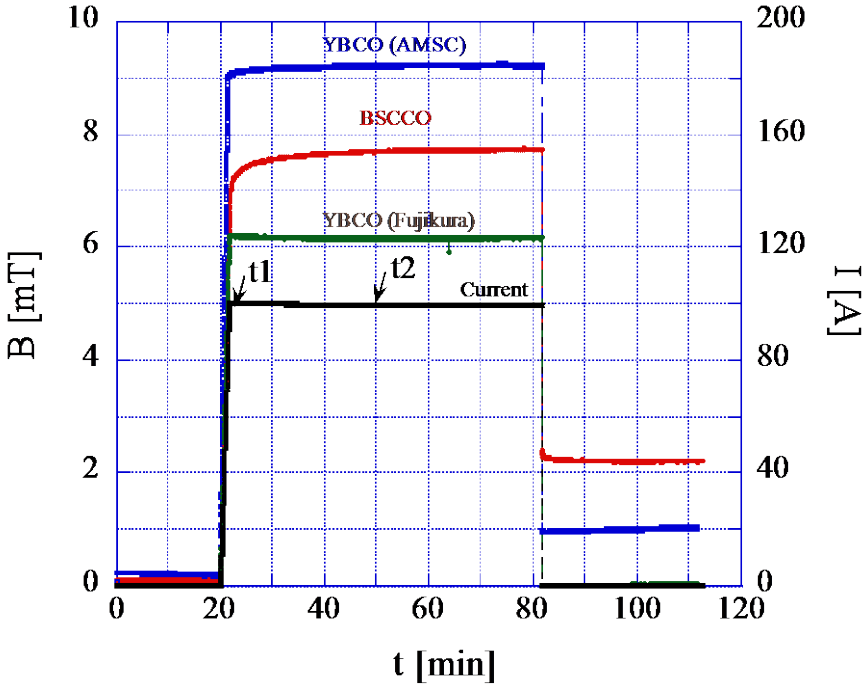

Fig. 50 Magnetic field profiles above HTS tapes edge on the normal operation.

After the self-magnetic field measurement above HTS tapes' edge, we scan its perpendicular component along the width of the three HTS tapes on two different times (t1=22 min, t2= 51 min) of the normal and over-current operations shown in figures 49 and 50.

5.6.2 Self-magnetic field scan along the HTS tape width

We show in Fig. 51 the self-magnetic field profiles in the over-current pulse and normal operations applied to the BSCCO tape. First scanning time t1 is shown just after the current reaches 100 A for over current and normal operations. Second scanning time t2 is shown almost 30 minutes after the switch ON. During the scanning time (45 sec for the tape's width), the total current is constant within 0.1%. The self-magnetic field doesn't change so much (see Fig. 49 and

50, estimated to ~ 5%) during the scanning time above the BSCCO tape. The two self-magnetic field profiles at t1 and t2 are different from each other especially around the edge because it decreases. However for the normal operation, and since the self-magnetic field near the edge has been changing a little, the vertical components of the self-magnetic field profiles are almost same each other.

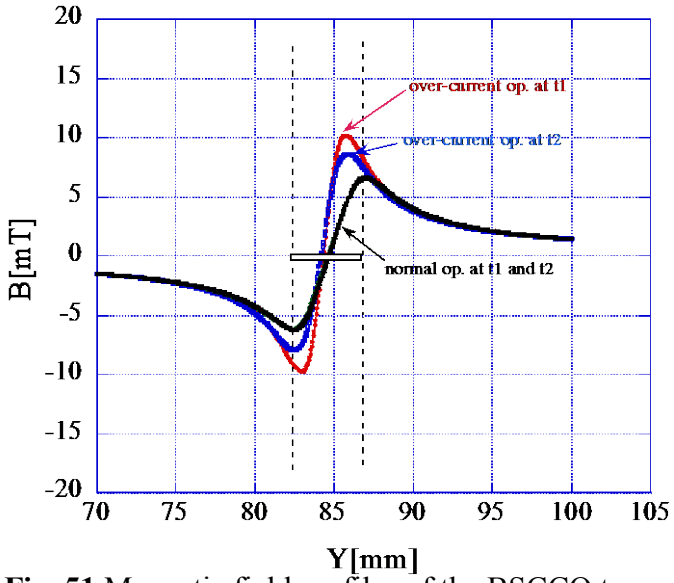

Fig. 51 Magnetic field profiles of the BSCCO tape.

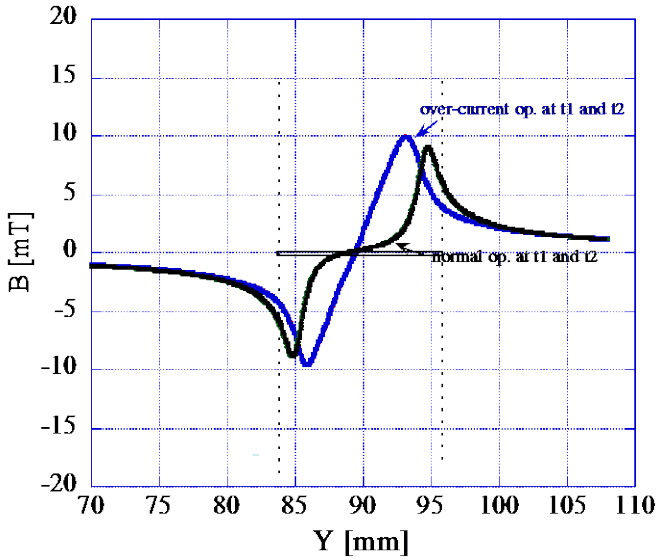

Fig. 52 Magnetic field profiles of the AMSC tape.

Figure 52 shows the self-magnetic field profiles in the over-current pulse and normal operations, applied to the YBCO (AMSC) tape at t1 and t2 as in Figs. 49 and 50.

Figure 53 shows the self-magnetic field profiles in the over-current and normal operations, applied to the YBCO (Fujikura) tape at t1 and t2 as in Figs. 43 and 44. As the other coated conductor, for the over-current and normal operations, the two self-magnetic field profiles at t1 and t2 are same.

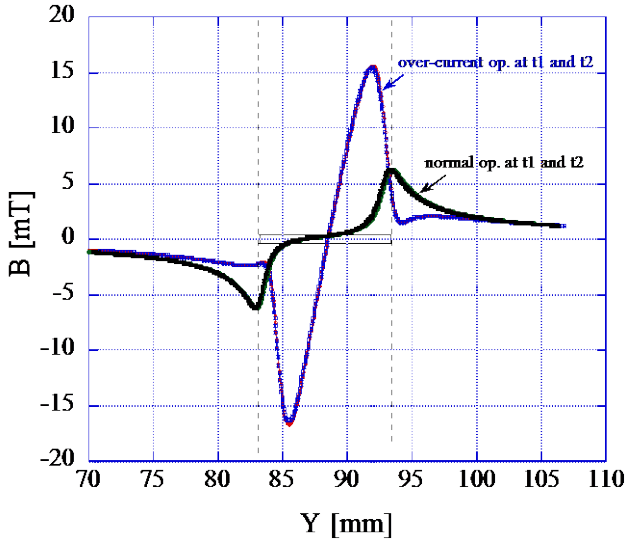

Fig. 53 Magnetic field profiles of the Fujikura tape.

5.6.3 Magnetic field penetration theory

The self-magnetic field diffusion and the current density diffusion times are the same because they must obey the same equation [59]. The skin depth s of the current density and the self-magnetic field is given by $s = 2\sqrt{\kappa_0 \cdot t}$ [A1] where κ_0 is the magnetic diffusivity and is given by

$\kappa_0 = \frac{\eta}{\mu}$ [A2] where η is the electrical resistivity, and μ is the magnetic permeability.

When the value of η is ~10^{-9} Ωm at 77K and μ is equal to the magnetic permeability of vacuum, the skin depth is ~ 2.5 mm for 5ms. This is almost 8 to 20 times longer than the thickness of the HTS tapes (see table 5). The critical currents of the HTS tapes are lower than 900 A, therefore, the superconducting current is not the major parts of current, and mainly the tapes' matrix carries the current. HTS tape current density profiles during the pulse would be flat because the matrix of the HTS tape is uniform. After the short but large current pulse, the operation current of the experiment was set back to 100 A, and this current of 100 A should be superconducting current because it is lower than the critical currents. Therefore, the process from 900 A to 100 A is called the self-magnetic field relaxations and depends on the whole structures of the HTS tapes including the HTS and the copper or silver stabilizers, the characteristics and the structures of the HTS filaments for Bi2223 and the HTS thin films for Y123, and so on. Actually, the self-magnetic field at the edge of the Bi2223 tape changes with time, and its characteristic time is several minutes shown in Figs. 49 and 50. The time length is longer than the self-magnetic diffusion time of the matrix and shorter than the self-magnetic diffusion time of the HTS itself. This means that the interaction between the HTS and the matrix would be important.

5.7 Residual magnetic field scan

5.7.1 One-dimensional residual magnetic field scan

In this experiment, we applied the two scenarios of the current-off operation to investigate the current-off operation effect on the permanent magnetic fields. We start scanning the perpendicular component of the residual magnetic field of each HTS tape along the Y-direction to cover the tape width and we change then the X position along the longitudinal direction with repeating these measurements for both slow current-off operation (slow op.) and fast current-off

operation (fast op.). Because of the similar structure to include a stabilizer layer we chose for these operations only two HTS tapes, which are the BSCCO tape and the YBCO (AMSC) tape. The perpendicular component of the residual magnetic field of BSCCO tape was scanned at three positions along the X direction with 10 mm distance separate each for both operations are shown in Fig. 54. The perpendicular component of the residual magnetic field of YBCO tape was scanned also at three X positions with 10 mm separate each for both operations as the Fig. 55.

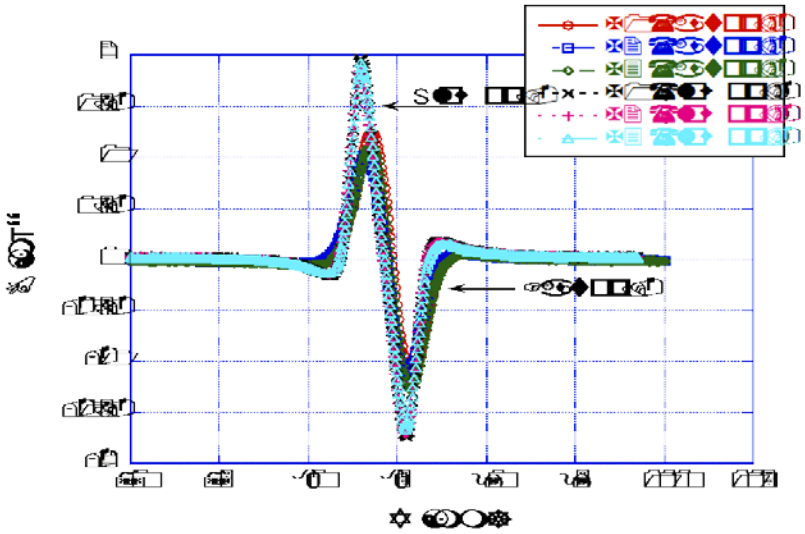

Fig. 54 Residual magnetic field profiles of the BSCCO tape.

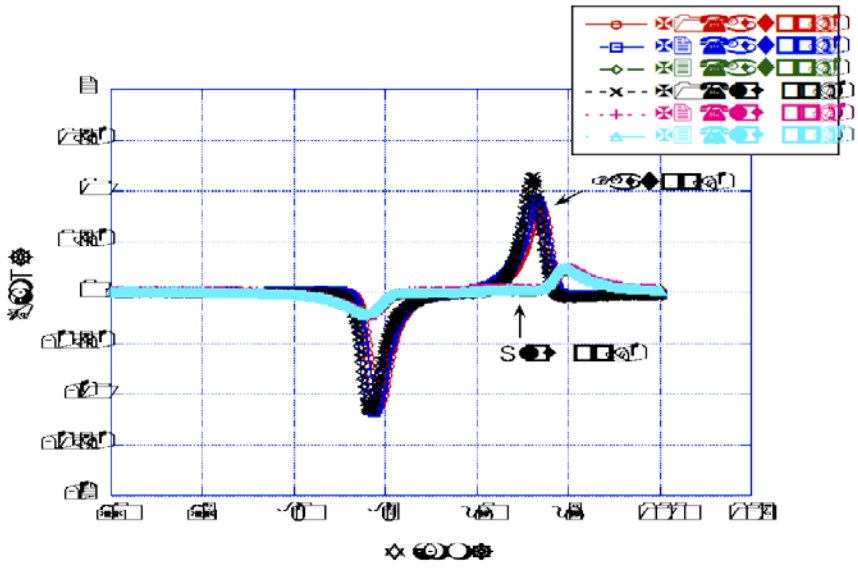

Fig. 55 Residual magnetic field profiles of the YBCO tape.

5.7.2 Homogeneity investigation along HTS tapes' length

In this section we measured also with BSCCO and SWCC tapes the residual magnetic fields of the YBCO AMSC tape. In fact, the AMSC and SWCC had a different dimension and critical current amplitudes as cited in table.2. However, both of these YBCO tapes have the same manufacturing process, which is metal organic deposition (MOD). That's why they were chosen for the residual magnetic field study and for the tape's homogeneity investigation. The current cut-off for this experiment is only the fast-cut off operation.

The perpendicular component of the residual magnetic field of BSCCO tape was scanned at three positions along the X-direction with 20 mm covered area (See Fig. 56). And the perpendicular component of the residual magnetic field of YBCO SWCC tape was scanned also at three X positions with 60 mm covered area (See Fig. 57). The third tape is YBCO AMSC tape. Its perpendicular component of the residual magnetic field was scanned at four positions with 50 mm covered area at 100 A and 250 A applied DC current (See Fig. 58 and 59).

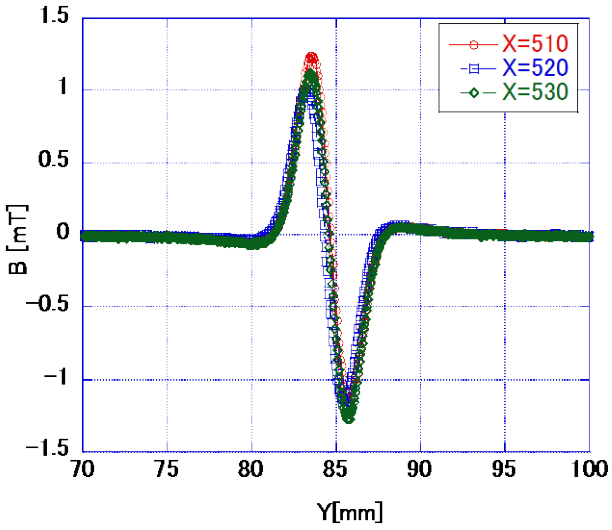

Fig. 56 Residual magnetic fields profiles of the BSCCO tape in different X positions.

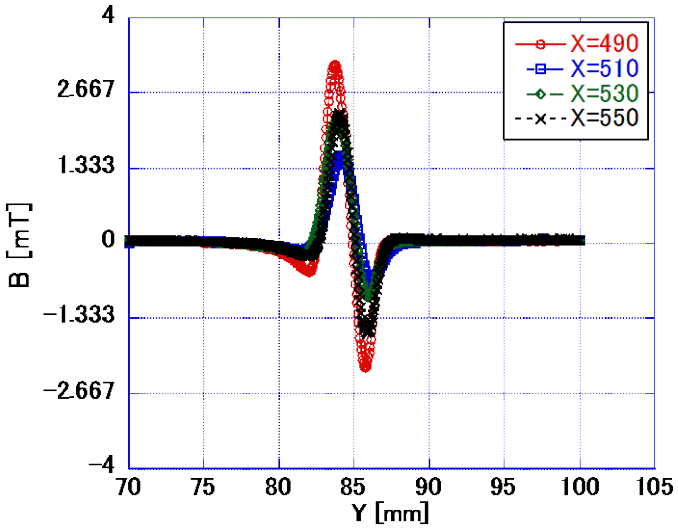

Fig. 57 Residual magnetic fields profiles of the SWCC tape in different X positions.

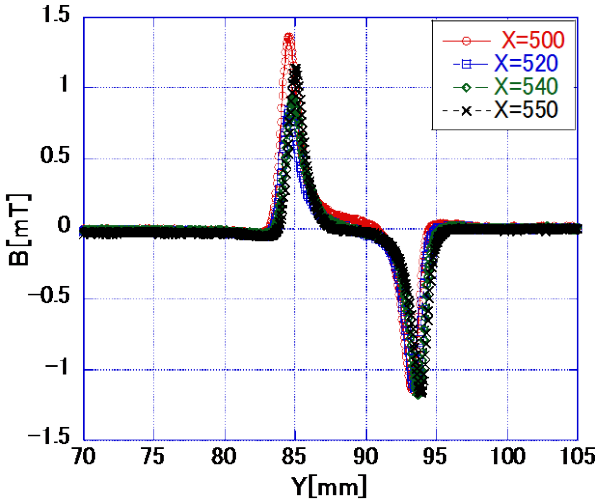

Fig. 58 Residual magnetic fields profiles of the AMSC tape in different X positions (I=100A).

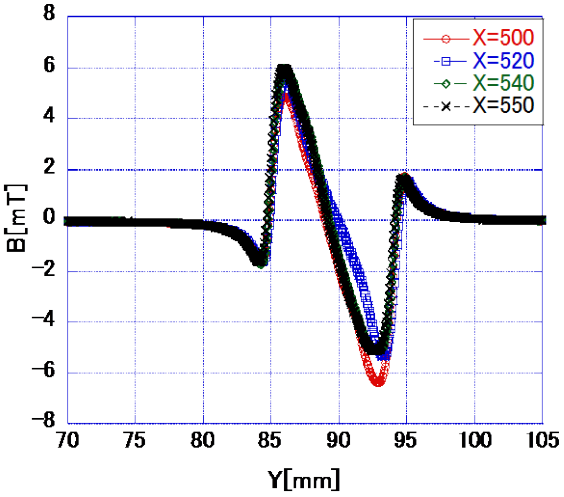

Fig. 59 Residual magnetic fields profiles of the AMSC tape in different X positions (I=200A).

5.7.3 Three-dimensional residual magnetic field scan

The DC current switch-off operation in this experiment is a fast switch-off, similar to the previous one-dimensional residual magnetic field measurement for HTS tapes' homogeneity study discussed in the previous section. The chosen HTS tapes for this experiment are BSCCO, AMSC, and Fujikura tapes. The Fujikura tape used in this experiment has a stabilizer layer (Fujikura tape 2 from the table. 5). The 3D Hall probes system moves across the tape along the Y-direction (Tape's width) and along the X direction (tape's length) at 0.3 mm altitude from the tape surface by the two 0.1mm stepping motor systems (X and Y directions). We start scanning the three components of the residual magnetic field (B*z*, B*y* and B*x*) of each HTS tape along the Y direction to cover the tape width with 0.1mm per step. Afterward, we change the longitudinal direction (X direction) of 3D-Hall probe system position by 0.1mm and we repeat scanning for Y direction again. Total scanning area along the X direction is 1cm for each HTS tape (see Figs. 60, 61 and 62). During the experiment, we keep the constant level of LN2 in the open cryostat.

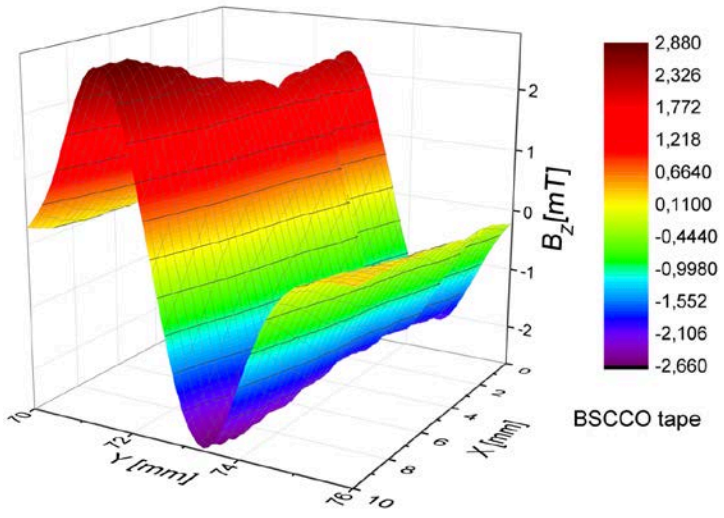

Fig. 60.a B*z* components of the 3D self-magnetic field map (BSCCO tape).

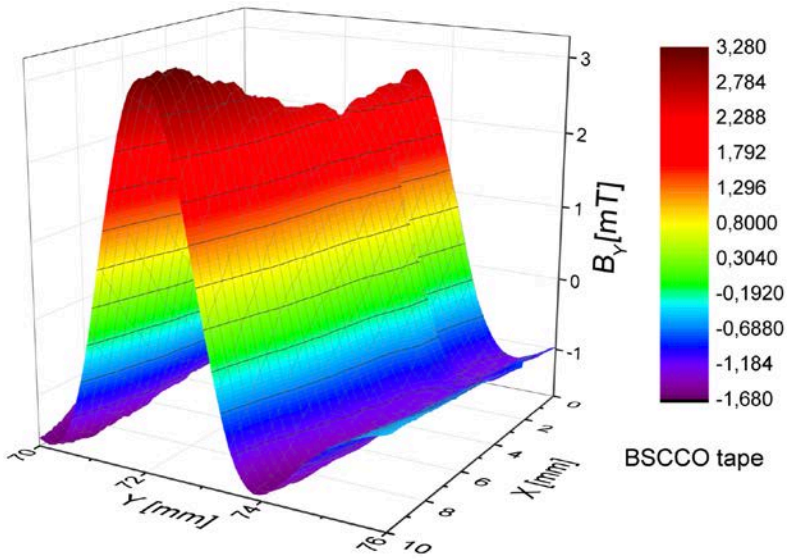

Fig. 60.b B*y* components of the 3D self-magnetic field map (BSCCO tape).

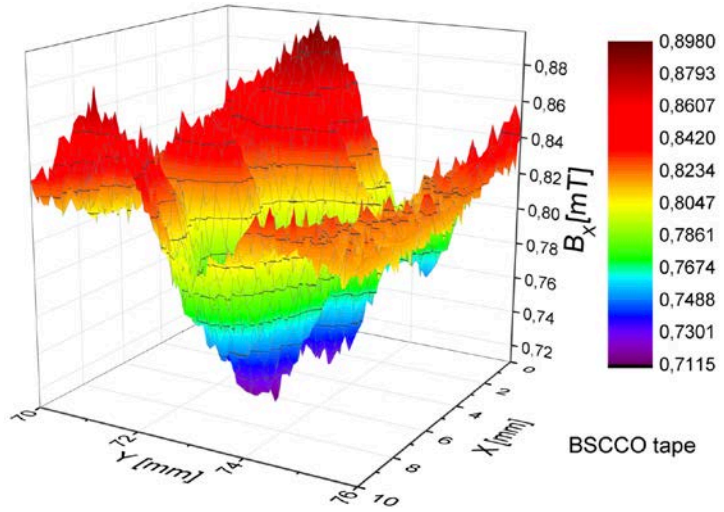

Fig. 60.c B*x* components of the 3D self-magnetic field map (BSCCO tape).

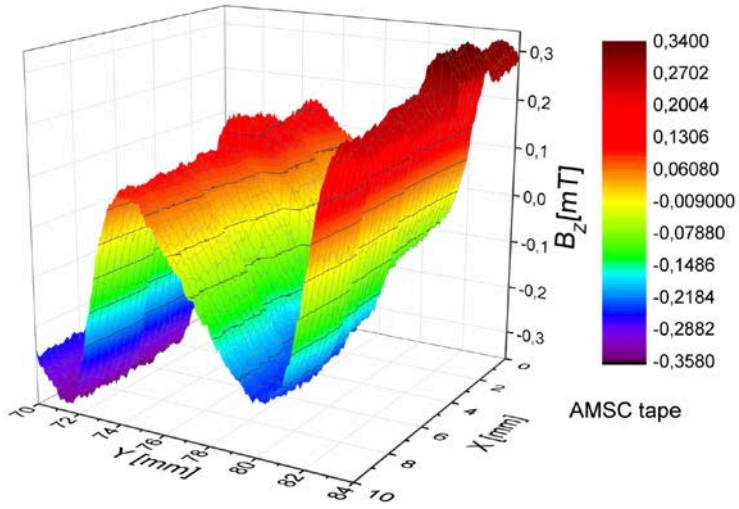

Fig. 61.a B*z* components of the 3D self-magnetic field map (AMSC tape).

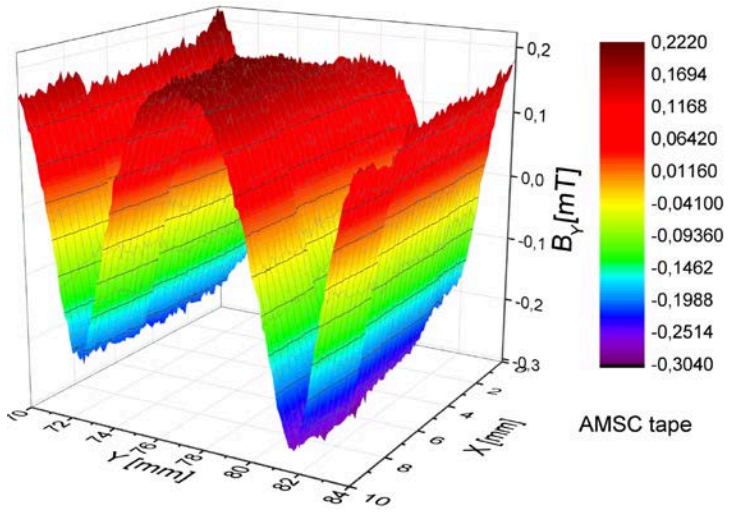

Fig. 61.b B*y* components of the 3D self-magnetic field map (AMSC tape).

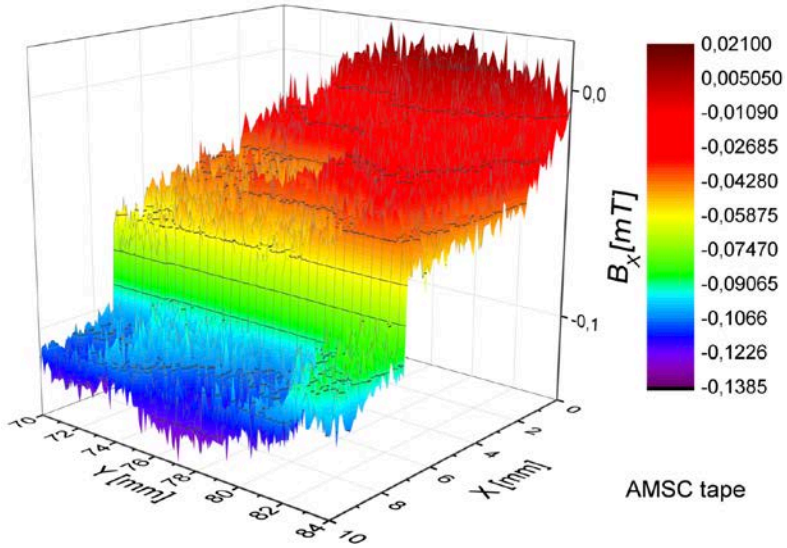

Fig. 61.c B*x* components of the 3D self-magnetic field map (AMSC tape).

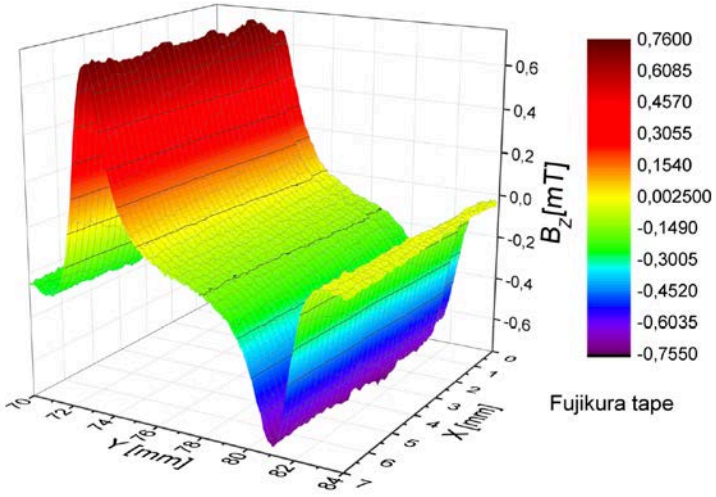

Fig. 62.a B*z* components of the 3D self-magnetic field map (Fujikura tape).

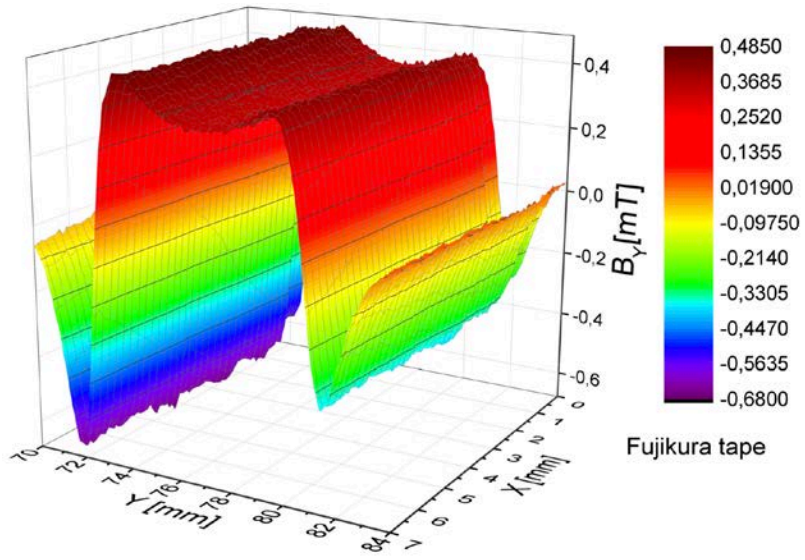

Fig. 62.b B*y* components of the 3D self-magnetic field map (Fujikura tape).

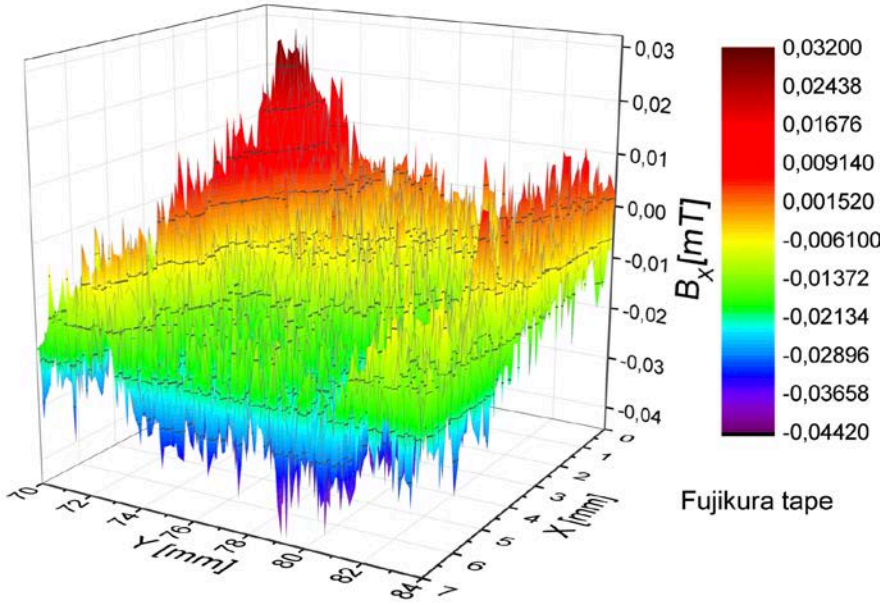

Fig. 62.c B*x* components of the 3D self-magnetic field map (Fujikura tape).

5.8 Summary

We present in this chapter the experiment set-up used in this thesis and the different current feed operation of direct and remnant DC current operations. The Self magnetic field measurements and scanning were presented with the study of the homogeneity of the residual magnetic field profiles of the different HTS tapes. These results will help us to calculate different current and remnant current density profiles that correspond to each current feed operations and which will be presented in the next chapters.

Contribution: This chapter is based on the following papers:

- M. Tallouli, J. Sun, A. Ninomia, M. Hamabe, H. Watanabe, et al, '' Residual magnetic field measurement of BSCCO and YBCO tapes by a Hall probe, '' *IEEE Trans. Appl. Supercond*., vol. 25, p. 8000704, June 2015, (4 pp.)

- J. Sun, Tallouli Mohamed, Oleg Shyshkin, Makoto Hamabe, Hirofumi Watanabe, Noriko Chikumoto, O. Shyshkin, '' Residual magnetic field profiles and their current density profiles of coated conductors for fast and slow-cut-off current operations,'' Progress in Supercond. And Cryogen., vol. 15, pp. 17-20, March 2015.

- Oleg Shyshkin, Yuri Kazarinov, Moahmed Tallouli, Tosin Famakinwa, Satarou Yamaguchi, '' Inverse Problem Solution Algorithms for Current Density Distribution Calculation in Different HTS Tape Configurations Basing on Minimum Self- Magnetic Field Measurements,'' *IEEE Trans. Appl. Supercond.,* vol. 26, no. 3, p. 9000404, Apr. 2016. (4 pp.)

- M. Tallouli, J. Sun, Noriko Chikumoto, O. Shyshkin, E.S Otabe, et al, '' Observation of self-magnetic field relaxations in Bi2223 and Y123 HTS tapes after over-current pulse and DC current operation,'' **submitted to** *Cryogenics.*

- M. Tallouli, J. Sun, M. Hamabe, H. Watanabe, Noriko Chikumoto, et al, '' Study of residual current density profiles of BSCCO and YBCO HTS tapes by a 3D Hall probe system,'' *IEEE Trans. On Appl. Supercond.,* vol. 26, Issue 3, 2016. (5 pp.)

CHAPTER 6. CURRENT AND RESIDUAL CURRENT DENSITIES CALCULATION MODEL

6.1. Introduction

Current distribution along and across the high temperature superconducting (HTS) tape provides sufficient information about the quality of the tape performance in different current feeding regimes. In this chapter, we present an algorithm for the inverse problem solution aimed to the calculation of 1D and 2D current density distributions from the residual and self-magnetic field measurement around the HTS tape. The crucial point of the study, presented in this thesis, is the fact that a minimum possible data for the self-magnetic field is provided with a solution of a lowest error level and simple linear equations. The calculation is performed for several single HTS tapes and the current density redistribution is analysed for different current feeding regimes.

6.2. Current density calculation models

6.2.1 One-dimensional current density calculation model

In order to measure the perpendicular component of the magnetic field of the HTSC tape, the Hall probe moving at the specified altitude above the tape was used. In this section, we present the inverse problem solution algorithm that allows us to calculate the current density profile in the HTS tape basing on the measurements of the magnetic field above the tape.

As in Fig. 63 the schematic representation of the experimental layout for the B_z measurements is shown. We put the HTS tape in Cartesian coordinates, which are used for the calculations, along the, in the plane Z=0 so that crosses the tape. The Hall probe path line goes parallel Y-axis on the defined altitude z_d above the tape.

Here we have to make several assumptions to simplify the analytical treatment of this problem and speed up the numerical calculations. Firstly we assume the thickness of the tape to be infinitesimal so that all the current running within the tape could be considered as a surface current presented through the surface current density **J** (see Fig. 63). Further, we suppose that all the current is running along the tape so that the only -component of the current density exists. The current density doesn't depend on X coordinate and is a function only of Y coordinate $J = J_x(Y)$. In this case, we can make a discretization of the tape (i.e., divide the tape into a number of sub-tapes) with the fixed current density value J_i in each sub-tape.

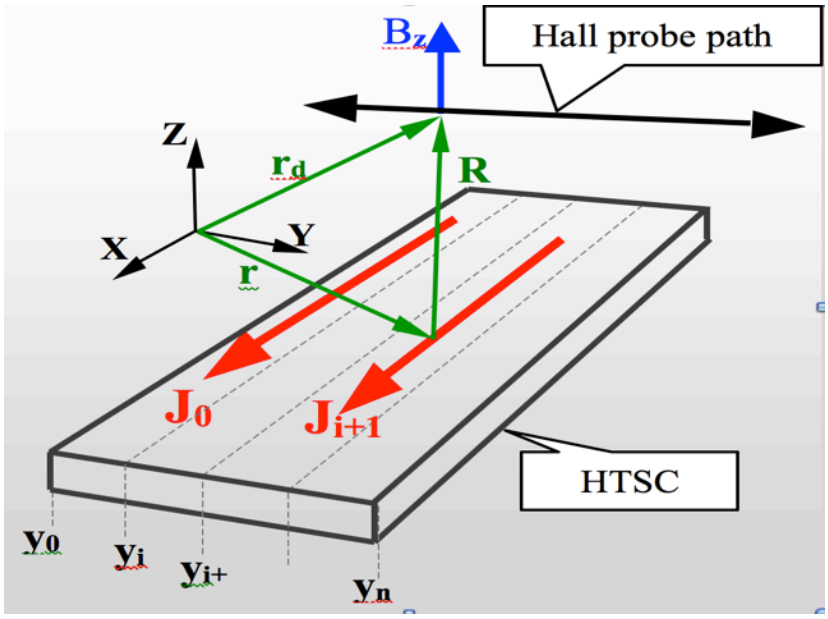

Fig. 63 HTS tape discretization used for the inverse problem solution algorithm of the inverse problem.

A detector in position $\vec{r} \equiv (x, y, z)$ measures the perpendicular component of the self-magnetic field B_z. Vector $\vec{r} \equiv (x, y, z)$ determines the coordinates of each current element on HTS tape. The distance between the separate current element and the arbitrary coordinate of the

detector is presented by the vector $\vec{R} = \vec{r}_d - \vec{r}$ with its absolute value $R=\sqrt{R_x^2+R_y^2+z_d^2}$

where $R_x = x_d - x$ and $R_y = y_d - y$. All these notations will be used throughout further treatment.

Generally, the magnetic field **B** at an arbitrary position $\mathbf{r}_d$ could be calculated by the Biot-Savart equation as follow:

$$\vec{B}(r_d) = \frac{\mu_0}{4\pi}\int \frac{[\vec{J}\times\vec{R}]}{R^3} dS \qquad (1)$$

The integration in Equation (1) is performed through the surface Σ of the tape $dS = dx\,dy$, which is limited in Y-direction, by the width of the HTS tape and in the X-direction it could be either limited manually or the integration could be performed in the range $(-\infty, \infty)$. The fact that the magnetic field decays as $\sim \frac{1}{R^2}$ makes the impact of currents running on the large distances negligible. Including the mentioned above assumptions the Biot-Savart equation (1) after the integration along x-direction in the range $(-\infty, \infty)$ could be written as following

$$B_z(r_d) = \frac{\mu_0}{2\pi}\sum_{i=0}^{n-1}\int_{y_i}^{y_{i+1}} \frac{R_y J_i}{R_y^2+z_d^2} dy. \qquad (2)$$

The summation in expression (2) should be done over all sub-tapes with the current density elements. After the integration along Y-direction we obtain the final formula used for the inverse problem solution

$$B_z(\mathbf{r}_d) = \frac{\mu_0}{4\pi}\sum_{i=0}^{n-1}\mathbf{J}_i \ln\frac{(y_d - y_i)^2 + z_d^2}{(y_d - y_{i+1})^2 + z_d^2}. \quad (3)$$

This expression is similar to that presented and justified by M. Carrera et al. [63]. For a number of measurements of the vertical components of the magnetic field the expression (3) gives a system of linear equations with known magnetic field B_z and unknown current density elements J_i. We developed MATLAB code to solve this system of linear equations by means of Cramer's rule. As result of inverse problem solution, we obtain the current density profiles, which are presented further.

6.2.2 Two-dimensional current density calculation model

To solve the inverse problem aim at the calculation of two-dimensional current density distribution throughout the HTS tape we have used several methods. One is the solution for the set of linear algebra equations issued from the Biot-Savart law and the other is the method of least squares. It was found that in some cases the best way to the inverse problem solution when the highly accurate analysis is needed the combination of both methods would be beneficial.

To calculate the magnetic field above the HTS tape in the arbitrary position $\mathbf{r}_d$ the Biot-Savart law in general form is used.

$$\vec{B}(r_d) = \frac{\mu_0}{4\pi}\int\frac{[\vec{J}\times\vec{R}]}{R^3}dS \quad (1)$$

With $R = \sqrt{R_x^2 + R_y^2 + z_d^2}$ is the distance between the segment on the tape and the detector position. All the notations are shown in Fig. 62 together with the schematic representation of the experimental layout with the HTS tape discretization used for the inverse problem solution

algorithm.

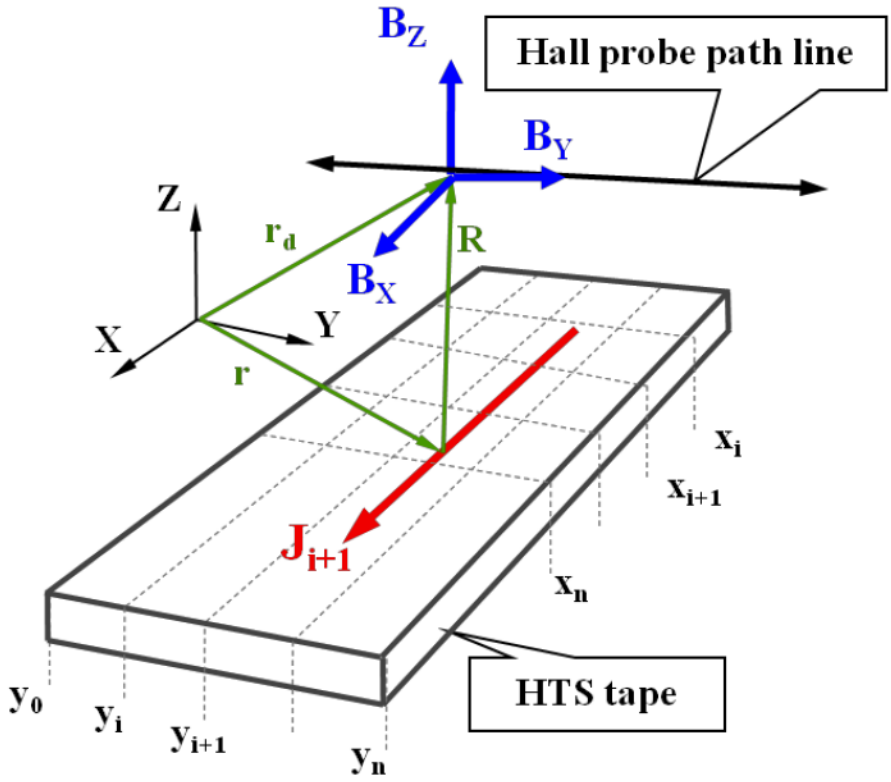

Fig. 64 The schematic representation of the experimental layout together with the HTS tape discretization used for the inverse problem solution algorithm.

The integration in expression (1) is performed through the surface Σ of the tape dS=dx Dy, which is limited in Y direction by the width of the tape and in the X direction it could be either limited manually or the integration could be performed in the range $(-\infty,+\infty)$. The fact that the magnetic field decays as ~$1/R^2$ make the impact of currents running on large distances negligible.

Three components of the magnetic field, as in Fig 64 could be represented by the integral notations as following

$$\mathrm{B}_X\left(\mathbf{r}_d\right)=\frac{\mu_0}{4\pi}\int_{\Sigma}\frac{J_Y R_Z}{R^3}\,dx\,dy, \qquad (2)$$

$$\mathrm{B}_Y\left(\mathbf{r}_d\right) = -\frac{\mu_0}{4\pi}\int_{\Sigma}\frac{J_X R_Z}{R^3}\,dx\,dy, \qquad (3)$$

$$\mathrm{B}_Z\left(\mathbf{r}_d\right) = \frac{\mu_0}{4\pi}\int_{\Sigma}\frac{J_X R_Y - J_Y R_X}{R^3}\,dx\,dy. \qquad (4)$$

After the integration throughout the tape surface including the fact of fast magnetic field decays with the distance and assuming the local symmetry of the perpendicular current J_Y we obtain the following set of linear equations

$$\mathrm{B}_X(\mathrm{r}_d) = 2\cdot 10^{-7}\sum J_{Yi}\left(\arctan\frac{y_i - y_d}{z_d} - \arctan\frac{y_{i-1} - y_d}{z_d}\right) \qquad (5)$$

$$\mathrm{B}_Y(\mathrm{r}_d) = -2\cdot 10^{-7}\sum J_{Xi}\left(\arctan\frac{y_i - y_d}{z_d} - \arctan\frac{y_{i-1} - y_d}{z_d}\right) \qquad (6)$$

$$\mathrm{B}_Z(\mathrm{r}_d) = 10^{-7}\sum_i^n J_{Xi}\frac{(y_d - y_{i-1})^2 + z_d^2}{(y_d - y_{i-1})^2 + z_d^2} \qquad (7)$$

The expression (7) fits to that used for calculations of 1D current distribution. These equations could be presented in more compact form

$$B_{Xk} = \sum_{i=1}^{n} A_{ki}\, J_{Yi}, \qquad (8)$$

$$B_{Yk} = \sum_{i=1}^{n} B_{ki}\, J_{Xi}, \qquad (9)$$

$$B_{Zk} = \sum_{i=1}^{n} C_{ki} J_{Xi}, \qquad (10)$$

Where A_{ki}, B_{ki} and C_{ki} are the components of the matrixes representing distances between the segment with the current element on the tape and detector position.

Afterwards, the equations could be solved by Cramer's rule, which is more stable for our case. Among the advantages of this method are the fast calculation and low error level. It is suitable perfectly for a single HTS tape analysis. Concerning the disadvantages of this method, one could mention the limited number of the current elements that could be resolved. In our calculations, the maximum number is 36 data points for current density profile obtained for a single HTS tape. This limitation is caused by the fact that the determinants of the matrixes consisting of elements approach to zero value with the increasing of data points. For the stacked conductor the number of data points is just 11. Also, there is a problem, to control the multiple solutions for stacked conductor. To avoid these problems the method of least squares could be used [63].

Method of Least Squares

The idea of the method of least squares is to minimize the value of the error function by varying the model of the current density profile

$$err = \sum \sqrt{\left(B_{\exp}(y_i) - B_{calc}(y_i)\right)^2} \qquad (15)$$

As soon as the error function goes to its possible minimal vale the model current density profile in its turn approaches the real current distribution in the tape. Here $B_{exp}(y_i)$ is the experimentally measured profile of the magnetic field, and $B_{calc}(y_i)$ is the magnetic field calculated from the model current density profile by means of Biot-Savart law. The crucial point of the method is to

present the initial model current density profiles that will be used to initiate calculation. The initial shape of current density profile could be an arbitrary, but in some cases, it will impact the final result of calculation.

The Combined Method

In the combined method as the first step, the method of solution of the set of linear equations is applied. It gives the preliminary solution, which is used as an input current density profile $B_{calc}(y_i)$ in the method of least squares. This combination of two methods provides us with more detailed and accurate analyse of current density distribution. Moreover, it allows the control of the multiple solution problems.

6.3 Check for the calculation model

In order to verify our current density calculations model, we use a 10mm width pure copper tape (99.99% pure copper) for 1D and 3D scanning experiment as explained in chapter 4. The copper is a normal conductor and its current density distributions in both one and two-dimensional distribution are known and represent a good tool to check our inverse problem solution adaptability.

First we applied a 40 A DC current to the copper tape and we made a 1D magnetic field scanning measurement of the self-magnetic field profile of the copper tape. Fig. 65 shows the scanned self-magnetic field profile.

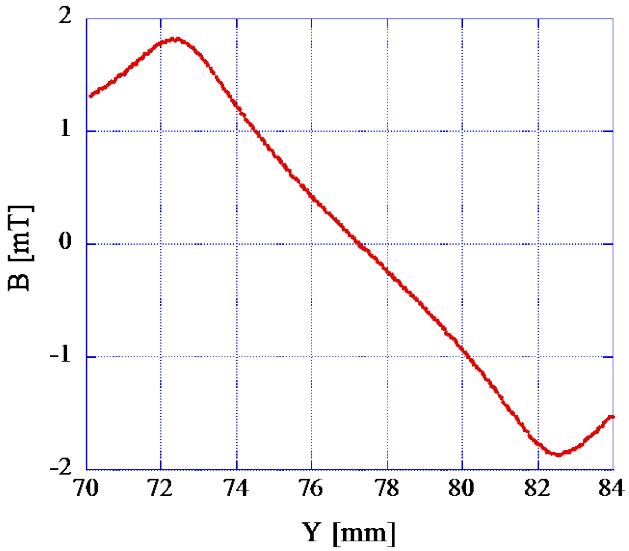

Fig. 65 Magnetic field profile of the copper tape.

We calculate then the 1D current distribution of the current density in the copper tape. Fig. 66 shows the one-dimensional current distribution in the copper tape. As we can see, the current density profile is almost uniform. This profile is, in fact, characteristic profile for a constant DC current conducted profile in pure conductors. We can confirm then that our method is useful to calculate the 1D current density distribution in HTS tapes.

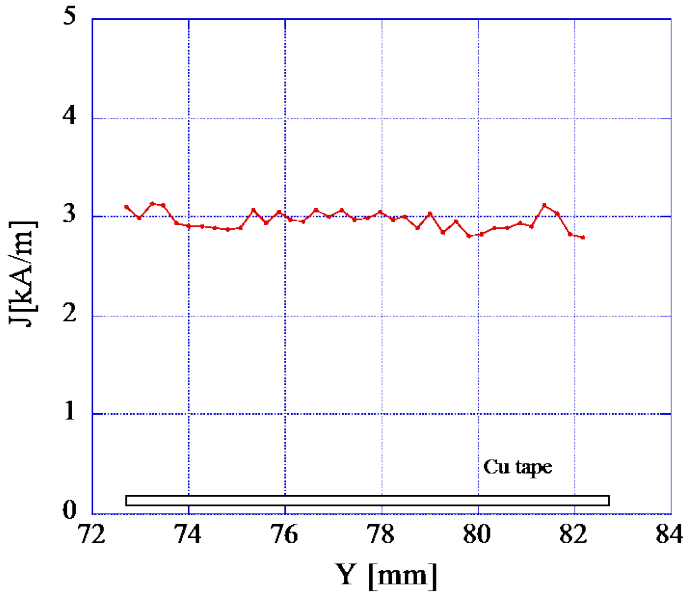

Fig. 66 One-dimensional current density profile of the copper tape.

In the case of the two-dimensional current density check we made the 3D self-magnetic field measurements via the 3D Hall probe when the copper tape is in the same condition as the HTS tapes at DC current feeding operation, means in liquid nitrogen and with 100 DC current applied current. We scanned 0.8 mm within the copper tape width along the Y-axis with 0.1 mm steps along X-axis and Y-axis. Fig. 67 shows the self-magnetic field profiles of the scanning operation. We show also the Bz, By and Bx component of the total scanning in figures 67.a, b, and c.

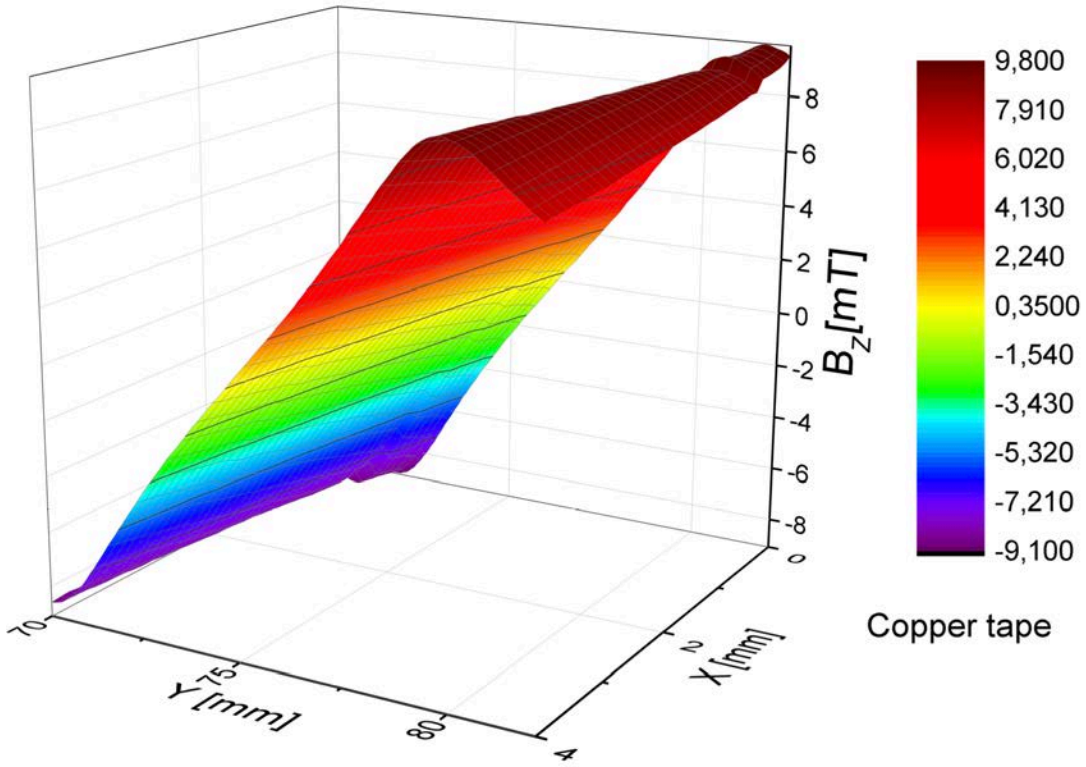

Fig. 67. a B*z* components of the 3D self-magnetic field map (copper tape).

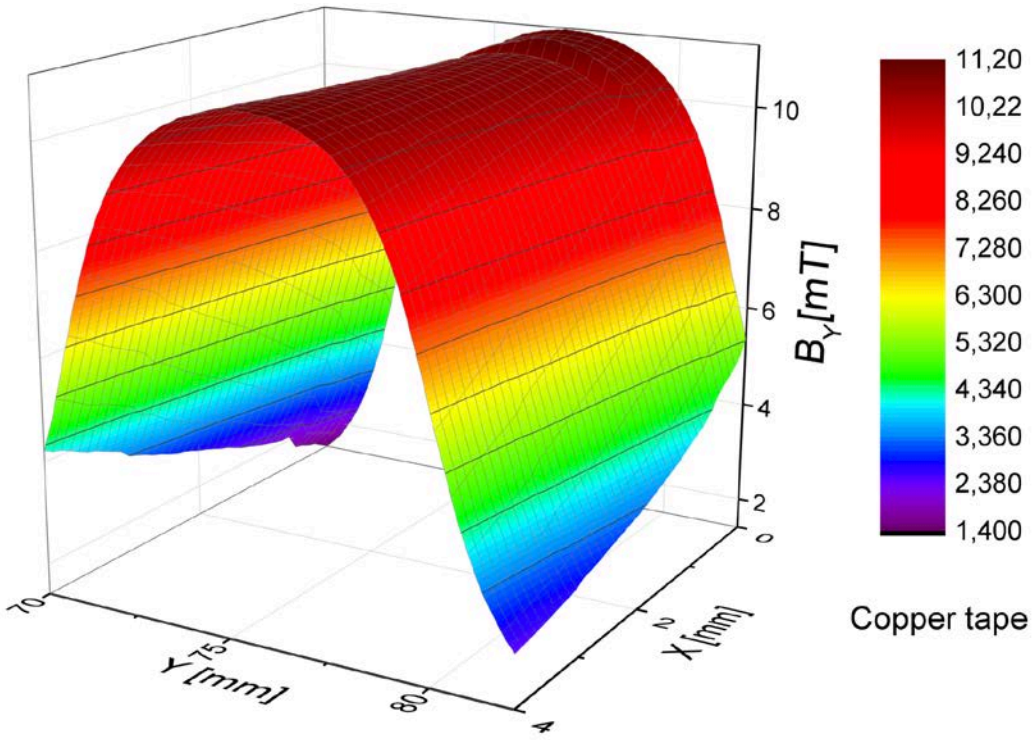

Fig. 67. b B*y* components of the 3D self-magnetic field map (copper tape).

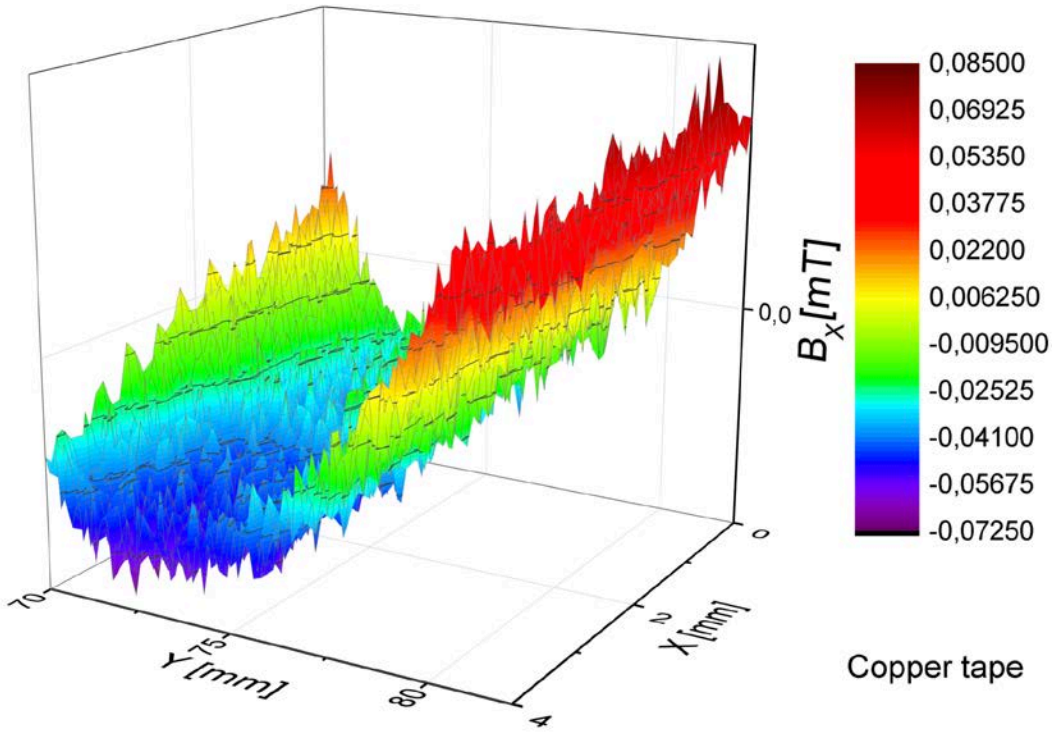

Fig. 67.c B*x* components of the 3D self-magnetic field map (copper tape).

We calculate then the two-dimensional distribution of the current density of the copper tape by the application of our two-dimensional current density calculation model. As the 1D current density distribution results, we got a uniform current distribution in the copper tape as shown in Fig. 68.a and Fig. 68.b. This distribution is almost uniform within the copper tape's width and we can assume that our method is relevant for 2D current density distribution in the HTS tapes.

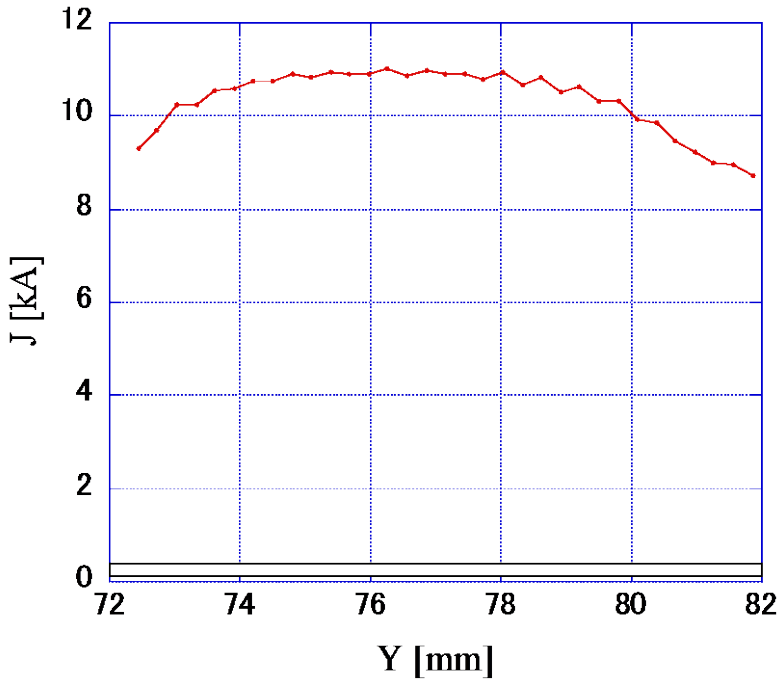

Fig. 68. a One-dimensional current density profile of the copper tape calculated from data in Fig. 67.a.

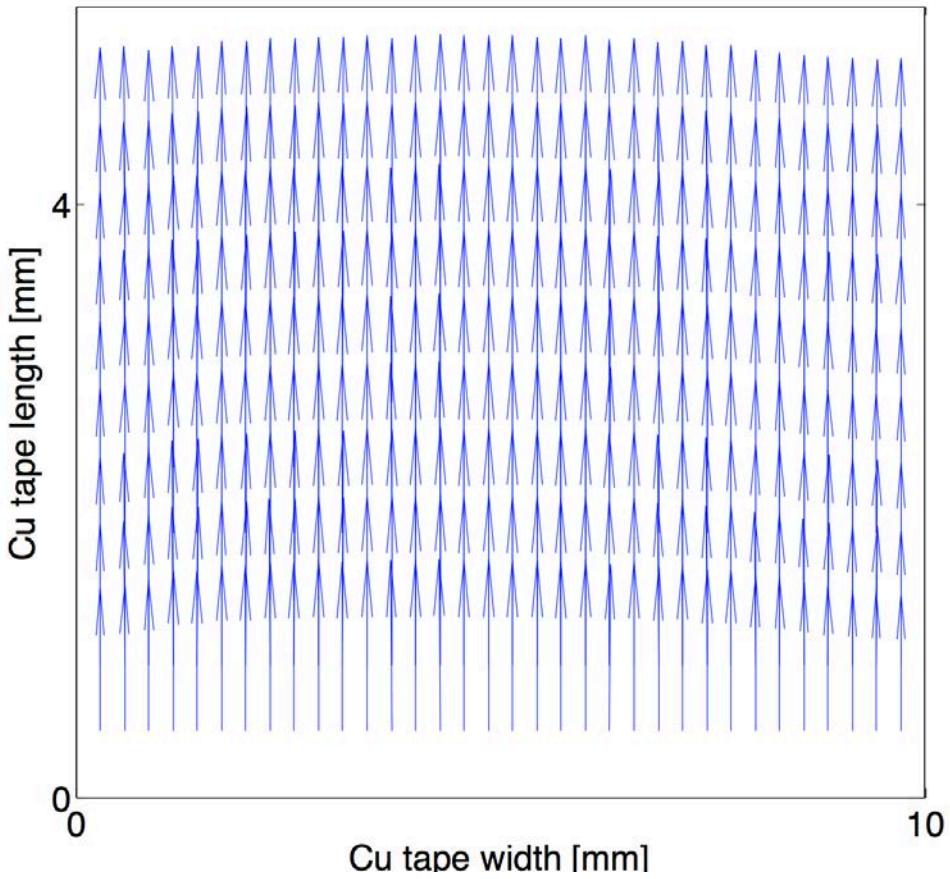

Fig. 68. b Two-dimensional current density profiles of the copper tape calculated from data in Fig. 67.

We conclude that our inverse problem method is useful to get one and two-dimensional current density distributions profiles for the HTS tapes used in this thesis.

6.4 Summary

A sample model of linear equation resolution method is used in the current distribution calculations basing on solving linear equations of the Biot-Savart inverse problem technique. The model of calculation of the one and two-dimensional distributions of the current density in the HTS tapes was presented. We used the current distribution of the a copper tape as a model to check the results and our results prove that our model of calculation gives prevented results and shows the ability to solve the inverse problem in the case of the HTS tape used in this thesis.

Contribution: This chapter is based on the following papers:

- M. Tallouli, J. Sun, A. Ninomia, M. Hamabe, H. Watanabe, et al, '' Residual magnetic field measurement of BSCCO and YBCO tapes by a Hall probe, '' *IEEE Trans. Appl. Supercond*., vol. 25, p. 8000704, June 2015, (4 pp.)

- Oleg Shyshkin, Yuri Kazarinov, Moahmed Tallouli, Tosin Famakinwa, Satarou Yamaguchi, '' Inverse Problem Solution Algorithms for Current Density Distribution Calculation in Different HTS Tape Configurations Basing on Minimum Self- Magnetic Field Measurements,'' *IEEE Trans. Appl. Supercond.,* vol. 26, no. 3, p. 9000404, Apr. 2016. (4 pp.)

CHAPTER 7. CALCULATION RESULTS

7. 1. Introduction

The new step in the world electric power supply systems is the use of long-length HTS tapes in electric power transmission cables to transport large DC currents. It is obvious that long-length cables are exposed to the fault conditions or technical defects during the operation of DC power transmission lines [65, 66]. One of the crucial events that could affect the performance of the current transport is the over-current pulse that originates from defects electrical power devices. The value of the current during the over-current pulse exceeds the critical current significantly, so it could locally affect the superconductivity. The resulting heating effects and thermal instabilities could sometimes damage the HTS tapes. That is an important reason to study the over-current pulse effect on the transport current distribution in superconducting tapes, from the point of view to examine the restart-ability of the cables. To study the transport current density distribution in HTS tapes, the vertical component of the self-magnetic field was measured the by means of a Hall probe above the tape, and then the inverse problem was solved to obtain the current density profiles. Previous researchers, studying the over-current pulse effect on tapes, discussed the overall characteristics of the HTS tape and the power converter circuit, and did not discuss the current density profiles of the HTS tape and its related phenomena. The magnetic field decay or relaxation observed in Bi-2223 tapes is usually understood as the influence of relatively small value of n-value and the change of current profile after applying a high magnetic field pulse or an alternative current [67, 68]. And in the case of a thin strip such as YBCO coated conductor, the analytical solution also was obtained by the critical state mode [69, 70]. But, in this thesis, we show relaxations of the vertical component of the self-magnetic field above the BSCCO tape edge and a constant self-magnetic field for the YBCO AMSC tape without

application of an external magnetic field pulse or alternant current. We show also a loop of current in the case of the YBCO tape, not observed in BSCCO tape after an over-current pulse operation. These self-magnetic field relaxations above tape's edges last for almost 30 min and is an evidence of current density redistribution in the tape during the DC current feeding phase.

HIGH temperature superconductor tapes are a key issue of superconducting technologies such as power cables. Power grid assembled from the HTS power cables can have problems caused by short circuit or overcurrent. Therefore a quick interruption is required in such fault conditions to protect superconductor cable. To restart the system, we should consider the remnant current density profiles after the transport current cut-off. These remnant current density profiles affect the performance of the cable and depend on the transport current cut-off speed. Scanning Hall probe measurement of residual magnetic field followed by a current density calculation constitutes a direct tool to study such characteristic [71, 72].

In the other hand, Hall probe scanning has the potential for the simple and non-destructive study of the quality of longitudinal uniformity of HTS tapes. And because HTS tapes are key issues of important various superconducting technologies such as power cables and superconducting magnets, these technologies require high-quality HTS tapes characteristics including longitudinal current density uniformity even for the phase of current-off. Therefore, we made a scanning Hall probe measurement of the residual magnetic field followed by a current density calculation constitutes a simple and direct tool to study such characteristic [73]. In this chapter, we present the calculations of the current density distribution from the magnetic field profiles obtained by means of the one-dimensional hall probe measurement and performed by the inverse problem solution.

7.2. Over-current pulse effect on current density distribution in HTS tapes

7.2.1 Over-current effect on the current density profiles

We present here the results of the current density distribution of the HTS tapes after applying the over current pulse operation. For the BSCCO tape, the current density profiles changed with time because the self-magnetic field decay at edges, as shown at Fig. 69.

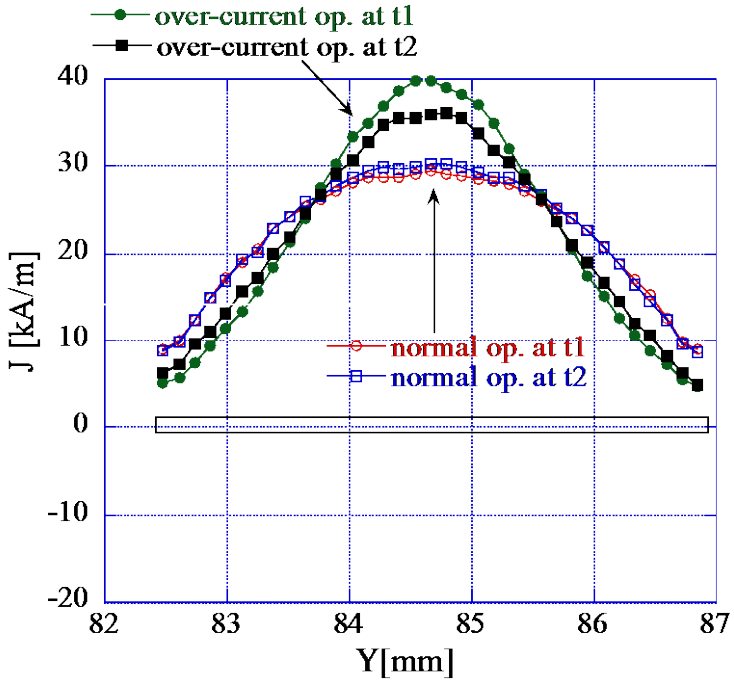

Fig. 69 The current density profiles measure above of the BSCCO tape from data shown in Fig. 51.

We used two-dimensional model (sheet current model), so the unit of current density is ampere per meter (A/m). The thickness of the HTS tape is 0.25 mm without the copper-alloy lamination for the BSCCO tape and 1 μm for the YBCO tape. Therefore, For the BSCCO tape, the actual current density at the peak decays from 160 A/mm^2 to 140 A/mm^2 within 30 minutes, which corresponds to 2 mT of measured magnetic field decay at the edge. The current density profile is broadening during this 30 minutes. The full width at half maximum corresponds to

almost 2 mm, which means almost 50% of the tape width (width= 4.5 mm). And current density profiles are peaked at the center.

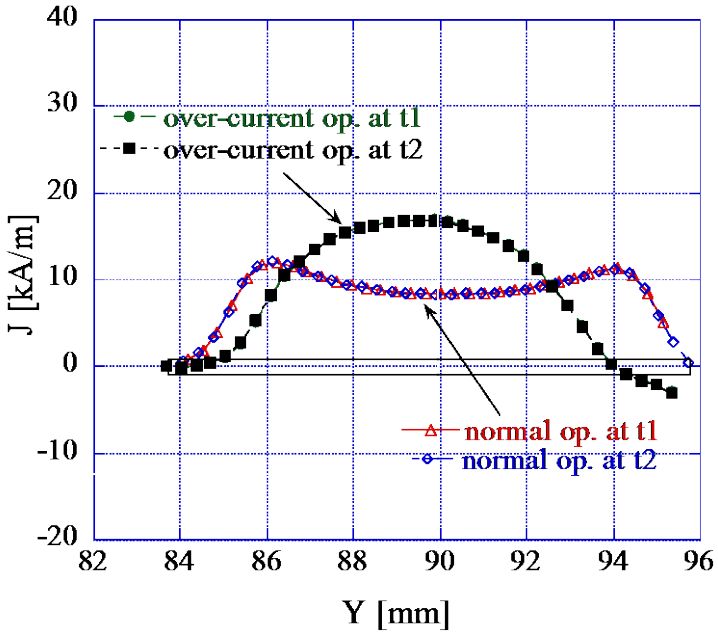

Fig. 70 The current density profiles measure above of the AMSC tape from data shown in Fig. 52.

For the YBCO (AMSC) tape as in Fig. 70, the two current density profiles at t1 and t2 for the normal operation are identical, and same thing for over-current operation. The current density is peaked for the over-current operation and boards for the normal operation. The current density at the center is 16700 A/mm^2 for the over-current operation and 9000 A/mm^2 for the normal one. The full width at half maximum corresponds to almost 10 mm corresponds to 83% decrease to only 6mm correspond to 50 % for the over-current operation. However, the applied current is positive, we remark a negative distribution of the current density close to one edge of the HTS tape that reaches 1000 A/mm^2 conducted by almost 2 mm from one tape's edge. This distribution can be related to current loop caused by the over-current pulse.

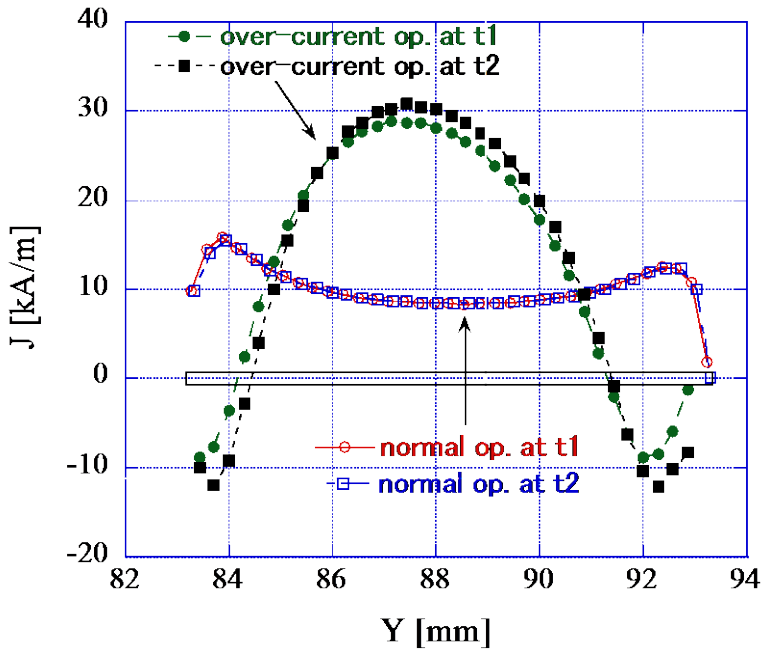

Fig. 71 The current density profiles measure above of the Fujikura tape from data shown in Fig. 53.

For the YBCO (Fujikura) tape as in Fig. 71, the two current density profiles at t1 and t2 for the normal operation are also identical, and the same thing for over-current operation. The current density is peaked for the over-current operation and boarded for the normal operation. The current density at the center is 30000 A/mm^2 for the over-current operation and almost 9000 A/mm^2 for the normal one. The full width at half maximum corresponds to almost 10 mm corresponds to 100% decrease to 6 mm corresponds to 45 % in over-current operation. We remark also for this HTS tape, a negative distribution of the current density close to both edges that reaches -10000 A/mm^2 conducted by almost 2 mm from each tape's edges.

7.2.2 Discussion of the over-current pulse effect-on the current distributions

For the normal operation, the current is conducted by the superconductor part of the HTS tape (superconductor filaments for BSCCO and the superconductor layer for YBCO tapes). The current density profile for BSCCO tape is a hill profile. The current density at the centre of the

BSCCO tape is maximal because the density of the superconductor filaments is higher at the centre of the HTS tape. The magnetic diffusion time depends on both superconducting filaments and the silver matrix because the measured self-magnetic field at the edges was changing with time for 10 min. However, for the YBCO tapes, the profile is hollow profile. The current is higher at the edge of the YBCO tape due to the low self-magnetic field penetration from the edges. In the case of the AMSC tape, the current density profile is symmetrical for the tape's centre because the uniform structure includes the superconductor layer and the copper and Ag stabilizers of the tape cross-section. In spite of not using the metal stabilizer in Fujikura tape, a symmetrical profile is observed, too.

The self-magnetic fields at the edges of BSCCO and AMSC tapes are changing with time. Their characteristic time is around 10 min, which is longer than the self- magnetic field penetration time in a silver matrix, and shorter than YBCO superconductor layer magnetic diffusion time. Therefore, in order to understand the phenomena, we should study the interaction research of superconductor and silver matrix.

When we applied an over-current pulse reaching 900 A during 5 ms to the BSCCO tape, current exceeds its critical current (Ic = 200 A). The silver matrix near the edge would mainly conduct the current during the pulse. After the pulse, the superconducting filaments carry the current around the centre.

The quick reduce of the current pulse from 900 A to 100 A induces an opposite electric field to reduce the current. This electric field generates eddy current at the edges zone, which opposes the current density diffusion, and reduces the current density especially near edges. The current density profile is then peaked at centre and current density around edges is lower than those of the normal operation.

When the constant current (100 A) is conducted on the BSCCO tape, the self-magnetic field at the edges is relaxing for almost one hour because is changing at the edge as shown in the experiment results (Fig. 45)

The magnetic field diffusion in a tape [59] corresponds to the general solution of the two-dimensional diffusion equation given by:

$$\frac{\partial^2 B_z}{\partial x^2}+\frac{\partial^2 B_z}{\partial y^2}=\frac{1}{\kappa_0}\frac{\partial B_z}{\partial t}$$

Where $\kappa_0=\frac{\eta}{\mu}$ is the magnetic diffusivity, η is the electrical resistivity and μ is the magnetic permeability.

If we consider the decay of the magnetic field in a rectangular tape with side 2a and 2b, general solution can be simplified to

$$B_z(x,y,t)=\frac{16}{\pi^2}B_0\exp\left\{-\frac{1}{4}\pi^2\kappa_0 t(\frac{1}{a^2}+\frac{1}{b^2})\right\}\cos\frac{\pi x}{2a}\cos\frac{\pi x}{2b}$$

B_0 is the magnetic field peak after pulse. Here we see that the characteristic decay time τ_0 is

$$\tau_0=\frac{4}{\pi^2(\frac{1}{a^2}+\frac{1}{b^2})\kappa_0}$$

The magnetic diffusivity coefficient $\kappa_0=\frac{\eta}{\mu}$ contains: the magnetic permeability μ (that can be very large compare to μ_0 for ferromagnetic materials [9]) and the resistivity coefficient η(for the copper/silver matrix $\eta\sim10^{-9}\Omega m$). Thus for diffusion process the AMSC tape, which contains Ni-5at%W ferromagnetic texture, behaves as if its conductivity increased by a factor μ_R. The time decay is then very short for the AMSC tape.

However the time decay for BSCCO tape is long which might correspond to a small magnetic diffusivity and then long relaxation process.

Never though, the long relaxation process of the self-magnetic field near the tape's edge is a subject for future research.

After the over-current pulse operation, since the negative electric field is induced, the current density near the edge is negative for the YBCO tapes. And this situation also induces a peaked current density profiles at the centre carrying the constant 100 A. In the case of the AMSC tape the silver matrix is used as stabilizer. Therefore, the silver matrix consumes this electric current. On the other hand, for the Fujikura case, silver matrix is not used. Therefore the electric current is not consumed and a negative magnetic field at the edge is higher than those of the AMSC's tape (see Figs. 66 and 67).

This phenomenon might depend on the permanent current near the tape's edge, and it's a subject for further research. A negative value of the current density for the AMSC tape is measured in one side, due to the symmetry of tape structure. But for the Fujikura tape, which doesn't contain a stabilizer, we should discuss the self-magnetic field diffusion process in the superconducting layer, because the superconducting layer is insulated from the Hastelloy tape and the HTS protection layer.

Since the self-magnetic field at the edges of the AMSC tape is not constant for 100 A DC current, magnetic field relaxation process should exist. The current is not conducted with the superconducting YBCO layer only. The current is peaked almost at centre sharply in opposition to the normal operation for HTS tapes. Only for the AMSC and BSCCO tapes, the limited time over-current pulse changes the current density profiles but didn't harm the HTS tape. That should be considered for power cable restart and design. Because HTS tapes make the power

cable, current-off operations will affect current density profiles and it is indispensable to have a stabilizer in HTS tapes for power application.

7.3 Calculation of the permanent current in HTS tapes

7.3.1 One-dimensional permanent current calculation

We used in this the inverse problem technique discussed in chapter 6 to calculate the remnant current density profiles corresponding to each HTS tape measured at the different X positions.

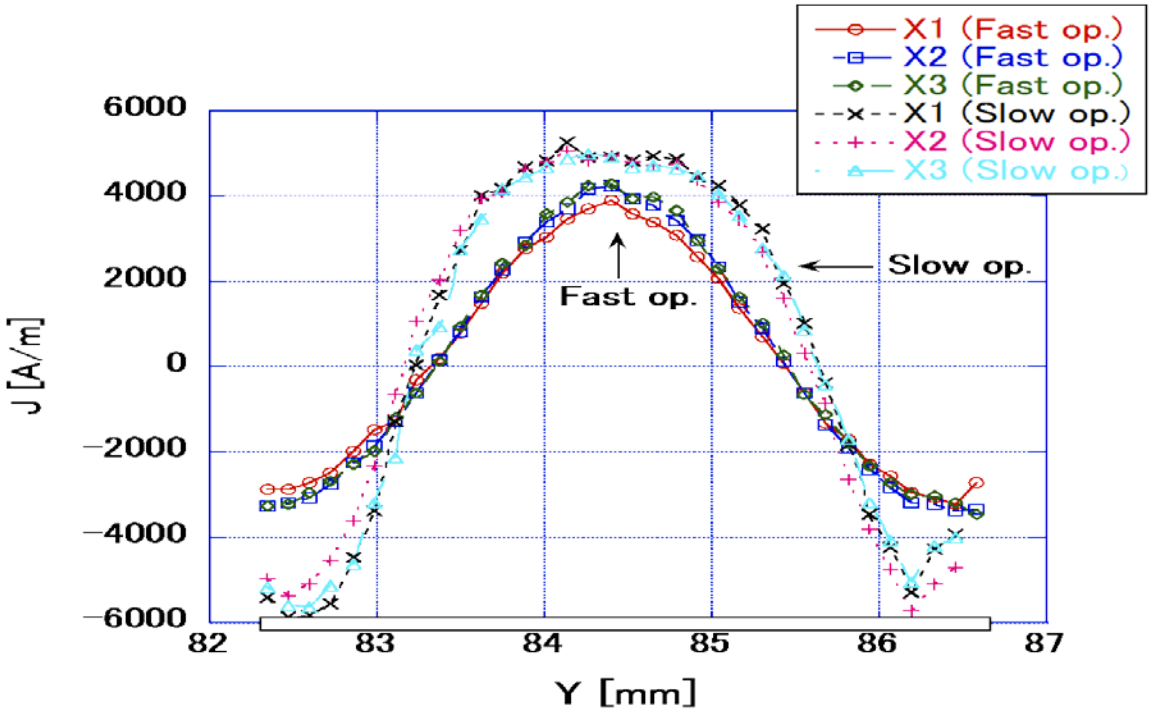

Fig. 72 Current density profiles of the BSCCO tape at different longitudinal positions calculated from data shown in Fig. 54.

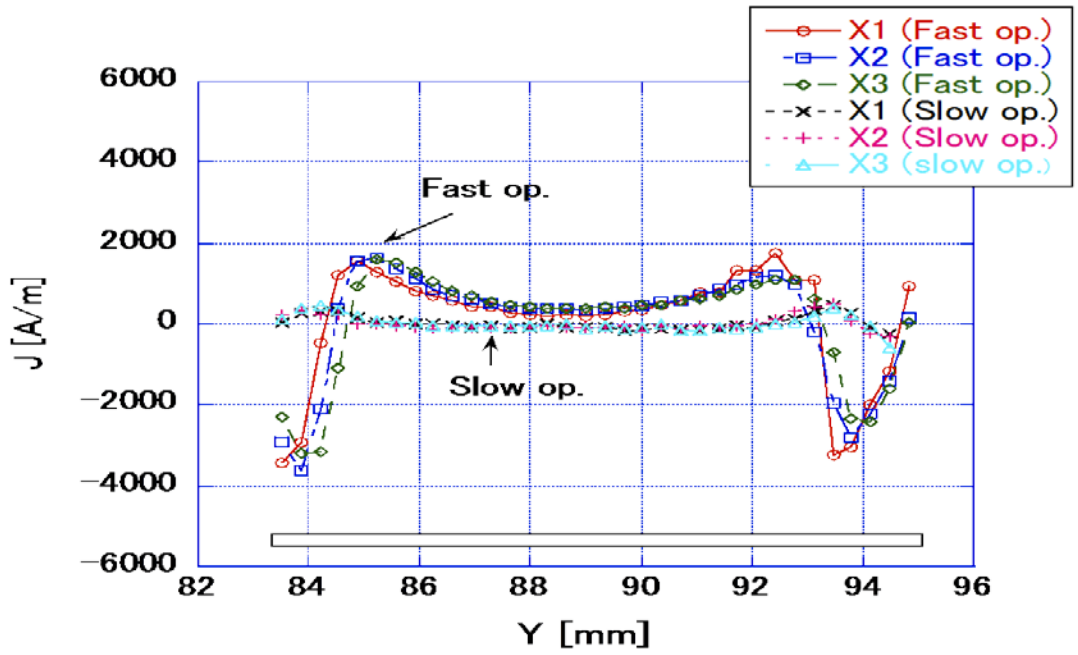

Fig. 73 Current density profiles of the YBCO tape at different longitudinal positions calculated from data shown in Fig. 55.

From each vertical component of the residual magnetic field we calculated the current density profile. For the BSCCO tape and the YBCO tape we got six current densities. For both cut-off operations we got three current density profiles corresponding to X-axis positions along the HTS tape as in Fig. 72 and Fig. 73.

7.3.2 One-dimensional current density distribution in both current-off operations

The profiles of the residual magnetic fields in BSCCO tape are almost the same on the direction of transport current. Therefore, their current density profiles along this direction are almost the same. They are almost symmetric for the center of the tape, which means that the uniformity of the BSCCO tape is high. In the case of YBCO tape, the residual magnetic fields are different for different coordinates along the tape that is the evidence of the inhomogeneity of the YBCO tape. This is the fundamental difference between these two tapes in the present

samples.

The peak current density is higher for the slow cut-off operation as compared with the fast cut-off operation for BSCCO tape, and this tendency is reverse of the resistive materials, such as copper. The reason would be the shielding effect of the matrix material. The copper and silver are used as the matrix materials for BSCCO, and these materials would consume high electric energy before it comes to the superconductor filaments. In case of 1 A/s decreasing operation, high electric field can penetrate into the HTS tape, and induce the permanent current.

Different magnetic field profiles can be observed for YBCO tape. They are not high uniform like the BSCCO ones. The amplitude of current densities in fast cut-off operation is almost four times higher than these of the slow cut-off operation.

The quality of the BSCCO filaments near the edge would be lower than the centre's. This is one of the reasons why the current density profile is peaked at the center, which is not true for YBCO. We should consider the shielding effect of the superconducting filaments and the matrix materials, such as copper and silver. These resistive materials can consumes electric power. On the other hands, the quality of the superconducting layer of the YBCO tape would be the same all over the tape. This is the reason that the current density is high near the edge.

Since the behaviours of the YBCO and BSCCO tapes are different each other for the fast and slow current cut-off operations, we should consider these phenomena for HTS cable applications.

7.4 Homogeneity of the HTS tapes

7.4.1 One-dimensional current density distribution and homogeneity

As it was mentioned before, the magnetic field scans of BSCCO tape indicate the uniformity of the current distribution along the tape (See Fig. 74). One can see that all three current density

curves match each other very accurately. The constraint of the calculation involves the total current of zero. The current maximum corresponds to the tape center and its distribution is symmetric and uniform along the X direction. The full width at half altitude corresponds almost to half the tape.

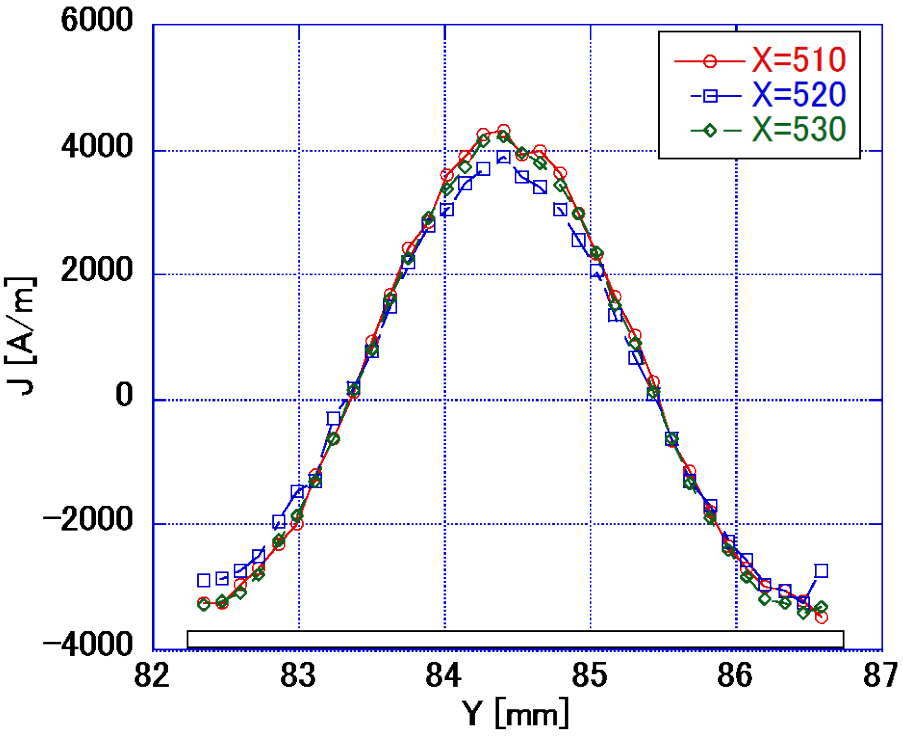

Fig. 74 Current density profiles at different X-axis positions of BSCCO tape calculated from data shown in Fig. 56.

In the case of YBCO tapes, with layer structure and different from the BSCCO with filament structure, we observe quite different behaviours of current density profiles. The perpendicular components of residual magnetic fields and their corresponding current densities change in amplitude and shape along the X direction.

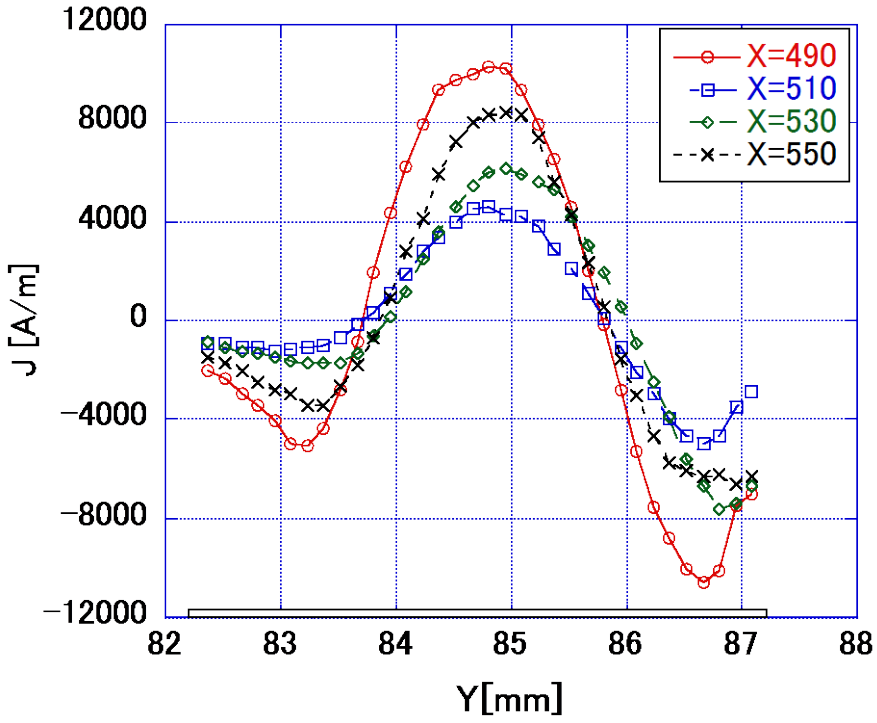

Fig. 75 Current density profiles at different X-axis positions of YBCO SWCC tape calculated from data shown in Fig. 57.

For YBCO SWCC tape, the perpendicular component of the magnetic fields is not symmetry for the center axis of the taper and identical along the longitudinal direction (See Fig. 71). And consequently, as it was expected, their corresponding current density profiles are also not uniform and symmetry for the center axis of the tape. They are different in shape and amplitude along the X direction. Here, we should point that the applied transport current of 100A is close to the critical current of YBCO SWCC tape. In cases of BSCCO tape and AMSC tape, the transport current of 100A is far below their critical current.

Concerning YBCO AMSC tape, it is wider than BSCCO so in result even the perpendicular component of the residual magnetic field amplitude is not high like the other tape, and almost the same (see Figs. 76 and 77) their corresponding current density profiles are lower compare to BSCCO and less uniform along the longitudinal axe as their residual magnetic fields source. (But it is rather better than SWCC tape)

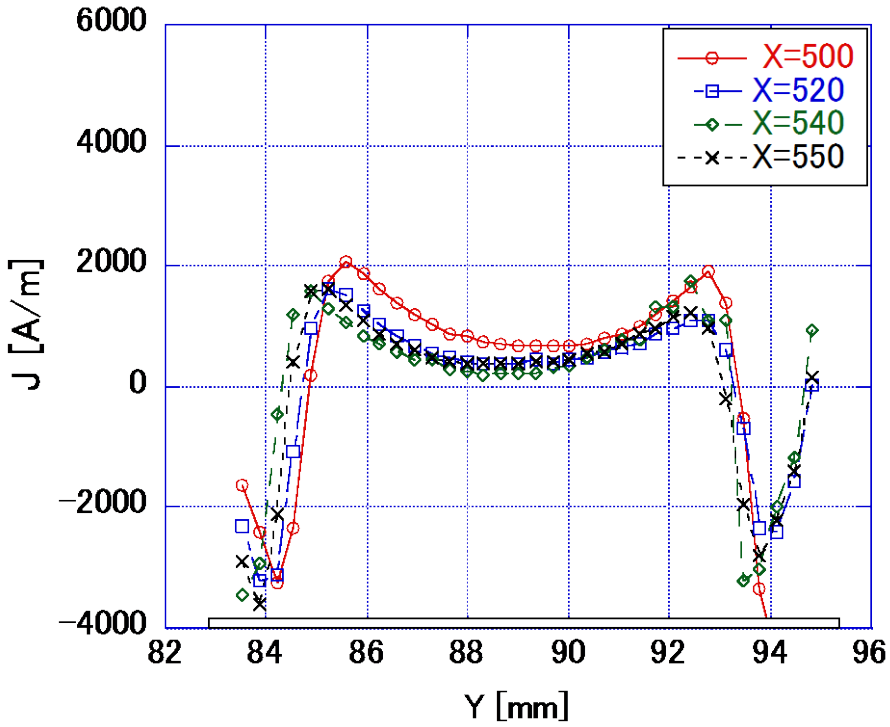

Fig. 76 Current density profiles at different X-axis positions of YBCO AMSC tape (Applied current =100A) calculated from data shown in Fig. 58.

When we raised up the applied current to 250 A for 20 min before cutting the current which is close to the corresponding critical current, we remark that the inhomogeneity of AMSC current density profiles becomes higher and the profile is asymmetry for the center axis of the tape. This tendency is closer to SWCC current density profiles ones (see Fig. 73).

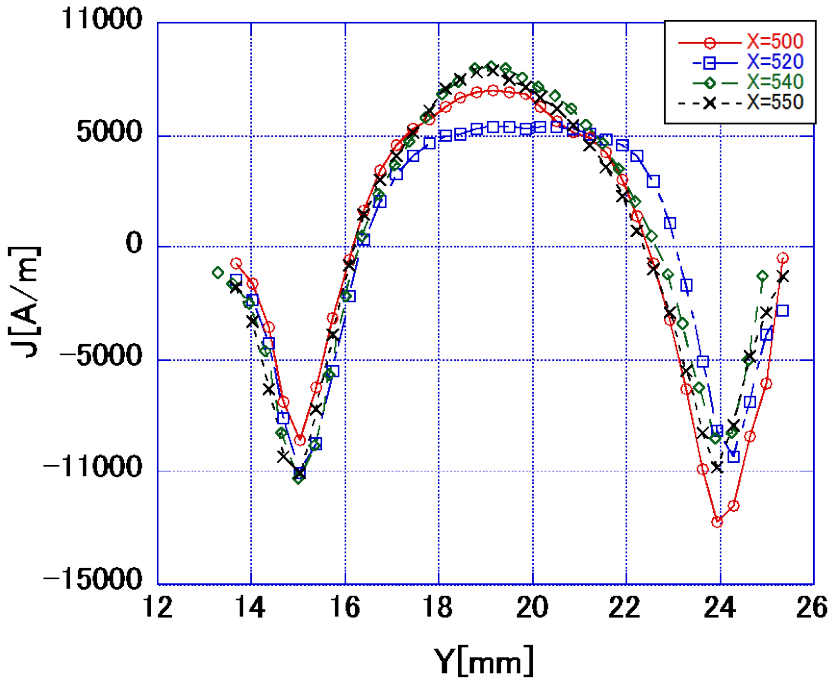

Fig. 77 Current density profiles at different X-axis positions of YBCO AMSC tape (Applied current =250A) calculated from data shown in Fig. 59.

7.4.2 Effect of the HTS tapes structures on the current density homogeneity

The perpendicular component of the residual magnetic field and their corresponding current density profiles for three types of HTS tape are demonstrated in this paper.

To study current density homogeneity we calculated the total remnant current for each BSCCO and YBCO tapes corresponding to each longitudinal positions. We integrate then the positive part of current density profiles, which we called Ipos and then we deduced the total current or remnant current Itot which is equal to Itot= 2 * Ipos.

BSCO (100A)	CURRENT DENSITY PROFILES	
X=510	Ipos=5.618A	Itot=11.236A
X=520	Ipos=4.912A	Itot=9.824A
X=530	Ipos=5.424A	Itot=10.848A

Table 7. Total remnant current in BSCCO tape.

YBCO SWCC (100A)	CURRENT DENSITY PROFILES	
X=510	Ipos=14.083A	Itot=28.166A
X=520	Ipos=5.838A	Itot=11.676A
X=530	Ipos=7.982A	Itot=15.964A
X=550	Ipos=10.497A	Itot=20.94A

Table 8. Total remnant current in SWCC tape.

The average of the remnant current after applying 100 A of DC current to BSCCO tape is 10.64 A and the Standard deviation quantity StD used to indicate amplitude fluctuation between current density profiles is 0.7% which is low. We can say then that current density profiles for BSCCO tape are highly homogeneous.

For YBCO SWCC tape the remnant current is equal to 19.2 A, which is higher than BSCCO tape for the same applied current and the StD is 7.1% (almost 10 times StD of BSCCO). We can see that the remnant current for the same 100 A of applied current for BSCCO and SWCC YBCO tape are different. It's higher but less homogeneous in the case of SWCC YBCO tape.

To compare SWCC and AMSC tapes we calculated the remnant current of AMSC HTS tape with 100 A of applied current.

YBCO AMSC (250A)	CURRENT DENSITY PROFILES	
X=500	Ipos=28.928A	Itot=57.856A
X=520	Ipos=25.638A	Itot=51.276A
X=540	Ipos=26.843A	Itot=53.686A
X=550	Ipos=26.915A	Itot=53.83A

Table 9. Total remnant current in AMSC tape (After 100 A of DC current).

After current density integration we had Itot = 14 A and the StD= 3%. We can assume that AMSC is more homogenous than YBCO tape but still lower than BSCCO. This property of AMSC tape can be related to its high critical current and wider size compare to SWCC tapes (see Table. I).

For this reason we calculated the remnant current for AMSC tape after 20 minutes of 250 A of DC applied current.

YBCO AMSC (100A)	CURRENT DENSITY PROFILES	
X=500	Ipos=9.307A	Itot=18.614A
X=520	Ipos=6.217A	Itot=12.434A
X=540	Ipos=6.301A	Itot=12.602A
X=550	Ipos=6.09A	Itot=12.18A

Table 10. Total remnant current in AMSC tape (After 250 A of DC current).

In this case Itot is equal to 54.16 A which is almost 7 times higher than the case of 100 A of applied current for the same tape. StD is 2.7% means almost same with the case of 100 A of applied current. Homogeneity then becomes higher for higher HTS tape critical current amplitude (119 A for SWCC and 300 A for AMSC).

We can conclude that the inhomogeneity of the HTS tapes may depend on the magnitude of the applied current, processes of manufacturing, the critical current and the width of the HTS tape. We conclude also that if the HTS tape critical current is low, the inhomogeneity is high. Which means that the homogeneity of the BSCCO tape is high relatively. Among a temperature range from 4K to 89K, the persistent current shows a slow decay at low temperature. However, the current of sintered YBCO at 77K shows a fast decay. In case of melt-textured YBCO and sintered BSCCO, the current decays slowly in any temperatures. The homogeneity of the current density profiles and the residual magnetic field profiles would so show the performance of the HTS tapes.

In case of BSCCO tape we observe the fact that the magnetic field scans are almost the same along the tape that confirms the homogeneity of current distribution along the tape.

Rather different situation is observed in case of two other tapes. The magnetic field scans are very different for each tape that predicts the strong inhomogeneity of current distribution in the case of YBCO SWCC tape which was operated under the current close to the critical one. Less inhomogeneity is observed in the case of YBCO AMSC tape. The results obtained from the experiments provide a way to compare distribution and longitudinal uniformity of current density profiles in different HTS tapes. The conclusion can be drawn regarding this experiment:

- The longitudinal uniformity of BSCCO tape is better than YBCO tapes'.

- The YBCO tape structure has a strong impact on the longitudinal uniformity of the current density that is confirmed by the measurements of amplitude, shape and distribution of the perpendicular component of the residual magnetic field.

7.5 2D permanent current

7.5.1 2D residual current density configuration in the HTS tapes

We discuss here the results of the fast switch of operation on the two-dimensional remnant current density. We used the inverse problem technique discussed above to calculate 2D current density map corresponding to each HTS tape. We get then 1D current density for each magnetic field scanning along the Y-direction for the three tapes. And after scanning all the 1cm area we got the 2D current density distribution. Three components of the residual magnetic field and their corresponding 1D and 2D current density profiles for three types of HTS tape are demonstrated in this chapter.

To study current density homogeneity we calculated the total remnant current for each BSCCO and YBCO tapes corresponding to each longitudinal positions. We draw then the 2D configuration of the residual current density of HTS tapes. We can conclude that the inhomogeneity of the HTS tapes may depend on the magnitude of the applied current, processes of manufacturing, the critical current and the width of the HTS tape. In Fig. 78 we see the results for the residual current distribution of the BSCCO tape. An arrow presents the amplitude of the current density and its direction. More the arrow is long more the amplitude of the current is higher. The current densities of the other two YBCO tapes are also presented, at 10 mm along the AMSC tape and 7 mm along the Fujikura tape as shown in Fig. 79 and 80.

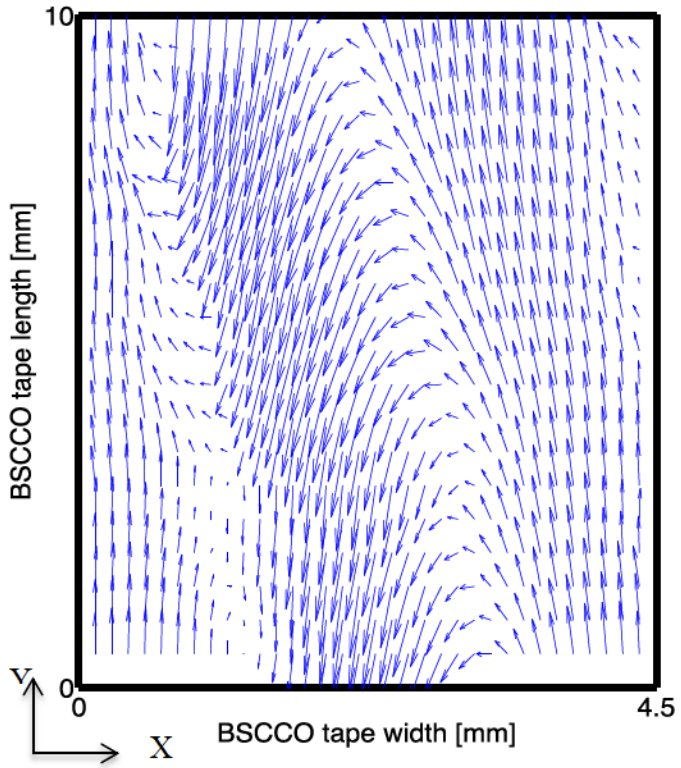

Fig. 78 2D short circuit current density profiles of the BSCCO tape calculated from data shown in Fig. 60.

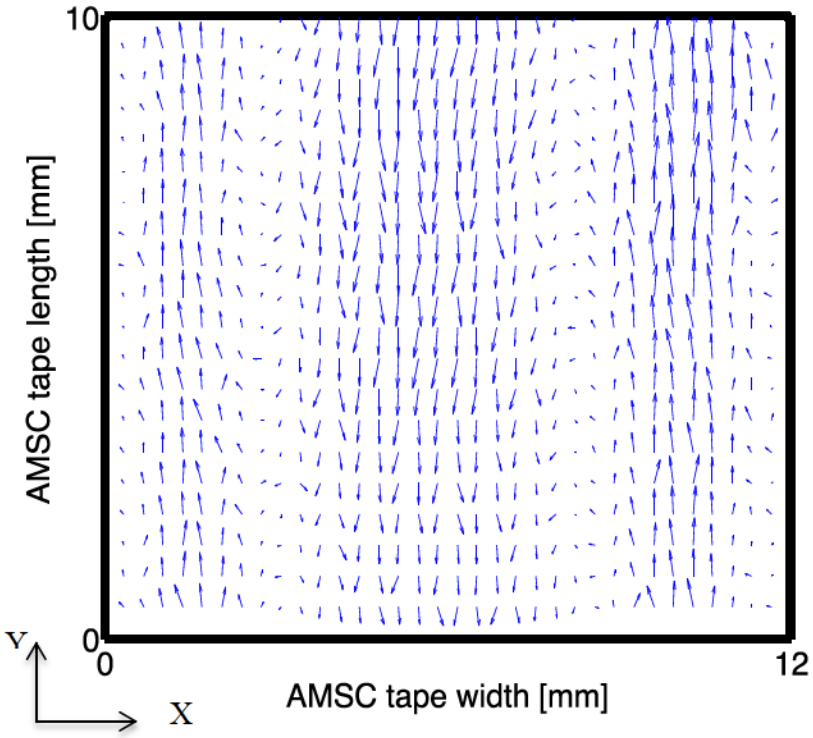

Fig. 79 2D short circuit current density profiles of the AMSC tape calculated from data shown in Fig. 61.

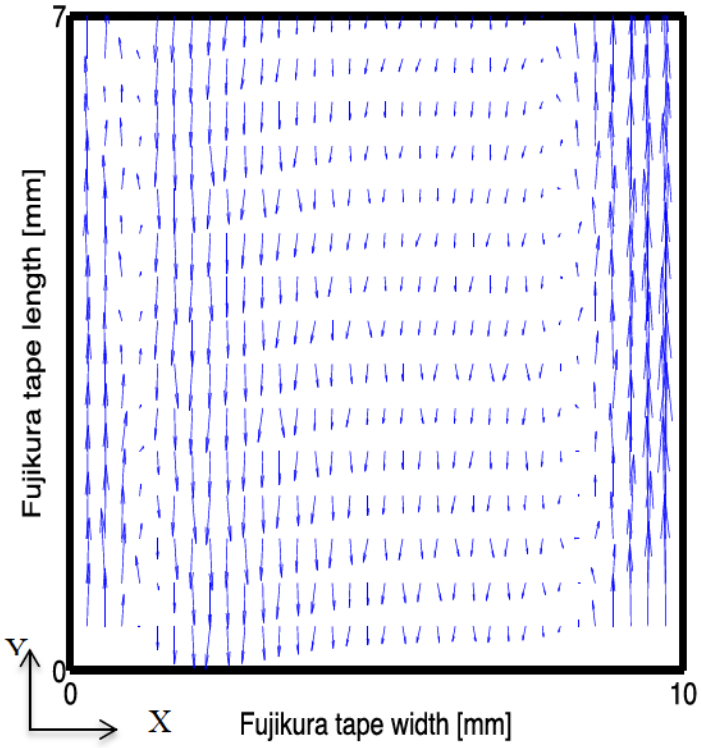

Fig. 80 2D short circuit current density profiles of the Fujikura tape calculated from data shown in Fig. 62.

7.5.2 Discussion of 2D residual current density distribution in the HTS tapes

For the BSCCO tape, we observe different 3D magnetic field maps along the tape. In fact, Bz amplitude changes in 10 mm part of the BSCCO tape. That predicts an inhomogeneity of current density distribution and might depend on the manufacturing of this tape.

In Fig. 78 the 2D residual current density distribution shows a high density of superconducting filaments at the center and two directions of the current. One direction is via the tape's edges and the second direction via the tape's center. The residual current density at the edges is not symmetric, which proves that the quality of the superconductor filaments is not same. Our observation might indicate a defection of the BSCCO tape observed in the 2D residual current density distribution.

On the other hand, the residual current flow at the center is not parallel to the tape's length direction. The superconductor filaments inside the BSCCO tape might be overlapped due to fabrication procedure. The quality of superconducting filaments is then not homogenous.

We can observe also in Fig. 74 a vortex-like structure of current density vectors inside the BSCCO tape.

For the YBCO tapes, the 3D self-magnetic field scans are almost the same along the tape longitudinal direction, indicating a high homogeneity. We show in Figs. 61 and 62 the magnetic field components of the AMSC and Fujikura tapes.

In the 2D residual current density profiles shown in Figs. 79 and 80 we observe also two directions of the current via tape's edges and center.

For the AMSC tape, the residual current density at the edges is almost symmetric along the X direction and penetrates to the tape's center (see Fig. 79). However for Fujikura tape, the residual current density profiles are not symmetric along edges (see Fig. 80).

Residual current shows lower penetration to the Fujikura tape's center comparing to the wider AMSC tape. As, the critical current of Fujikura tape is more than five times higher than the transport current, before switch off, comparing to the critical current of AMSC tape, which is three times higher than the transport current (See Table. 5).

The results demonstrate the strong asymmetry and vortex-like structure of 2D residual current density profile in BSCCO tape while the current flow pattern in YBCO tapes is symmetric about the center of the tape. That could be explained by the manufacturing specifics of the BSCCO tape that results in filament structure of it while the structure of YBCO tape is uniform. The significant difference in the shape and amplitude of the residual current density profiles is observed as well.

7.6 Summary

We discussed in this chapter the over-current pulse operation effect on the current density of the HTS tapes. We studied the self-magnetic field of the BSCCO and YBCO tapes. The self-magnetic field distribution on the BSCCO and YBCO tapes showed a relaxation of the self-magnetic field above the BSCCO tapes edge where the self-magnetic filed above the YBCO tapes is constant.

These relaxations represent a current density distribution inside the HTS tapes after the over-current pulse operations. A negative current distribution, different between AMSC and Fujikura tapes, near the YBCO tapes' edges after the over-current pulse are also shown and. Current density profiles also show different profiles related to the characteristics of each HTS tape.

The remnant current of the BSCCO and YBCO tapes was calculated in this chapter. The way to cut the DC current was shown that it plays a role in the current distribution of HTS tapes. We relate this observation to the HTS tapes characteristics. We used also the current density profiles study to check the homogeneities of each HTS tapes, regarding the critical currents and manufacturing processes.

Contribution: This chapter is based on the following papers:

- M. Tallouli, J. Sun, A. Ninomia, M. Hamabe, H. Watanabe, et al, '' Residual magnetic field measurement of BSCCO and YBCO tapes by a Hall probe, '' *IEEE Trans. Appl. Supercond*., vol. 25, p. 8000704, June 2015, (4 pp.)

- J. Sun, Tallouli Mohamed, Oleg Shyshkin, Makoto Hamabe, Hirofumi Watanabe, Noriko Chikumoto, O. Shyshkin, '' Residual magnetic field profiles and their current density profiles of coated conductors for fast and slow-cut-off current operations,'' Progress in Supercond. And Cryogen., vol. 15, pp. 17-20, March 2015.

- Oleg Shyshkin, Yuri Kazarinov, Moahmed Tallouli, Tosin Famakinwa, Satarou Yamaguchi, '' Inverse Problem Solution Algorithms for Current Density Distribution Calculation in Different HTS Tape Configurations Basing on Minimum Self- Magnetic Field Measurements,'' *IEEE Trans. Appl. Supercond.,* vol. 26, no. 3, p. 9000404, Apr. 2016. (4 pp.)

- M. Tallouli, J. Sun, Noriko Chikumoto, O. Shyshkin, E.S Otabe, et al, '' Observation of self-magnetic field relaxations in Bi2223 and Y123 HTS tapes after over-current pulse and DC current operation,'' **submitted to** *Cryogenics.*

- M. Tallouli, J. Sun, M. Hamabe, H. Watanabe, Noriko Chikumoto, et al, '' Study of residual current density profiles of BSCCO and YBCO HTS tapes by a 3D Hall probe system,'' *IEEE Trans. On Appl. Supercond.,* vol. 26, Issue 3, 2016. (5 pp.)

CHAPTER 8. THESIS SUMMARY

8.1 Summary

High superconducting tapes with high homogeneity are required to transport high DC current via DC superconducting power transmission lines. However, there are still some challenges to avoid some fault conditions in current feeding that can occur, which requires a complete study of current density redistributions in these tapes in such conditions. This thesis focused on fault condition simulations and current density distribution calculations.

One-dimensional and two-dimensional current distributions after over-current pulse or quick switch off of DC current reveal inhomogeneous and time dependence distribution of current in specific HTS tapes. The quality of the BSCCO filaments near the edge would be lower than the center's. It is one of the reasons why the current density profile is peaked at the tape' s center, which is not true for YBCO because the shielding effect of the superconducting filaments and the matrix materials, such as copper and silver. These resistive materials can consume electric power. The quality of the superconducting layer of the YBCO tape would be the same all over the tape and the current density is high near the edge. The inhomogeneity of the HTS tapes may depend then on the magnitude of the applied current, processes of manufacturing, the critical current and the width of the HTS tape. We conclude also that if the HTS tape's critical current is low, the inhomogeneity is high. Which means that the homogeneity of the BSCCO tape is high relatively. That is why when we applied an over-current pulse current exceeds HTS tapes' critical current, the silver matrix near the edge would mainly conduct the current during the pulse. And after the pulse, the superconducting components of the HTS tapes carry the current around the center. The quick reduce of the current pulse, induces an opposite electric field to reduce the

current. This electric field generates eddy current at the edges zone, which opposes the current density diffusion, and reduces the current density especially near edges, where the silver matrix consumes this electric current. The current density profile is then peaked at center and the current density around tapes' edges is lower than those of the normal operation.

The homogeneity of the HTS tapes differed on the HTS tape characteristics and the current cut method (fast or slow). Homogeneity was almost symmetric on the BSCCO tape's center, which means that the uniformity of the BSCCO tape is high, but was not highly uniform in the case of YBCO tapes where the amplitude of current densities in fast cut-off operation is almost four times higher than these of the slow cut-off operation. Along the HTS tapes also, The magnetic field scans are very different for each tape that predicts a strong inhomogeneity of current distribution in the case of YBCO SWCC tape which was operated under current close to the critical one. Less inhomogeneity is observed in the case of YBCO AMSC tape.

Chapter 1 presented a background and history of superconductivity.

Chapter 2 described briefly the properties of HTS tapes especially BSCCO and YBCO. And gives some method and model to investigate and calculate current density distribution in these tapes.

In **chapter 3**, superconducting power transmission cables are described and the advantage of the DC power transmission technologies compare to AC one were discussed.

In **chapter 4**, some of the cryogenic engineering techniques developed in Chubu University for the DC superconducting power transmission line were described.

In c**hapter 5**, the experiment set-up and different techniques used to simulate fault and normal

conditions of the DC current feeding operations was shown. Measurement of direct and remnant HTS tapes self and residual magnetic field method are also explained. Different magnetic field measurement in each current feed operation with the Hall probe scanning technique was described. The results of the Hall probe scanning and measurement were also shown.

In **chapter 6**, our model for solving current density distributions in HTS tapes is suggested. Then, the model is verified by the current density distribution profile in copper tapes. In the model, it is was assumed that the thickness of the tape is infinitesimal so that all the current running within the tape could be considered as a surface current presented through the surface current density. Further, we supposed that all the current is running along the tape so that only one component of the current density exists. The current density doesn't depend on X coordinate and is a function only of Y coordinate. For a number of measurements of the vertical components of the magnetic field for one-dimensional current density distribution and three vertical components for the two-dimensional current density distribution, we got a system of linear equations with known magnetic field and unknown current density elements. A code solves this system of linear equations by means of Cramer's rule. As a result, of inverse problem solution, we obtained the current density profiles. And to solve the inverse problem aim at the calculation of two-dimensional current density distribution throughout the HTS tape the solution for the set of linear algebra equations issued from the Biot-Savart law and the method of least squares was combined.

Chapter 7 presented the results of the self-magnetic field calculation after fault conditions simulation presented in chapter5 and the current density calculation method presented in chapter 6. Self-magnetic field relaxation was observed above HTS tapes edges proving the current density distribution after an over-current pulse. However, this long time relaxation

process depends in the existence of the stabilizer layer, which consumes an opposite induced electric field near the tapes' edges and the HTS components which differ current density profiles in BSCCO and YBCO tapes.

This chapter described also one-dimensional remnant current distribution results after slow and quick interventions of DC current presented in chapter 5 and remnant current density calculation presented in chapter 6. The results obtained from the experiments provide a way to compare the distribution and longitudinal uniformity of current density profiles in different HTS tapes. With the two-dimensional current density calculation, it was observed that the 3D residual magnetic field scans are not the same along the tape longitudinal direction. Bz and By amplitudes changes in just 1cm part of the BSCCO tape. That predicts a longitudinal inhomogeneity of current distribution in this tape, which was operated under current equals half the critical one. The superconductor filaments inside the BSCCO tape might be not parallel to the BSCCO longitudinal direction due to the fabrication procedure. For YBCO the superconductor lattice via the longitudinal direction is homogeneous. The remnant current density in the edges is almost symmetric and rises a little on one tape's edge side along the length direction.

8.2 Contributions

This thesis presented a simple and direct way to calculate and draw current density distribution in HTS tapes. It gives also a deeper understanding of the current density distribution in HTS tapes after different situation of DC current feeding that DC power transmission cable can face. This thesis contributes then to the energy transport field in a number of ways. First it studies the different ways to transport energy and clarify the advantages of the DC power transmission technology. Second it describes some phenomena occurring in superconductor cables after over-current pulses such as self–magnetic field relaxation process and inhomogeneity of HTS tapes

after quick current off intervention which is important for the DC power cable running and restart proceeding.

8.3 Future Work

While this thesis provides the basic framework for DC power transmission technology, more work is needed in several areas. In fact, when the constant current is conducted on the HTS tapes, the self-magnetic field at the edges is relaxing and changing for a long time process. The long relaxation process of the self-magnetic field near the tape's edge, which might depend on the permanent current near the tape's edge, is a subject for future research to design the superconducting cable.

In the other hand, even our method gives a simple way to resolve the linear equation of Biot-Savart law; more data with more high-resolution magnetic field measurement might be required for a deeper investigation of current redistribution in the HTS tapes during and after fault conditions.

REFERENCES

[1] H. Kamerlingh Onnes, "Investigations into the properties of substances at low temperatures, which have led, amongst other things, to the preparation of liquid helium" *Nobel Lecture*, pp. 306-336, December 1913.

[2] R. Heeb, D.F. Agterberg, "Ginzburg-Landau theory for a p-wave Sr2RuO4 superconductor: Vortex core structure and extended London theory", *Phys. Rev. B ,* vol. 59, pp. 7076-7082, March 1999.

[3] J. Bardeen, L. N. Cooper and J. R. Schrieffer, "Microscopic theory of superconductivity", *Phys. Rev,* vol. 106, p. 1175, December 1957.

[4] J. Bardeen, "Electron-Vibration interaction and superconductivity", Rev. of Modern Physics, vol. 23, p.261-270, July 1951.

[5] P. W. Anderson and B. T. Matthias, "Superconductivity, " *Science*, vol. 144, pp. 373-381, April 1964.

[6] M. K. Wu, J. R. Ashburn and C. J. Torng. "Superconductivity at 93 K in New mixed-phase Y-Ba-Cu-O compound system at ambient pressure", *Phys. Rev. Letter C,* vol. 58, p. 908, March 1987.

[7] http://www.futurescience.com/manual/sc1000.html

[8] Ch. Kittel, book "Introduction to solid state physics, " [John Wiley and Sons, Inc] New York, 1996. (Book)

[9] https://simpliphy.wordpress.com/2012/05/06/superconductivity/

[10] http://hyperphysics.phy-astr.gsu.edu/hbase/solids/scbc.html

[11] F and H. London, "The Electromagnetic Equations of the Superconductor", *Proceed. Of the Roy. Of London Soc. Series A: Math. Phys. And Eng. Sc.,* vol. 149, pp. 71-88, 1935.

[12] https://commons.wikimedia.org/wiki/File:Magnetisation_and_superconductors.png.

[13] http://www.msm.cam.ac.uk/ascg/lectures/fundamentals/fluxpenetration.php

[14] Mangin, "Superconductivity is a physical condensate", Presented in a conference at Ecole de Mines de Nancy, France, IFR materials conference. 23-24, Jun 2003. (French)

[15] O. Narayan, "Driving force on an Abrikozov vortex," *J. Phys. A: Math. Gen*, vol. 36, pp. 373-377, 2003

[16] H.T. Coeffey, "Distribution of magnetic fields and currents in superconductors," vol. 7, pp. 73-77, December 1967.

[17] X. L. Wang and A.H. Li, S. Yu, S. Ooi, K. Hirata, et al., "Thermally assisted flux flow and individual vortex pinning in $Bi_2Sr_2Ca_2Cu_3O_{10}$ single crystals grown by the traveling solvent floating zone technique," *Journal of Appl. Phys*., vol 97, pp. 10B114-1 - 10B114-3, May 2005.

[18] C. Attasnasio, L. Mariato, S.L Prishepa, and R. Scafuro, "Flux Creep effects in the transport properties of C-axis oriented BSCCO thin films," *Journal of Supercond*, Vol. 5, pp. 107-114, 1999.

[19] V. Meerovich, V. Sokolovsky, L. Prigozhin and D. Rozman, "Dynamic response of HTS composite to pulsed currents," *Supercond. Sc. And Tech*., vol 19, p. 267, February 2006.

[20] F. Grilli, E. Pardo, A. Stenvall,D. Nguyen, W. Yuan et al., "Computation of losses in HTS under the action of varying magnetic fields and current, *" IEEE Trans. Appl. Supercond.,* vol. 24, p. 8200433, Jun 2014.

[21] M. Inoue, K. Abiru, Y. Honda, T. Kiss, Y. Iiijimaet al., "Observation of current distribution in high superconducting tape using scanning Hall-probe microscope, " *IEEE Trans. On Appl. Supercond.*, vol. 19, pp. 2847-2850, June 2009.

[22] J. R. Kirtley, m. B. Ketchen, K. G. Stawiaz, J. Z. Sun, W. J. Gallagher, et al., "High-resolution scanning SQUID microscope, " *App. Phys. Let.,* vol. 66, pp. 1138-1140, 1995.

[23] http://www.physics.rutgers.edu/~eandrei/389/faraday.pdf

[24] H. Song, M. W. Davidson and J. Schwartz, "Dynamic magneto-optical imaging of transport current redistribution and normal zone propagation in $YBa_2Cu_3O_{7-\delta}$ coated conductor, " *Supercond. Sci. Tech.*, vol.22, p. 062001, May 2009.

[25] C. P. Bean, "Magnetization of hard superconductors, " *Phys. Rev. Lett.* Vol 8, pp. 250-253, March 1962B. Oswald, M. Krone, T. Staber, K. –J. Best, M. Soll, H. –J. Gutt, et al. "Design of HTS reluctance motors up to several hundred kW, " *Physica C*, vol. 372-378, pp. 1513-1516, 2002.

[26] Y. B. Kim, "Flux-flow resistance in type II superconductors, " *Phys. Rev.,* vol 139, pp. A1170-A1172, August 1965.

[27] L. Bottura and O.C. Zienkiewicz, " Quench analysis of large superconducting magnets. Part I: model description, " *Cryogenics,* vol. 32, pp 659-667, 1992.

[28] https://en.wikipedia.org/wiki/Superconducting_magnet

[29] H. Piekarz, J. Blowers, S. hays, Y. Huang and V. Shieltzef, "Design study and test arrangement of HTS transmission line power cable for cycling accelerator magnets, " *IEEE. Trans. Appl. Supercond.* , vol. 20, pp.1304-1307, June 2010.

[30] B. Oswald, M. Krone, T. Straber, K.-J. Best, M. Soll, W. Gawalek, H. –J. Gutt, et al., "Design of HTS reclutance motors up to several hundred kW, " *Physica C,* vol. 372-376, pp.1513-1516, 2002.

[31] http://www.azom.com/article.aspx?ArticleID=949

[32] J. O. Walbrecker, B. Kalisky, D. Grombacher, J. Kirtley, K. A. Moler, R. Knight, "Direct measurement of internal magnetic fields in natural sands using scanning squid microscopy, " *Jrnl. Magn. Reson.,* vol. 242, pp.10-17, 2014.

[33] K. Hattori, M. Hazumi, H. Ishino, M. Kawai, A. Kibayashi, N. Kimura, et el. "Developpement of superconducting detectors for measurement of cosmic microwave background, " *Phys. Proc.*, vol. 37, pp.1406-1412, 2012.

[34] H. Maeda, Y. Tanaka, M. Fukutumi, and T. Ansano, "A New High-Tc Oxide Superconductor without a Rare Earth Element". *Jpn. J. Appl. Phys*., vol. 27, pp. L209-L210, 1988.

[35] http://cesur.ankara.edu.tr.

[36] D. I. dos Santos, D. Rodrigues Jr, E. Ap.A. Rubo, E. Cursino, "Processing and properties of Ag/BSCCO PIT tapes containing different proportions of silver metal powder, " *Physica C Proceed of ICMM of Supercond*, vol. 408-410, pp 52-53, 2004.

[37] M. Kikuchi, N. Ayai, T. Ishida, K. Tatamidani, et al., "Development of new type of DI-BSCCO, " *SEI Tech. Rev.,* Number 66, pp. 73-79, April 2008.

[38] A. D, Caplin, S. M. Cassidy, L. F. Cohen, M. N. Cuthbert, et al. " 'Strong' grain boundaries in Ag-BSCCO(2223) tapes, " *Physica C,* vol. 209, pp. 167-170, April 1993.

[39] M. K. Wu, J. R. Ashburn, and C. J. Torng, "Superconductivity at 93 K in a new mixed-phase Y-Ba-Cu-O compound system at ambient pressure, " *Phys. Rev. Let.,* vol.58, p. 908, March 1987.

[40] C. Yang, Y. Xia, F. Zhang, B. Tao and J. Xiong "The effect of grain boundaries on the current Transport properties in YBCO coated conductors, " *Nanoscale Res. Let*., vol. 10, p. 416, 2008.

[41] http://www.windpowerengineering.com/design/materials/why-the-wind-industry-should-cheer-superconductivity/

[42] V. Matias and R. H. Hammond, "YBCO superconductor wire based on IBAD-textured templates and RCE of YBCO: Process Economics, " *Physica C*, vol. 36, pp. 1440-1444, Superconductor Centennial Conference 2012.

[43] V. Matias and R. H. Hammond, "YBCO superconductor wire based on IBAD-textured templates and RCE of YBCO: Process Economics, " *Physica C*, vol. 36, pp. 1440-1444, Superconductor Centennial Conference 2012.

[44] M. Igarashi, Ch. Tashita, T. Hayashida, Y. Hanada, S. Hanyu, H. Fuji, et al., "RE123 coated conductors, " *Fujikura Tech. Rev.,* pp. 46-54, 2009.

[45] Y. Iijima, "High-performance Y-based superconducting wire and their applications, " *Fujikura Tech. Rev*., pp. 117-121, 2013.

[46] Showa Electric Wire and Cable Co. Ltd., "Wire Handbook, ", 2011. (Japanese book).

[47] http://www.yoshinogawa.co.jp/english/etech4.html

[48] http://lhc-machine-outreach.web.cern.ch/lhc-machine-outreach/components/cable.htm

[49] http://mri-q.com/superconductive-design.html.

[50] https://en.wikipedia.org/wiki/SCMaglev.

[51] S. Yamaguchi, T. Fujii, M. Sugino, M. Hamabe, H. Watanabe, T. Kawahara, and A. Iiyoshi, " Iron-steel cryogenic pipe for DC superconducting power transmission line, " IEEE. Trans. Appl. Supecond, vol. 21, pp. 1046-1049, June 2011.

[52] J. Sun, S. Yamaguchi, M. Sugino, H. Watanabe, M. Hamabe, T. Kawahara, S. Yamaguchi, "Critical current measurement for design of superconducting DC transmission power cable, " *Physica C*, vol. 471, pp. 1313-1316, November 2011.

[53] J. Sun et al. " Development and operation of the measurement system for 200 m HTS cable, " Proc. Of ICEC 23-ICMC 2010, pp. 1035-1040, 2011.

[54] Y. Ivanov, A. Radovinsky, A. Zhukovsky, A. Saaki, H. Watanabe, T. Kawahara, and S.Yamaguchi, "A compact cooling for HTS power cable based on thermal siphon for circulation of LN_2 , " *AIP Conf. Proc*., vol. 1218, pp. 865-870, 2010.

[55] M. Hamabe, A. Sasaki, T. S. Famakinwa, A. Ninomiya, Y. Ishiguro, and S. Yamaguchi, "Cryogenic system for DC superconducting power transmission line , *" IEEE. Trans. Appl. Supercond.,* vol. 17, pp. 1722-1725, June 2007.

[56] N. Ayaki, K. Yamazaki, M. Kikuchi, G. Osabe, H. Takaaze, et al. “Electrical and Mechanical Proprties of DI-BSCCO Type HT Reinforced With Metallic Sheathes,” *IEEE Trans. Appl. Supercond*, vol. 19, pp. 3014-3017, June 2009

[57] Y. Yamada, S. Sakai, K. Shiohara, Y. Ishii, K. Tachikawa, T. Koizumi, Y. Aoki, and T. Hasegawa, “Development of HTS Current Leads Prepared by the TFA-MOD Processed YBCO Tapes,” *IEEE Trans. Appl. Supercond.,* vol 20, pp. 1714-1717, June 2010.

[58] M. W. Rupich, X. Li, S. Sathyamurthy, C.L.H. Thieme, K. DeMoranville, J. Gannon, and S. Fleshler, “Second Generation Wire Development at AMSC,” *IEEE Trans. Appl. Supercond*., vol. 23, p. 6601205, 2013, (5pp).

[59] H. Knoepfel “Pulsed high magnetic field fields, ” pp 46-72, North-Holland Publishing Company, 1970.

[60] P. Usak, " Measurement of the transport current distribution in a superconducting tape, " *Physica C*, vol. 316, pp. 229-233, 1999.

[61] Y. Honda, K. Higashikawa, M. Inoue, T. Kiss, N. Ayai, M. Kikuchi, et al, " Study on critical current distribution in CT-OP Bi2223 tape based on the scanning Hall probe magnetic microscopy, " *Physica C*, vol. 484, pp. 1377-1379, 2010.

[62] M. Carrera, X. Granados, J. Amoros, R. Maynou, T. Puig, and X. Obrados, "Current distribution in HTSC tapes obtained by inverse problem calculation, " *J. Phys.: Conf. Ser.*, vol. 470, p. 012009, 2010.

[63] O. A Shyshkin, Y. G. Kazarinov, M. Tallouli, T. Famakinwa, S. Yamaguchi, " Inverse problem solution algorithms for current density distribution calculation in different HTS tape configuration basing on minimum self magnetic field measurement, " accepted for publication in *IEEE Trans. Appl. Supercond*, 2015.

[64] http://www.arepoc.sk/uploaded/download/HallProbes.PDF.

[65] J.H. Kim, M. Park, M. H. Ali, J. Cho, S. Kim, H. Kim et al, "Investigation of the over current characteristics of HTS tapes considering the application for HTS power devices, " *IEEE Trans. Appl. Supercond.*, vol. 18 , pp. 1139-1142, June 2008.

[66] T. Ishigohka, and K. Kurahashi, "An over current withstanding design of superconducting power cables, " *Elect. Eng. in Japan*, vol. 141, pp. 34-38, 2002.

[67] K. Rogacki, A. Gilewski, M. Newson, H Jones, B. A. Glowacki, J. Klamut, " Pulsed transport critical currents of Bi2212 tapes in pulsed magnetic fields, " *Supercond. Sci. and Technol.* vol. 15, p. 1151, 2002.

[68] S. Ochiai, D. Doko, H. Okuda, S. S. Oh , D. W. Ha, “Distribution of local critical current along sample length and its relation to overall current in a long Bi2223/Ag superconducting composite tape.” *Supercond. Sci. Technol.*, vol. 19, pp. 1097–1103, September 2006.

[69] Y. Lee, H. Yamasaki, M. Furuse, "Magnetic field angle dependent critical current densities and flux pinning in commercial YBCO tapes below liquid nitrogen temperature, " *Physica C*, vol. 471, pp. 1017–1020, 2011.

[70] I. Falorio, E. A. Young, Y. Young, "Flux pinning and E-J characteristics of 2G YBCO tapes, " *J. Physics: Conf. Ser.* vol. 507, p. 022004, 2014.

[71] C. Gu, Timing Qu, and Z. Han, "Measurement and calculation of residual magnetic field in a Bi2223/Ag Magnet," *IEEE Trans. Appl. Supercond.,* vol. 17, pp. 2394-2397, 2007.

[72] R. Inada, S. Baba, R. Ohtsu, T. Makihara, S. Sakamoto, and A. Oota, "Longitudinal Uniformity of Commercial Bi2223 Characterized by Scanning Hall-Probe," *IEEE Trans. Appl. Supercond,* vol. *21, pp. 2816-2819, 2011.*

[73] P. Usak, M. Polak, and P. Mozola, "Measurement of the lateral Transport Current Distribution in YBCO Tape," *IEEE Trans. Appl. Supercond.,* vol. 19, pp. 2839-2842, 2009.

Publications in Review Journals

Title	Journal	Author
Residual magnetic field measurement of BSCCO and YBCO HTS tapes by a Hall probe.	*IEEE Trans. On Appl. Supercond*., vol. 25, no. 3, p. 8000704, Jun. 2015. (4 pp.)	**Mohamed Tallouli** Jian Sun Oleg Shyshkin Akira Ninomiya Makoto Hamabe Hirofumi Watanabe Noriko Chikumoto Samia Charfi-Kaddour Satarou Yamaguchi
Residual magnetic field profiles and their current density profiles of coated conductors for fast and slow-cut-off current operations.	*Progress in Supercond. And Cryogen.,* vol. 15, no. 1, pp. 17-20, Mar. 2015.	Jian Sun **Mohamed Tallouli** Oleg Shyshkin Makoto Hamabe Hirofumi Watanabe Noriko Chikumoto Satarou Yamaguchi

Study of residual current density profiles of BSCCO and YBCO HTS tapes by a 3D Hall probe system	*IEEE Trans. On Appl. Supercond.,* vol. 26, Issue 3, 2016. (5 pp.)	**Moahmed Tallouli** Jian Sun Oleg Shyshkin Makoto Hamabe Hirofumi Watanabe Noriko Chikumoto Samia Charfi-Kaddour Satarou Yamaguchi
Inverse Problem Solution Algorithms for Current Density Distribution Calculation in Different HTS Tape Configurations Basing on Minimum Self- Magnetic Field Measurements	*IEEE Trans. On Appl. Supercond.,* vol. 26, no. 3, p. 9000404, Apr. 2016. (4 pp.)	Oleg Shyshkin Yurij Kazarinov **Moahmed Tallouli** Tosin Famakinwa Satarou Yamaguchi

Presentation at International Conferences

Title	Conference	Author
Magnetic field measurement of HTS tape conductors	25th International Symposium on Superconductivity, Tokyo, Japan, WTP-035, 2013, 2013. (Poster)	**Mohamed Tallouli** Jian Sun Hirofumi Watanabe Makoto Hamabe Toshio Kawahara Satarou Yamaguchi Akira Ninomiya Edmund Soji Otabe Teng Zhang Samia Charfi-Kaddour
Residual magnetic field measurement of BSCCO and YBCO HTS tapes by a Hall probe.	2014 Applied Superconductivity Conference, Charlotte, USA, 3MPo1C-08, 2014. (Poster)	**Mohamed Tallouli** Jian Sun Oleg Shyshkin Akira Ninomiya Makoto Hamabe Hirofumi Watanabe Noriko Chikumoto Samia Charfi-Kaddour Satarou Yamaguchi

1D and 2D current and remnant current density profiles of BSCCO and YBCO HTS tapes by 3D Hall probe system.	12th European Conference on Applied Superconductivity, Lyon, France, 1A-WT-P-01.01, 2015. (Poster)	**Mohamed Tallouli** Jian Sun Hirofumi Watanabe Makoto Hamabe Yuri Ivanov Toshio Kawahara Satarou Yamaguchi Edmund Soji Otabe Oleg Shyshkin Samia Charfi-Kaddour

Presentation at local Conferences

Title	Conference	Author
Magnetic field measurement of HTS tapes.	The 60th Japanese Applied Physics Society meeting, 27a-G3-1, 2013. (Oral)	**Mohamed Tallouli** Toki Yoshinubu Hisato Ohara Jian Sun Hirofumi Watanabe Makoto Hamabe Toshio Kawahra Satarou Yamaguchi
Observation of inhomogeneous profiles of current density in BSCCO and YBCO tapes from residual magnetic field measurement	The 62th Japanese Applied Physics Society meeting, 12a-P9-16, 2015. (Poster)	**Mohamed Tallouli** Jian Sun Oleg Shyshkin Satarou Yamaguchi Samia Charfi-Kaddour
Magnetic field measurement of HTS tape conductors	Abstract of Cryogenics and Superconductivity Society of Japan Conference, 1P-p14. Vol. 88 (2013) 77. (Poster)	**Mohamed Tallouli** Jian Sun Yuri Ivanov Hirofumi Watanabe Makoto Hamabe

		Noriko Chikumoto Oleg Shyshkin Samia Charfi-Kaddour Satarou Yamaguchi